AD-A252 572

REPORT DOCUMENTATION PAGE

Form Approved
OMB No 0704-0188

REPORT DATE	3. REPORT TYPE AND DATES COVERED
1992	THESIS

4. TITLE AND SUBTITLE
Development of a Real-Time Fiber Analyzer: A Feasibility Study

5. FUNDING NUMBERS

6. AUTHOR(S)
Philip John Becker, Captain

7. PERFORMING ORGANIZATION NAME(S) AND ADDRESS(ES)
AFIT Student Attending: University of Minnesota

8. PERFORMING ORGANIZATION REPORT NUMBER
AFIT/CI/CIA- 92-022

9. SPONSORING/MONITORING AGENCY NAME(S) AND ADDRESS(ES)
AFIT/CI
Wright-Patterson AFB OH 45433-6583

10. SPONSORING/MONITORING AGENCY REPORT NUMBER

11. SUPPLEMENTARY NOTES

12a. DISTRIBUTION/AVAILABILITY STATEMENT
Approved for Public Release IAW 190-1
Distributed Unlimited
ERNEST A. HAYGOOD, Captain, USAF
Executive Officer

12b. DISTRIBUTION CODE

13. ABSTRACT (Maximum 200 words)

92-17923

14. SUBJECT TERMS

15. NUMBER OF PAGES
124

16. PRICE CODE

17. SECURITY CLASSIFICATION OF REPORT	18. SECURITY CLASSIFICATION OF THIS PAGE	19. SECURITY CLASSIFICATION OF ABSTRACT	20. LIMITATION OF ABSTRACT

DEVELOPMENT OF A REAL-TIME FIBER ANALYZER: A FEASIBILITY STUDY

A THESIS
SUBMITTED TO THE FACULTY OF THE GRADUATE SCHOOL
OF THE UNIVERSITY OF MINNESOTA
BY

PHILIP JOHN BECKER

IN PARTIAL FULFILLMENT OF THE REQUIREMENTS
FOR THE DEGREE OF
MASTER OF SCIENCE

MARCH 1992

UNIVERSITY OF MINNESOTA

This is to certify that I have examined this bound copy of a M.S. thesis by

PHILIP J. BECKER

and have found that it is complete and satisfactory in all respects, and that any and all revisions required by the final examining committee have been made.

DAVID Y. H. PUI
Name of Faculty Adviser(s)

David Y. H. Pui
Signature of Faculty Adviser(s)

March 25, 1992
Date

GRADUATE SCHOOL

ACKNOWLEDGMENTS

I am indebted to Dr. David Pui for the support, encouragement, and direction provided to me over the last year. Dr. Pui always had time for me and never lacked enthusiasm. This experience has been an excellent one thanks to him. I must also thank the other Particle Technology Laboratory students for their friendship and help. Yan Ye and Seung-Ki Chae especially gave much of their time answering questions on the computer programs used in this thesis. Dexian Zhang also deserves my thanks for providing me with a digital oscilloscope.

I appreciated the help I received from Rob Caldow and Stan Kaufman of TSI and also appreciate the SiC fibers provided by Tai Chan of General Motors.

I gratefully acknowledge the support of the United States Air Force which gave me the opportunity to complete this work through the Air Force Institute of Technology Civilian Institutes Program.

Finally, I am grateful to my parents for their encouragement and for showing confidence in me always and to my parents-in-law for their support. Most of all, I thank Lisa and little Molly, without whose love, support, sacrifice, and smiles this work would not have been possible.

ABSTRACT

The feasibility of creating an instrument which could distinguish fibrous particles from spherical particles and measure the dimensions of those fibers in real-time by modifying a TSI Aerodynamic Particle Sizer (APS) was examined. The main concept for the instrument is to align fibers so their polar axis is perpendicular to the incident laser beams in the APS. The pulse pairs generated can then be used to measure fiber length, diameter, and aerodynamic diameter.

Two main aspects of the instrument were studied, the fiber orientation within the APS and the light scattering characteristics of a fiber in the APS. The possibility that fibers would be aligned properly by simply using the shear flow in the APS nozzle assembly was investigated using a computer model. The results indicated that fibers would align themselves properly. With this information, a computer model was used to find the light scattering characteristics of an infinitely long cylinder in the APS for a normally incident beam. The results showed it would be possible to distinguish fibers from spherical particles by comparing their pulse pairs.

The feasibility of the proposed instrument was experimentally tested by sampling 2.0 μm diameter silicon carbide (SiC) fibers with a mean length of 31.2 μm into an APS and viewing their pulse pairs on an oscilloscope. The light scattering characteristics determined from the computer analysis were borne out by the experimental results but proper fiber orientation was not found in all cases. SiC fibers were also sampled to Nuclepore filters by the same method and the concentration of single fibers determined. This was found to be in good agreement with the single fiber concentration as determined from viewing the APS pulse pairs.

Overall, the proposed instrument was determined to be feasible. Further research into the light scattering of fibers and fiber orientation is recommended. The direction of instrument development and some possible modifications to be made to the APS are discussed. These include providing electrostatic fiber alignment, modifying the APS collecting optics, and modifying the incident laser beams.

Table of Contents

List of Figures

CHAPTER 1
INTRODUCTION

The objectives of this feasibility study are: 1) to investigate the possibility of distinguishing fibrous particles from spherical particles in an aerosol and measuring the length, diameter, and aerodynamic diameter of the fibrous particles in real-time, and 2) if the instrument proves feasible, to provide recommendations and direction for future development. A particle's aerodynamic diameter is the diameter of a unit density sphere that has the same settling velocity as the particle. This allows irregular shaped particles to be quantified by their aerodynamic properties. The aerodynamic diameter is an important property for fibers as it is used as a measure of such things as the deposition of fibers in human airways. The new instrument will be referred to as the Real-time Fiber Analyzer (RFA) and its hardware is based on an instrument made by TSI called the Aerodynamic Particle Sizer (APS). The APS is currently used to measure the aerodynamic diameter of aerosol particles in a size range from 0.5μm to 30μm. It does this by relating a particle's time-of-flight between two points to the particle's aerodynamic diameter.

The need for an instrument which would distinguish fibers from other particles in an aerosol and size them all in real-time is great. Applications for the RFA would include such things as asbestos fiber sampling for health and safety reasons or for quality control and environmental safety for fibers being used in the manufacture of composite materials. Currently, accepted fiber measurement techniques involve sampling the aerosol in the field and then returning to a lab for analysis. Some of the measurement and counting techniques include using phase contrast microscopy or electron microscopy. Many manual methods of counting exist as well as a few forms of automatic image analysis. The automatic image analysis is markedly faster than the manual techniques but in all cases a good deal of time elapses between when the samples are taken and when the results are known.

In a specific example Chan *et. al.* (1991) notes that health hazards must be considered when using Silicon Carbide (SiC) whiskers in manufacturing

metal matrix compounds. It was found that the sampling time needed to meet the requirements of the counting method used was 40 minutes. Chan *et. al.* also noted that there is a need to develop a method of instantaneous fiber detection and physical characterization of airborne fibers. This specific example is pertinent to this work because Chan provided 2.0μm SiC fibers for experimental use in this study. Throughout the study, SiC fibers are used in the numerical models because they were available for experimental use although the study was not limited to this application only.

Several methods of automatic, real-time fiber measurement have been explored by others. One method has resulted in a commercially available instrument, the MIE Fiber Aerosol Monitor. In Chapter 2 some background information on fiber mechanics is presented followed by a review of the other fiber measurement methods in Chapter 3. This provided a good starting point for exploring the feasibility of the RFA.

The idea for an instrument based on the APS was brought forth by Professor David Y.H. Pui (University of Minnesota). It was briefly studied in an honors thesis by Corpron (1990). This study builds on that work. The concepts for the operation of the instrument are discussed in detail in Chapter 4. Basically, a fiber is accelerated through a nozzle into the APS viewing volume where it crosses two laser beams. As it crosses each beam, light is scattered and collected by a photomultiplier tube (PMT). The PMT generates a voltage pulse pair corresponding to the amount of light scattered from each beam. Information can then be extracted from the pulse pair to determine fiber aerodynamic diameter, length, and diameter.

In developing this new instrument, numerous aspects must be considered, sampling efficiency, signal processing, and coincidence error to name a few. This study, however, focuses on two of the main aspects of the instrument around which its operation hinges. These two aspects are, the orientation of fibers as they pass through the APS, and the light scattering characteristics of fibers in the APS. Chapter 5 provides some insight into these two matters using computer models to simulate the conditions in the APS.

The APS was tested with 2.0μm SiC fibers in experiments to discover if it could actually perform as a fiber analyzer. The experimental methods and results are discussed in Chapter 6. No modifications were made to the APS used for the experiments. In other words, an RFA was not built and tested for this study. Nevertheless, the performance of the unmodified APS is directly related

to the feasibility of constructing a working RFA. The overall results of the study lead to some recommended modifications and possible directions for instrument development which are outlined in Chapter 7.

CHAPTER 2
FIBER MECHANICS

Before progressing further, it will be helpful to review some background information on fiber mechanics. This information includes a prolate ellipsoid model of fibers, calculation of fiber aerodynamic diameter, a look at fiber rotation, and fiber losses due to interception. The prolate ellipsoid model is used as an approximation for a cylindrical fiber for use in modeling flow around the fiber and fiber translation and rotation. The aerodynamic diameter of a fiber is important as it provides a way to characterize a fiber's aerodynamic behavior. It differs from that of a sphere in that it depends on the orientation of the fiber in the flow. Fiber rotation and orientation in a flow becomes very important for many fiber measurement instruments and the RFA is no exception. Two methods of orienting the fibers in the instrument are discussed. Finally, the transport losses due to fiber interception are briefly covered.

2.1 PROLATE ELLIPSOID MODEL

Aerodynamic properties of a fiber, which is basically a cylinder, can be developed using a prolate ellipsoid approximation. The prolate ellipsoid is shown in Figure 2.1 with major axis, b, and minor axis, a. Fiber length therefore is $L = 2b$ and fiber diameter, $d = 2a$.

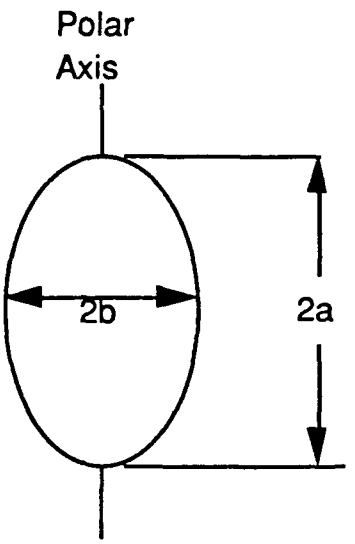

Figure 2.1 Prolate Ellipsoid

The drag force exerted on the ellipsoid when moving through a fluid is given by Fuchs (1964) as

$$F_d = 6\pi\mu avK \qquad (1)$$

where μ is the fluid viscosity, a is the ellipsoid radius, and v is the ellipsoid velocity relative to the fluid. The coefficient K depends on the fiber orientation with respect to the flow direction. If the fiber has its polar axis parallel to the fluid motion, K = K' where

$$K' = 4/3\ (\beta^2-1)/ \{[(2\beta^2-1)/(\beta^2-1)^{1/2}]\ \ln\ [\beta+(\beta^2-1)^{1/2}]-\beta\ \} \qquad (2)$$

If the fiber has its polar axis perpendicular to fluid flow, then K = K" where

$$K'' = 8/3(\beta^2-1)/ \{[(2\beta^2-3)/(\beta^2-1)^{1/2}]\ \ln[\beta+(\beta^2-1)^{1/2}]+\beta\} \qquad (3)$$

In these equations $\beta = b/a$ and is called the fiber aspect ratio. When the aerodynamic drag force equals the gravitational force, the fiber will attain a terminal settling speed v_s. It is given by

$$mg = 6\pi\mu a v_s K \qquad (4)$$

where m is the mass of the fiber and g is the acceleration of gravity. Since

$$m = (4/3)\pi a^3 \rho_p \beta \qquad (5)$$

where ρ_p is the particle density, then

$$v_s = 2a^2\rho_p g\beta/9\mu K \qquad (6)$$

2.2 AERODYNAMIC DIAMETER

The aerodynamic diameter of a particle is defined as the diameter of a unit density sphere having the same settling speed as the particle in question. The settling speed for a unit density sphere with radius a is:

$$v_s = 2a^2\rho_o g/9\mu \qquad (7)$$

where ρ_o is 1 g/cm^3. The aerodynamic radius of the fiber, a_a, can be found using Equations (6) and (7).

$$a_a = (\rho_p\beta/\rho_o K)^{1/2} a \qquad (8)$$

It follows that the aerodynamic diameter d_a is given by:

$$d_a = 2a_a \qquad (9)$$

The aerodynamic diameters for 2 μm diameter fibers of varying lengths for fibers falling vertically through the air (major axis parallel with the flow) and for fibers falling horizontally through the air (major axis perpendicular to the flow) are shown in Figure 2.2.

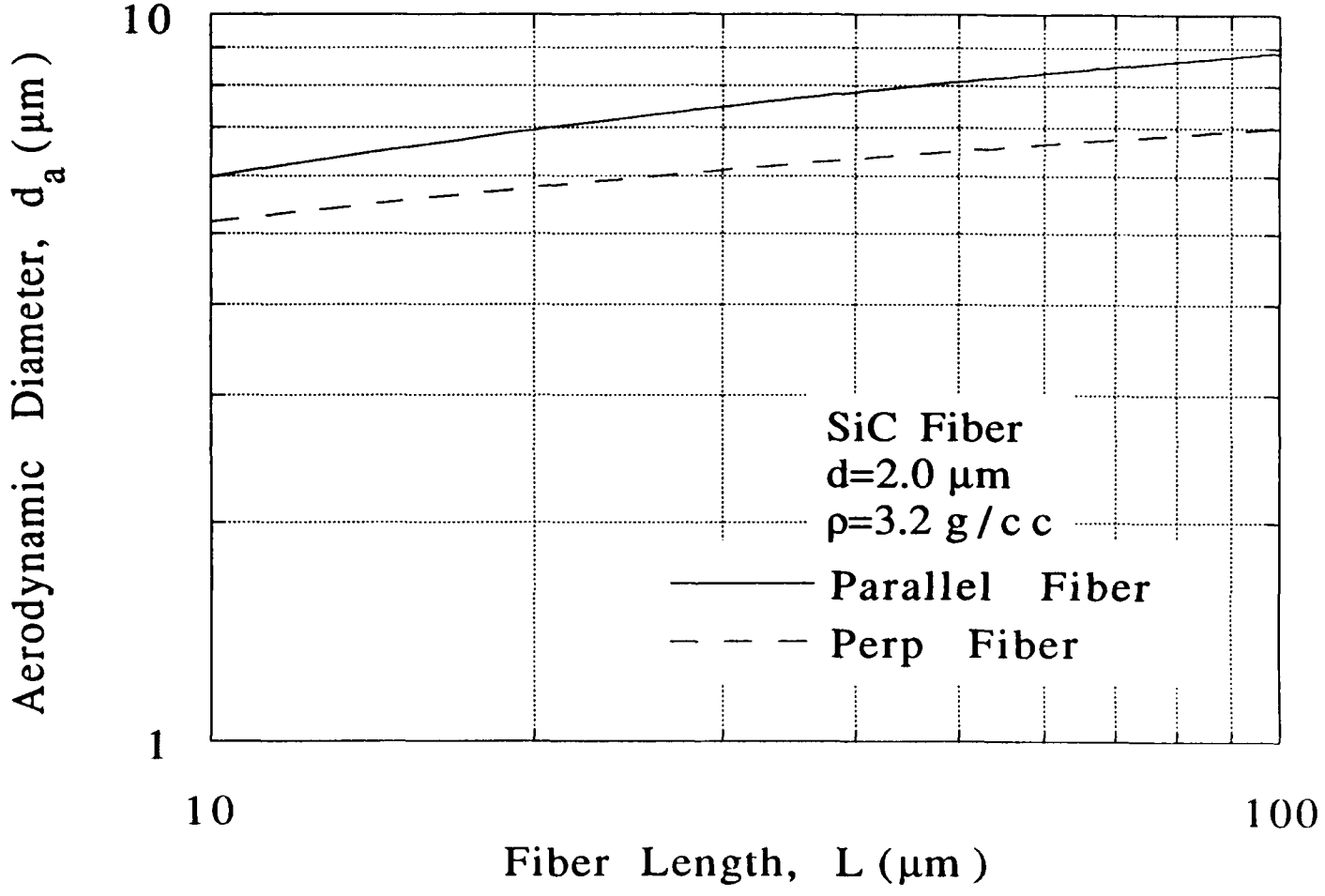

Figure 2.2 Aerodynamic Diameter of Fibers Aligned Parallel and Perpendicular to the Flow

It is easy to see that the aerodynamic diameter does not depend heavily on the fiber length but more so on the orientation and diameter.

2.3 FIBER ROTATION

An important part of any fiber measurement device would be the ability to know or control the orientation of the fibers at the time of measurement. For real-time fiber measurement instruments, two methods of controlling fiber orientation may be employed separately or in conjunction. The first is to orient the fiber using an electric field and the second is to orient the fiber using a shear flow.

2.3.1 Rotation in an Electric Field

The proposed method of real-time fiber measurement requires that the airborne fibers be aligned parallel with the flow. The mechanism discussed in this section which could be used to align the fibers, is an electric field. This mechanism has been thoroughly investigated by Lilienfeld (1985).

A fiber, which is exposed to an electric field, will be aligned with the fiber polar axis parallel to the electric field lines. (Note: Fibers aligned with their polar axes parallel to the flow or electric field will be hereby deemed aligned parallel with the flow while fibers aligned with their polar axes perpendicular to the flow or electric field will be hereby deemed aligned perpendicular to the flow.) This occurs in two steps. First, when the fiber is exposed to the field, the field will induce the fiber to become polarized. Second, the polarized fiber experiences torque due to the electric field and aligns itself with the electric field lines. For conductive particles, free electrons separate to opposite ends of the fiber. For nonconductive particles the molecules only polarize with the electric field. Therefore, the torque experienced by conductive fibers may be two to three orders of magnitude higher than nonconductive fibers. The surface adsorption of water, however, allows most particles to be considered conductive (Fuchs 1964) . Experiments (Lilienfeld et al., 1979) have shown that almost all fibers can be considered conductive when the ambient relative humidity exceeds about 30%.

The time it takes for the free charges in a fiber to travel to the opposing fiber ends is called the polarization time constant. This time constant is given by Lilienfeld (1985) as :

$$t = \varepsilon \rho d/4 \qquad (10)$$

where t = polarization time constant; ε = fiber dielectric constant; ρ = fiber surface resistivity; and d = fiber diameter. From this equation it is evident that the polarization time constant is independent of fiber length. Polarization times for fibers up to about 10 μm in diameter are typically around 1 μs. The equation assumes that the bulk resistivity of the fiber is infinitely high so that only water adsorption or like condition contributes to fiber conductivity.

Once a particle is polarized after being introduced to an electric field, a number of forces are acting on it. These include turbulence, drag force, bombardment of molecules from Brownian motion, and the torque on the polarized fiber induced by the electric field. The time it takes a fiber to rotate through a given angle θ in an electric field is found using equations given by Fuchs (1964). Assuming no turbulence, the equations are as follows:

$$d\theta/dt = B_\omega \tau_\theta = \omega \qquad (11)$$

and

$$\tau_\theta = d\Omega/d\theta \qquad (12)$$

where θ is the angular measure of orientation with respect to the electric field vector, B_ω is the rotational mobility, ω is the rate of rotation, τ_θ is the torque, and $d\Omega$ is the change in field energy caused by particle polarization. A prolate ellipsoid serves as a model for a fibrous particle as previously discussed. With that a general equation for the rotational mobility of a fiber is (Fuchs, 1964) :

$$B_\omega = 3\{[(2\beta^2-1)/(\beta^2-1)^{1/2}]\ \ln[\beta+(\beta^2-1)^{1/2}-\beta]\}/ 2\pi\eta d^3(\beta^4-1) \qquad (13)$$

where η is the viscosity of the gas and β is the aspect ratio of the fiber. The mean torque on the particle is found by differentiating the following expression (Fuchs, 1964) with respect to θ:

$$\Omega = -2\pi\varepsilon_o VE^2[(\cos^2\theta/X_1) + (\sin^2\theta/X_2] \qquad (14)$$

Where V is particle volume; E is electric field intensity in volts per meter; ε_o is the permittivity of free space; and X_1 and X_2 are ellipsoid shape factors. The shape factors are also given by Fuchs (1964):

$$X_1 = [1/(\beta^2-1)]\ \{[\beta/(\beta^2-1)^{1/2}]\ \ln[\beta+(\beta^2-1)^{1/2}-1]\} \qquad (15)$$

$$X_2 = [\beta/2(\beta^2-1)]\ \{\beta-[1/(\beta^2-1)]\ \ln[\beta+(\beta^2-1)^{1/2}]\} \qquad (16)$$

After differentiation, the torque is given by:

$$\tau_\theta = 4\pi\varepsilon_o VE^2\cos\theta\ \sin\theta[1/X_1-1/X_2] \qquad (17)$$

Then from Equation (11) the characteristic fiber axis rotation time is:

$$t_\theta \equiv 1/(B_\omega\tau_\theta) \qquad (18)$$

The previous equations were used to generate Figure 2.3, which shows various fiber rotation times for increasing fiber aspect ratios at three different electric field strengths. From Figure 2.3, the fiber rotation time varies little with aspect ratio for a given electric field intensity. However, the rotation time is greatly reduced for each increase in electric field intensity.

If an electric field is to be used as a method of fiber alignment it is important to know the fiber rotation time so that proper fiber alignment is assured prior to the fiber entering the sampling volume. For the standard APS

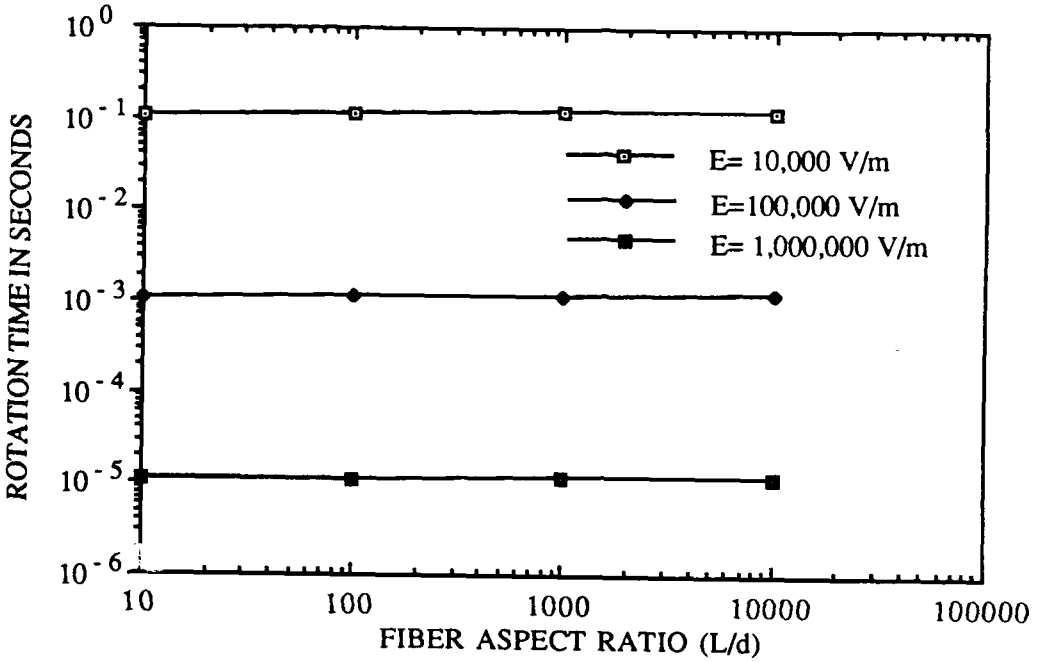

Figure 2.3 Rotational Times for Fibers of Various Aspect Ratio for Various Electric Field Strengths

nozzle the sampling flow rate is 1 LPM and the sampling tube is 0.32 cm in diameter and 8.5 cm in length. The velocity through the tube is then 207 cm/s and the fiber residence time in the tube is 0.04 s. The fiber residence time needs to be larger than the fiber rotation and polarization times to insure proper fiber alignment. From Figure 2.3, an electric field of 100,000 volts/m would be more than sufficient as the fiber rotation times are on the order of .001 s.

2.3.2 Rotation Using an Abrupt Contraction

Another method of insuring fiber alignment prior to measurement is to create a shear flow using an abrupt contraction. This is illustrated in Figure 2.4. Basically, a fiber that is perpendicular to the flow will experience a greater drag force on the end that is in a region of higher velocity than the center of the fiber. This will induce the fiber to rotate. This type of fiber rotation will be studied in greater detail using a computer model in Chapter 5.

2.4 FIBER INTERCEPTION

Bringing fibers into the instrument and transporting them to the viewing volume is not an insignificant task. If fibers of any diameter are oriented perpendicular to the flow and their lengths are longer than the tube diameter, the fibers will not enter the tube. Other shorter fibers may make it into the tube but may be intercepted by the tube wall during transport.

A model proposed by Fish (1974) can be used to determine the penetration efficiencies for fibers. Using this model, the penetration of randomly oriented fibers with diameters up to about 10 μm that are about 100 μm in length passing through an APS nozzle which has an opening of 0.8 μm diameter will be about 90%. Although particle losses in any instrument are of concern, they will not be explicitly considered in this feasibility study. It is recommended that they be considered for any future work.

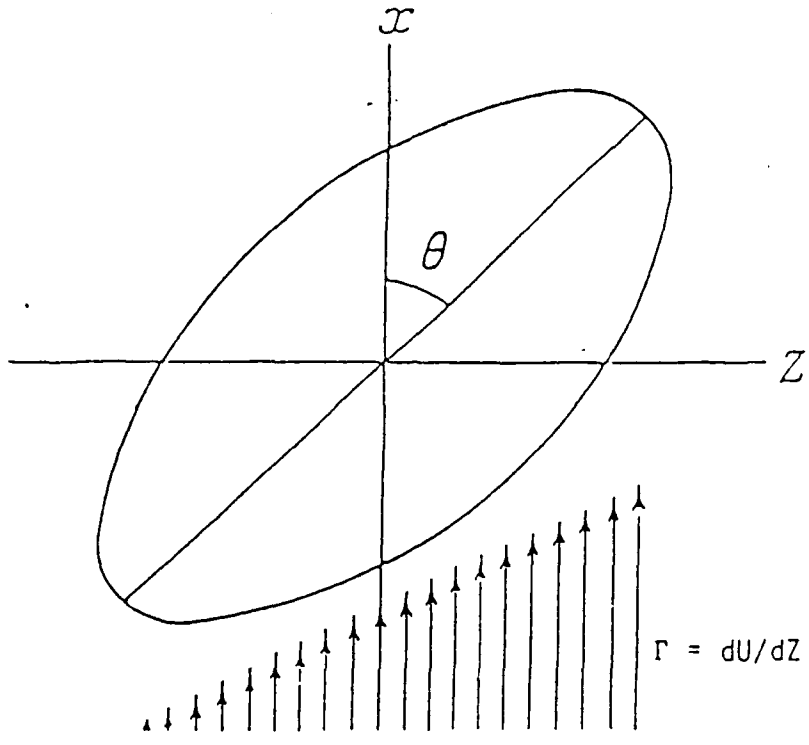

Figure 2.4 Fiber Rotation in Shear Flow

CHAPTER 3
REVIEW OF EXISTING FIBROUS AEROSOL MONITORS

Other automatic, real-time fiber measurement instruments have been or are being developed. One instrument, the MIE Fiber Aerosol Monitor, is even available commercially. These instruments all have limitations however. Some are not able to measure fiber diameter while others do not measure fiber length. None of the instruments discussed here are able to accomplish all the tasks of distinguishing fibers from spherical particles, measuring fiber length, measuring fiber diameter, and measuring fiber aerodynamic diameter. A summary of the theory and/or operating principles of some of these instruments is provided in this chapter.

3.1 UVM FIBER MONITOR

As described by Detenbeck (1980) the UVM (for University of Vermont) fibrous aerosol monitor discriminates fibers from other particles and counts them using a two-detector optical particle counter. The fibers can be distinguished by the asymmetry of their optical diffraction patterns. This concept is illustrated in Figure 3.1 (Detenbeck, 1980).

In this figure the fiber is oriented with its long axis perpendicular to the incident beam. The fiber orientation is accomplished using a combination of flow and electric field. The scattered light from the fiber forms a diffraction pattern on a screen behind it. The light scattered in the plane defined by the incident beam and the long dimension of the fiber is less than the light scattered in the plane defined by the incident beam and the fiber diameter. By placing photodetectors equidistant from the incident beam at the two locations (1 and 2) identified in Figure 3.1, the two different light intensities would be measured. A spherical particle on the other hand, would scatter an equal amount of light to each detector. In this way then, fibers can be distinguished from other particles.

A diagram of the instrument is shown in Figure 3.2 (Detenbeck, 1980). The laser used is a circularly polarized, 3 mW He-Ne laser. The viewing volume

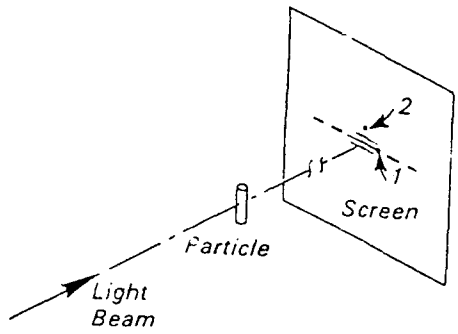

Figure 3.1 Asymmetry of Fiber Diffraction Pattern

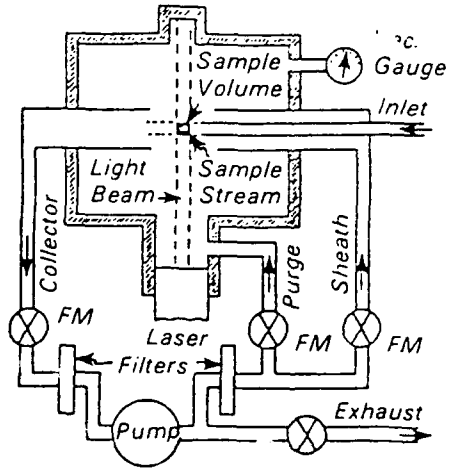

Figure 3.2 UVM Fiber Monitor

of the sample is about 1 mm^3. Sample air flows into the viewing volume surrounded by clean sheath air. The maximum air sampling rate is 5 cm^3/s in laminar flow, which corresponds to 2.5 cm of water vacuum in the sampling chamber. The sampling chamber also has a flow of purge air available for use during instrument start up.

The scattered light is detected by photomultiplier tubes located as shown in Figure 3.3. The angle θ is 20^o for each PMT although the sampling chamber is drilled to allow for the PMTs to be adjusted to scattering angles of 40^o and 90^o as well. The PMTs are set to work in a mode where they count photons. As light strikes a PMT, electrons are released from the PMT cathode and are amplified into an electric pulse. The pulses are then counted each 100 microseconds, and the sum is transferred to a computer. The number of pulses is proportional to the intensity of the scattered light.

When either of the PMTs detect an intensity in excess of a preset value, the computer knows that a particle is present. If the ratio of the output from both PMTs is found to exceed a preset value, the computer then knows that the particle is a fiber. The brighter of the two intensities is saved also, for it leads to the diameter of the fiber. The computer can give a number and size distribution based on fiber diameter at the end of sampling.

For the UVM fiber monitor the minimum fiber size measurable is limited by the signal to noise ratio. In other words, the amount of background scatter in the chamber when no particles are present. According to Detenbeck (1980) although it is theoretically possible to measure fibers down to a volume of .02 μm^3, it is actually only possible to detect fibers down to a minimum volume of 0.06 μm^3. This equates, for example, to about a 0.3 μm diameter fiber with an aspect ratio of 3. However, the UVM monitor is also limited in the maximum fiber size it can measure. This is due to the fact that the forward scattering intensities vary more widely with volume for fibers than for spheres. A prototype UVM monitor was built and subsequently tested, but it never went into commercial production.

3.2 MIE FIBROUS AEROSOL MONITOR

The MIE Fibrous Aerosol Monitor (FAM) is a commercially available real-time fiber measurement instrument. It is capable of discriminating fibers from other particles and it is capable of measuring fiber length and

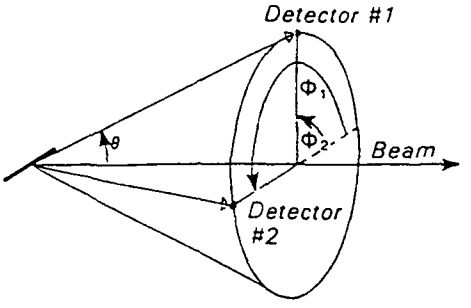

Figure 3.3 PMT Location for the UVM Monitor

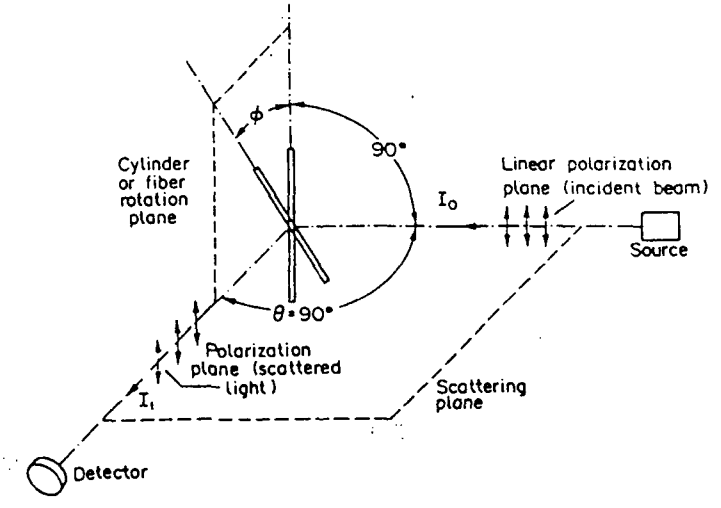

Figure 3.4 Fiber Light Scattering

number concentration. Because of its wide use, the theory and operation of this instrument will be described in greater detail than the other instruments described here. The basic principle behind this instrument is as follows. Sampled fibers are induced to rotate in a flow by applying a high-intensity fluctuating electric field. The rotating fibers are then illuminated by a monochromatic light source. The scattered light from the fibers is detected at a detection angle of 90 degrees and the pulses generated allow the fibers to be differentiated from other particles and measured.

3.2.1 Fiber Light Scattering

It is helpful to look at the light scattering signature of finite cylinders which are rotating in the plane perpendicular to the axis of illumination. Lilienfeld (1987) takes an in-depth look at this problem. Figure 3.4 (Lilienfeld, 1987) provides a schematic showing the orientation of the light source, the detector, and the fiber.

It can be shown that the perpendicularly polarized scattering intensity, I_1, for a cylinder, for a scattering angle θ of 90^o, is given by Lilienfeld (1987):

$$I_1 = I_0 l^2/\pi^2 r^2 [\sin(\pi l\phi/\lambda)/(\pi l\phi/\lambda)]^2 i_1$$

where I_0 is the intensity of the incident light, l is the fiber length, r is the distance between the cylinder axis and the detector, ϕ is the roll angle of the cylinder, λ is the wavelength of the incident light, and i_1 is the scattered intensity function for an infinitely long cylinder computed by Farone *et al.* (1963). The scattered intensity function for an infinitely long cylinder is shown in Figure 3.5 (Lilienfeld 1987). This will become important later in the discussion.

Because the previous equation is for linearly polarized light, the equation is only valid if the cylinder axis is constantly parallel to the plane of polarization. Therefore, the roll angle is not really the roll angle but rather the angle of detection. If the cylinder is tilted with respect to the linearly polarized incident wave, the scattered light then becomes elliptically polarized. However, because scattering occurs mostly in a narrow area around the equator of the cylinder, most of the scattered light remains within $\phi < \pm 6^o$. Therefore, the previous equation is a close approximation for scattered

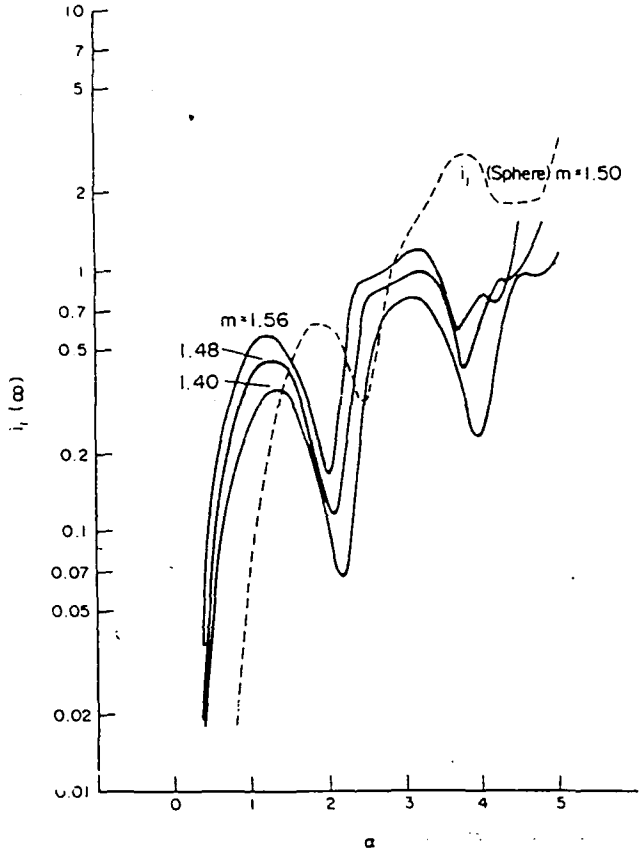

Figure 3.5 Scattered Intensity Function for Infinitely Long Cylinders at Perpendicular Incidence, for $\theta=90^{o}$ ($\alpha = 2\pi/\lambda a$, where a=Cylinder Radius, m= Index of Refraction)

intensity as a function of roll angle and the roll angle becomes equivalent to ϕ. With this then, the dependence of scattering on cylinder length and roll angle is given by Lilienfeld (1987):

$$I_1(l,f) \propto l^2[\sin(\pi l\phi/\lambda)/(\pi l\phi/\lambda]^2$$

From this it can be seen that a maximum scattering intensity occurs at $\phi = 0$, and the scattering pattern becomes more concentrated in the plane perpendicular to the cylinder axis, as the fiber increases in length. This can be used to determine fiber length.

The pulse from a detector at $\theta = 90^o$, generated by a rotating fiber, is likened to a search-light beam by Lilienfeld (1977). That is, the signal detected is very sharply peaked at its maximum and nearly zero at all other angles. As can be seen in Figure 3.6 (Lilienfeld 1977), as the fiber length increases, the pulse height and pulse sharpness increase. Thus the fiber length can be measured by sensing the pulse width for a given roll angel ϕ which is what is done in the actual instrument.

Measuring fiber diameter with this instrument, however, is not practical. Given non-monotonic nature of the scattering function for infinite cylinders shown in Figure 3.5, the fiber diameter cannot be determined. It would be possible to determine fiber diameter by simultaneously detecting the scattered light at angles other than 90^o, but this instrument is not so equipped.

3.2.2 Description of the Instrument

A schematic of the optical and flow systems of the FAM are shown in Figure 3.7 (Lilienfeld 1979). In the system shown, a 2mW He-Ne laser with greater than 500:1 polarization is used. The two 45 degree adjustable mirrors are used to fold the beam by 180 degrees and to align the beam with the optical axis of the flow tube. The flow tube has a Brewster window where the laser beam enters and an aperture to reduce the amount of stray light. At the end of the flow tube is a light trap. The detector used in the instrument is a 9-stage side-on PMT. The PMT has a multialkali photocathode. The detector is equipped with a 0.8 mm slit, limiting the angular scattering dispersion so that the necessary angular selectivity needed to gather the pulse sharpness is

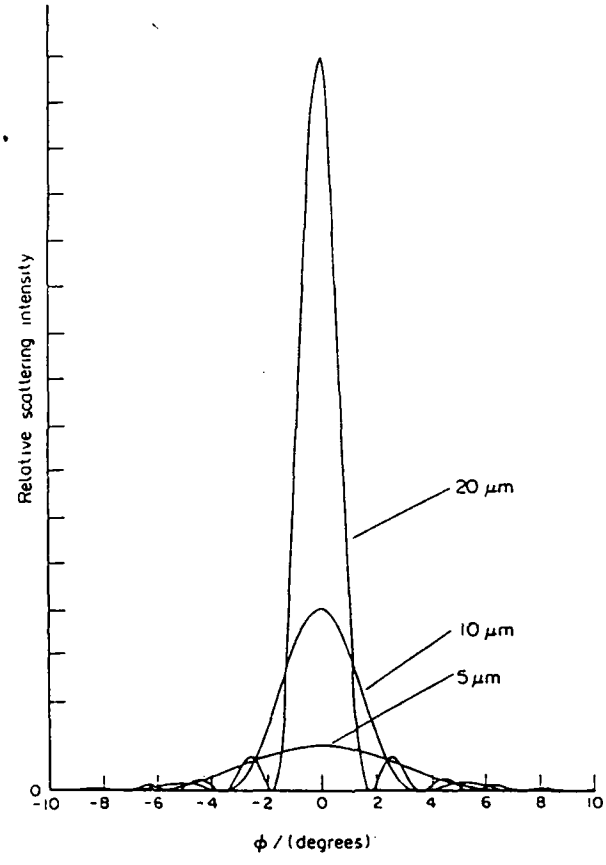

Figure 3.6 PMT Signal From Fiber

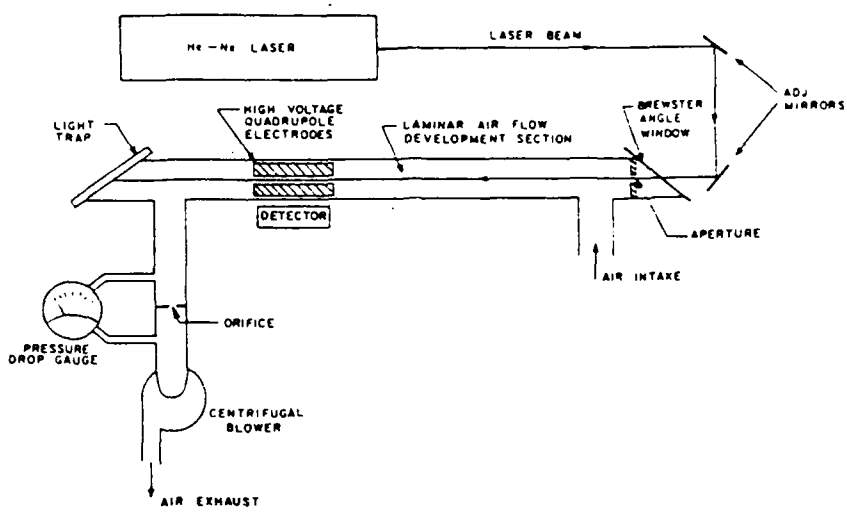

Figure 3.7 Diagram of the Fibrous Aerosol Monitor

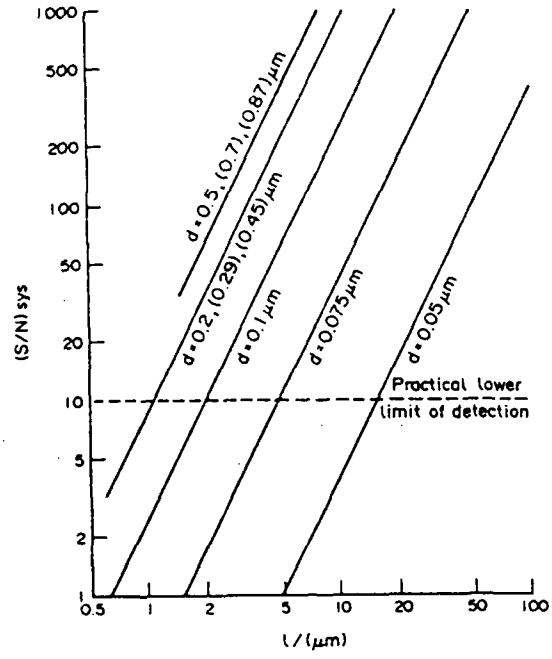

Figure 3.8 Signal to Noise Ratio vs Fiber Length and Diameter

preserved. The PMT views the sample volume through a gap in the high voltage quadrupole electrodes which are used to induce the fiber rotation.

One unique aspect of the FAM is its signal-to-noise ratio. Because the fibers rotate at a known frequency, the frequency of the light scattering pulses is known. Therefore, synchronous electronic detection is used to enhance the signal-to-noise ratio. This is shown by Lilienfeld (1987). The signal-to-noise ratio for the system is the signal-to-noise ratio of the photomultiplier tube multiplied by the square root of n where n is the number of pulses generated by the rotating fiber. Figure 3.8 (Lilienfeld 1987) shows the signal-to-noise ratios as a function of fiber length and diameter based on a refractive index of 1.56 which approximates the refractive index for typical asbestos fibers.

Lilienfeld suggests that the practical lower limit of the signal-to-noise ratio is 10. Therefore, for a 2 μm long fiber, the minimum detectable fiber diameter is around 0.1μm. For some of the lines representing given fiber diameters there are other diameters in parenthesis. This is a result of the fact that the scattered intensity function for an infinitely long cylinder is not monotonic for these diameters (See Figure 3.5).

3.3 POLARIZATION INDUCED FIBER DISCRIMINATION

According to Al-Chalabi *et al.* (1990), because the FAM described above uses scattered light collected at 90^{o}, irregular particles may be mistaken for fibers because the scattering is sensitive to shape. Also, the fibers must be oscillated in the flow. A technique which allows fibers to be detected and sized, which has minimal shape sensitivity, and which is not dependent on fiber orientation was proposed by Jones and Purewal (1982). The idea is to discriminate fibers on the basis of the polarization of their scattered light. The idea was expanded upon by Jones and Savaloni (1989,1990) and again by Al-Chalabi *et al.* (1990).

3.3.1 Fiber Light Scattering

Although a theory exists for the light scattering of an infinite cylinder at random orientation, the difficulty of matching the boundary conditions for the finite cylinder has prevented a solution. Using methods which approximate a finite cylinder, such as an ellipsoid, require extensive

computational efforts. With this in mind, Al-Chalabi *et al.* (1990) evaluated two approximate methods. The first modifies the infinite cylinder theory by multiplying it by Fraunhofer diffraction on the length. This describes the diffraction pattern correctly and works for long cylinders. However, it does not work well for short cylinders and does not describe the anisotropic nature of the light scattering. The other method evaluated was the Shifrin modification to the Rayleigh-Gans-Debye approximation. This method does describe the anisotropic scattering and qualitatively explains the results.

3.3.2 Instrument Description

The instrument theoretically works as follows. The incident beam onto the particles is circularly polarized. A spherical particle will scatter the incident light also with a circular polarization. The scattered light with the circular polarization will then pass through a quarter wave plate changing the polarization to linear. When the linearly polarized light is sent through a beam splitter, all of the light can be sent to one detector while another detector receives none. The polarization ratio would then be infinity. Elongated particles or fibers will scatter light with an elliptical polarization. The elliptically polarized light remains elliptically polarized as it passes through the quarter wave plate. As the scattered light goes through the beam splitter, some light will be sent to each detector making the ratio finite. In reality, however, the ratio of the detector's output is limited by the extinction ratio of the beam splitter. The instrument set-up is shown in Figure 3.9 (Al-Chalabi *et al.* 1990).

The expanded laser beam is imaged into the test space giving the beam a top-hat profile. This is done so the scattering is independent of the particle or fiber path through the beam. The first wave plate produces the circular polarization of the incident beam which makes the scattering independent of fiber rotation in the plane orthogonal to the beam.

The scattered light is collimated by a lens and sent through the next quarter wave plate. If the particle in the test chamber were spherical, the circularly-polarized, scattered light will become plane polarized. The light then passing though the beam splitter would lead to a detector ratio ideally equal to that of the beam splitter's extinction ratio. If the particle in the test chamber were a fiber, the scattered light would be elliptically polarized and after it passed through the second quarter wave plate it would not change. The

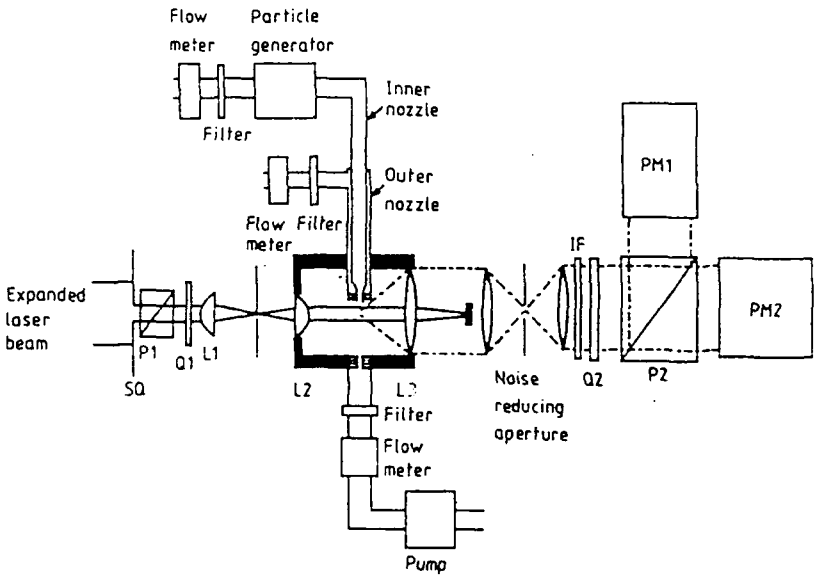

Figure 3.9 Polarization Induced Fiber Discriminator Set Up

signal ratio from the PMT's will then be smaller than what it was for the sphere.

The apparatus shown in Figure 3.9 was built and tested. For the beam splitter used, the extinction ratio should theoretically limit the photomultiplier response ratio to a maximum of 49. Testing revealed that the maximum ratio reached for the ballotini test spheres was 10. This was attributed to the ballotini not being perfect spheres and to "strains and aberrations in the optical components." The tests also showed that fibers and spheres can be sized down to a diameter of about 0.5 μm. Distinguishing fibers from spheres can only be accomplished at diameters down to 1 μm. Below this diameter the spread in polarization ratio due to noise, prevents discrimination (Al-Chalabi *et al.* 1990).

It is important to note that this instrument does not measure fiber length as of yet, nor is it commercially available. Al-Chalabi *et al.* (1990) included some suggested improvements to the instrument. These included using abberation-free optics.

3.4 TSI AERODYNAMIC PARTICLE SIZER

The TSI Aerodynamic Particle Sizer (APS) measures an aerosol's aerodynamic diameter size distribution. A particle's aerodynamic diameter is the equivalent diameter of a unit density sphere which has the same settling velocity as the particle. The aerodynamic diameter becomes an important quantity when respiratory deposition and the related health effects are under consideration. The instrument does this by accelerating an aerosol through a nozzle, then through two aligned laser beams. The aerosol is surrounded by a clean sheath air which forces the aerosol to go through the center of the laser beams where the illumination is uniform. The particles in the flow lag behind the flow velocity as it goes through the nozzle. When the particles flow through the two laser beams, scattered light in the near forward direction is focused onto a photomultiplier tube (PMT), generating two pulses. From these pulses, the time it takes a particle to travel from one beam to the other is found. With this information the particle aerodynamic diameter is found using a calibration curve set up for each APS. The instrument was designed for use with spherical particles or near spherical particles.

As noted by Griffiths *et al.* (1983), the APS can successfully measure fiber aerodynamic diameter. A Timbrell aerosol spectrometer was used together with an APS to check the accuracy of the APS in measuring the aerodynamic diameter of particles having the same settling velocity under gravity. A fiber's aerodynamic diameter depends on its orientation with respect to the flow however, and the fibers measured by Griffiths *et al.* (1983) were randomly oriented in the instrument. This random orientation caused some spread in the experimental data collected but the fiber aerodynamic diameter was measured with some accuracy. Nevertheless, the APS cannot measure fiber diameter or fiber length, nor can it differentiate fibers from other particles.

3.5 CONCLUSIONS

The literature review has shown three prototype instruments and one commercial instrument available for fiber sizing. The capabilities of the techniques are:

-Distinguishing fibers from spherical and irregular particles
-Measuring fiber length
-Measuring fiber diameter

Important fiber parameters that cannot be measured by the existing techniques are:

-Aerodynamic Diameter
-Simultaneous measurement of fiber diameter and length

The proposed RFA will be capable of distinguishing fibers from spherical and irregular particles, measuring fiber aerodynamic diameter, measuring fiber length, and measuring fiber diameter. It is proposed that the TSI APS can be modified to accomplish all of the tasks outlined above. Chapter 4 describes the theory and possible modifications.

CHAPTER 4
DEVELOPMENT OF THE REAL-TIME FIBER ANALYZER (RFA)

The last chapter finished with a brief look at the workings of the APS. This chapter will give a detailed discussion of the original thoughts behind converting the APS into an RFA before any detailed analysis had taken place. This will provide some insight into the direction of this study. It will be convenient to describe the normal APS operation in greater detail than what was presented in Chapter 3 prior to going over the ideas of how the RFA is to work.

4.1 NORMAL APS OPERATION

The TSI APS is made up of two main components, the sensor and what TSI calls the Data Analysis Center which consists of an IBM Personal Computer XT, a video monitor, and a dot matrix printer. The complete system is pictured in Figure 4.1(Kinney 1990).

Within the sensor are the accelerating orifice and the laser velocimeter. A schematic of the sensor is shown in Figure 4.2 (Kinney 1990). The accelerating orifice is actually made up of an outer and inner nozzle. With the outer nozzle being 1.0 mm in diameter, 80% of the flow into the APS inlet goes into the outer nozzle. The other 20% of the flow goes into the 0.8 mm diameter inner nozzle. The flow going into the outer nozzle is filtered, passed through a flowmeter, and then returned as sheath air to keep the particle laden flow from the inner nozzle in the central region of the jet where the flow velocity is uniform. With the total APS inlet flow being 5 liters per minute (LPM), 4 LPM is used as sheath air while the remaining 1 LPM continues through the inner nozzle to the viewing volume of the laser velocimeter. A pressure transducer is used to keep the sampling chamber at 125 cm of water below the ambient inlet pressure which translates into a constant orifice velocity of 150 m/s. The pressure transducer controls the vacuum pump which keeps the vacuum constant.

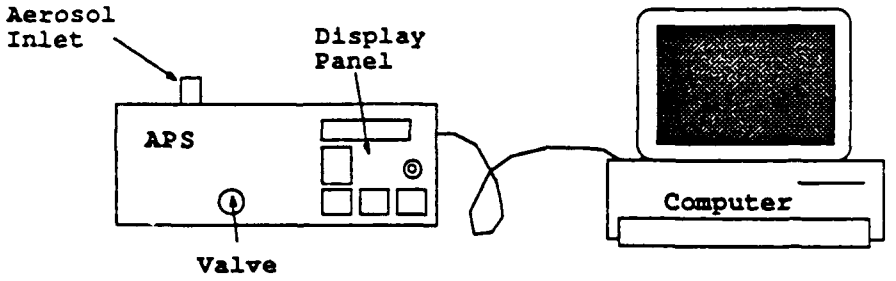

Figure 4.1 Complete APS System

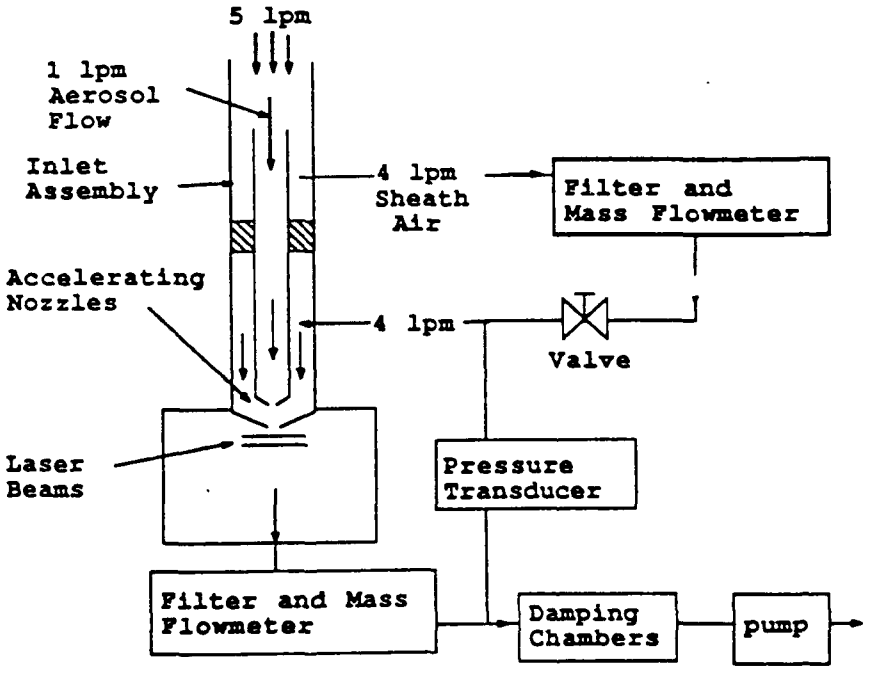

Figure 4.2 APS Sensor

The laser used in the laser velocimeter is a 2 mW, polarized He-Ne laser. The beam passes through a beam expander and is focussed by a positive lens. It continues through a calcite plate which splits the beam by polarization. A cylindrical lens forms the two rectangular spots in the viewing volume. The scattered light from the particles is collected in the near-forward direction while the main beams are blocked.

As a particle passes through the two beams, two pulses are generated as the photomultiplier tube (PMT) converts the scattered light into a voltage. These pulses are converted to digital pulses. The time interval between the pulses is measured by a high speed digital clock with a 2-nanosecond resolution. This information is stored and is then used for calculating particle aerodynamic diameter. The data processing takes place in the personal computer and the results can be presented in a variety of formats.

4.2 PRINCIPLE OF THE REAL-TIME FIBER ANALYZER (RFA)

The basic, original idea behind the operation of the RFA is using the pulse pairs generated by the light scattered from the fiber, much in the same manner as the APS operates. Before any of the analysis in the upcoming chapters was completed, it was thought that fibers could be distinguished from spherical particles by the width of their pulses. The RFA would first use the measured time of flight between the two beams to determine the fiber's acrodynamic diameter. The time of flight can also be used to find the fiber's velocity because the distance between the two beams is known. The velocity can then be used in conjunction with the pulse width to find the fiber's length. If the alignment of the fiber is fixed as it passes through the viewing volume then the aerodynamic diameter and the length can be used to calculate the fiber diameter using Equations (8) and (9) for a given density. Another possibility is that the pulse height generated by the scattered light could be directly related to fiber diameter. This process will be outlined in greater detail in section 4.2.1.

Several considerations need to be made in the development of this modified instrument. First, the fibers need to be consistently aligned with the flow prior to intersection with the laser beams to provide accurate light scattering measurements. Also if fiber alignment is not known, then neither the fiber length or diameter could be found. Second, the instrument should

have an adequate sampling efficiency for the fibers of different diameters and aspect ratios. Third, a determination must be made as to the accuracy of the correlation between the light scattering pulses and the fiber diameter.

These considerations lead to the possible modifications that need to be made to the APS for conversion to an RFA. Modifications to the inlet and inner nozzle may need to be made to insure fiber alignment and sampling efficiency are adequate without loss of resolution. The fiber alignment can be accomplished using a shear gradient, electrostatic alignment, or a combination of both. Undoubtedly, modifications will have to be made to the inlet for sampling efficiency but are not considered in this work. The APS processing circuit will require modifications to accommodate the new method of measurement. Finally, fiber light scattering needs to be studied for calibration purposes and extensive experimental work needs to be completed for final APS calibration and coincidence error evaluation.

4.2.1 Measurement Method and Calculation

Once accurate pulses are obtained for a fiber of known orientation, the information from the pulses can then be processed to obtain the aerodynamic diameter, length, and diameter. A representation of an expected fiber pulse pair is shown in Figure 4.3.

The shape of a pulse created by a spherical particle is that of an upside down "V". That is, it has a sharp peak at the top. As a fiber passes through each beam it was thought that the peak pulse height would be maintained at a constant level for the time that the fiber was fully illuminated by the beam. This would give it a flat top or square shape thus distinguishing it from a spherical particle. The height of the pulse (h) may lead directly to a fiber diameter. Otherwise, the time of flight (t), or transit time, leads to the fiber aerodynamic diameter through the APS calibration curve. It also gives the fiber velocity. The width of the pulse (l) can then be used to calculate the length of the fiber. As mentioned before, the aerodynamic diameter and fiber length can then be used to calculate fiber diameter for a given fiber density.

As will be seen in the next chapters, these expectations were only partially realised. However, another means of distinguishing fibers from spherical particles was discovered involving the fact that the APS laser beam is split into two beams by polarization.

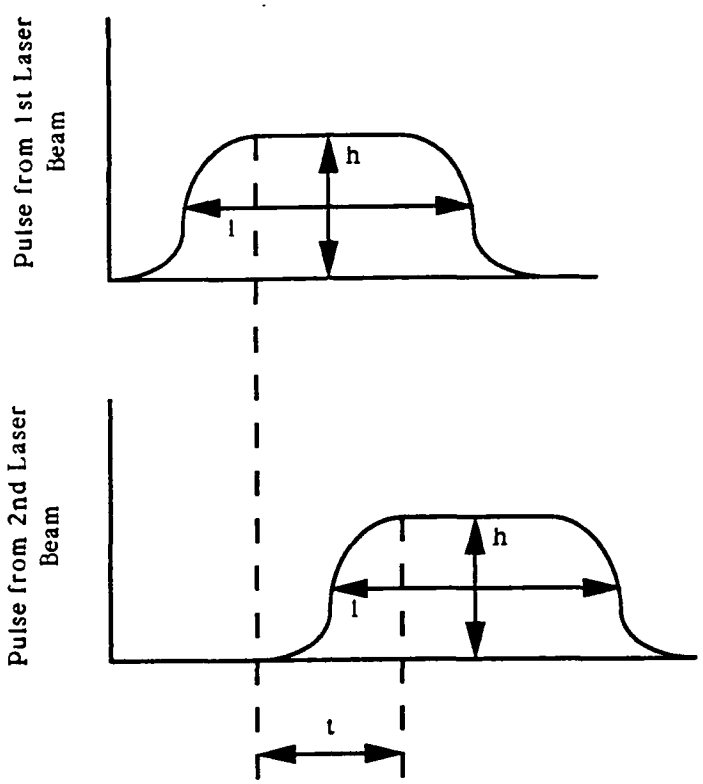

Figure 4.3 Expected Fiber Pulse Pair from Scattered Light Detected by the $\bar{I}$ - $\bar{II}$

It is evident from the expected fiber pulse pair that if a fiber is not aligned perpendicular to the laser beams then the pulse width (l) will not be a good measure of fiber length. Therefore, fiber alignment using the shear flow in the APS nozzle will be investigated.

4.2.2 Nozzles

Because it would require less modification, fiber orientation using the shear flow in the APS nozzle was studied first. If not successful, fiber orientation using the electrostatic methods discussed in Chapter 2 could be explored. The APS inner inlet has a 60^{o} nozzle which is shown in Figure 4.4 (Kinney 1990). In converting the APS to an RFA the two main concerns with nozzle design are fiber orientation and fiber penetration. The shear flow created at the nozzle will cause all fibers to become somewhat oriented parallel with the flow. The parallel orientation is required for accurate fiber measurements. Also fiber penetration through the nozzle should be as close to 100% as possible to insure a representative sample of aerosol is extracted from the sampling volume. Three inlets were investigated in this work, an abrupt 90^{o} contraction, the 60^{o} standard APS inlet, and a 2^{o} inlet, shown in Figure 4.5, developed by Kinney (1990). This evaluation is outlined in Chapter 5. The emphasis in this comparison is place on fiber orientation.

4.2.3 Optics

It was originally thought that the optical system of the APS itself would not require modification for the APS to function as a Real-time Fiber Analyzer. Two main points needed investigation. Will the pulse shapes from a fiber be wider, or more square than for spherical particles and would it be possible for fiber diameter to be determined directly from pulse height. This evaluation is also outlined in Chapter 5.

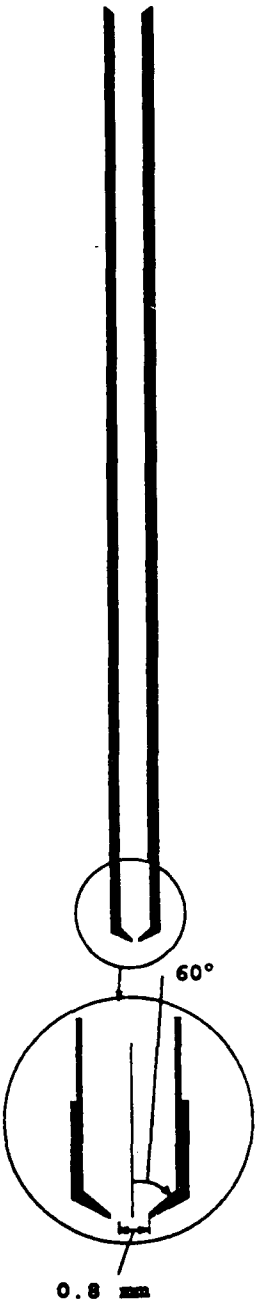

Figure 4.4 Standard 60^{o} Nozzle

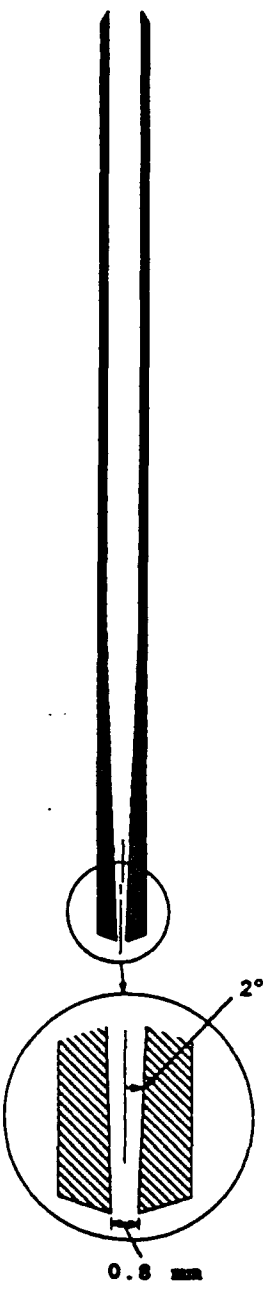

Figure 4.5 Modified 2^{o} APS Nozzle

CHAPTER 5

RFA NUMERICAL EVALUATION AND RESULTS

Two aspects of the proposed RFA were evaluated numerically. The first is the fiber orientation as it passes through the APS nozzle. The second is the light scattering response of the APS to a fiber. The fiber orientation was modeled for the three nozzles mentioned previously using simulated 2 μm diameter silicon carbide (SiC) fibers with an aspect ratio of 10. This fiber material and size was chosen for the model because it was readily available for experimental use. Further, it is more difficult to align and detect these fibers compared to the 8 μm diameter carbon graphite fibers which were also available for this study. Analysis was carried out and a nozzle selection was made based on fiber orientation and also instrument resolution. After the best nozzle was chosen, fibers of other sizes were modeled as well for that nozzle.

The light scattering models were based on programs from Bohren and Huffman (1983). One program for light scattered from infinite cylinders and one program for light scattered from homogeneous spheres. The spherical program was used to calculate the light scattering response of PSL spheres for comparison to the calculated light scattering response of SiC fibers determined from the infinite cylinder program.

5.1 FIBER ALIGNMENT

5.1.1 Numerical Methods

For the RFA to work as described, it is crucial that the fibers be aligned parallel with the flow direction (perpendicular to the incident laser beam). Therefore the rotational angle of a fiber as it flows through a nozzle was modeled by modifying a program developed by Ye and Pui (1990). A brief description of the model as found in Ye and Pui (1990) follows.

In studying the orientation of a fiber as it passes through a nozzle, it is assumed that the fiber experiences deterministic motion. In other words, the effect of molecular Brownian motion on the fiber is considered negligible with respect to the effects of aerodynamic drag force. Again, the fiber is simulated using a prolate ellipsoid model.

The translational and rotational equations for the fiber would be the same as for a spherical particle:

$$m d\mathbf{U}/dt = \mathbf{F}_f + \Sigma \mathbf{F}_{e,i} \tag{19}$$

$$d(\mathbf{I}_c \omega)/dt = \mathbf{M}_{c,f} + \Sigma \mathbf{M}_{c,e,i} \tag{20}$$

where $\mathbf{F}_f$ and $\mathbf{F}_{e,i}$ are respectively the aerodynamic force and the external force acting on the fiber. $\mathbf{M}_{c,f}$ and $\mathbf{M}_{c,e,i}$ are respectively the aerodynamic torque and the external torque acting on the fiber with respect to the center of mass. $\mathbf{I}_c$ is the moment of inertia of the fiber with respect to the center of mass. Because the fibers are symmetrical, the effect of simultaneous translation and rotation can be ignored and the aerodynamic force and torque can be given by:

$$\mathbf{F}_f = -\mu(\mathbf{K} \bullet \mathbf{U}) \tag{21}$$

$$\mathbf{M}_{c,f} = -\mu(\boldsymbol{\Omega} \bullet \boldsymbol{\omega}) \tag{22}$$

where $\mathbf{K}$ is the translation tensor, $\boldsymbol{\Omega}$ is the rotation tensor, $\mathbf{U}$ is the velocity vector, $\boldsymbol{\omega}$ is the angular velocity vector, and μ is the viscosity. The aerodynamic force and torque can be found by solving the Stokes equation. Quasi-steady motion can be assumed if the translational Reynolds number ($Re^{(t)} = D_p U/\nu$) and the rotational Reynolds number ($Re^{(r)} = \omega^2 D_p/n$) are small and the following Stokes equations are then valid:

$$-\nabla p + \mu \nabla^2 \mathbf{U} = 0 \tag{23}$$

$$\nabla \bullet \mathbf{U} = 0 \tag{24}$$

As previously stated, the prolate ellipsoid of revolution is used as a fiber model. In a coordinate system fixed to the particle body the surface of the ellipsoid can be given by:

$$x'^2/a^2 + y'^2/b^2 + z'^2/c^2 = 1 \tag{25}$$

where b is the polar semi-axis and a is the equatorial semi-axis (see Figure 2.1). With the aspect ratio $\beta = b/a$, let the eccentricity $e = (1-1/\beta^2)^{1/2}$. The aerodynamic force and torque on the ellipsoid are then given by:

$$F_{x'} = 6\pi\mu a\{8/3e^3[-2e + (1 + e^2)\ln\{(1+e)/(1-e)\}]^{-1}U_{x'}\}$$

$$F_{y'} = 6\pi\mu a\{16/3e^3[2e + (3e^2-1)\ln\{(1+e)/(1-e)\}]^{-1}U_{y'}\}$$

$$F_{z'} = 6\pi\mu a\{16/3e^3[2e + (3e^2-1)\ln\{(1+e)/(1-e)\}]^{-1}U_{z'}\} \qquad (26)$$

and

$$M_{x'} = 16\pi\mu/3\{[1/(b^2\beta_o + c^2\gamma_o)]\ [(b^2 - c^2)\varepsilon_{y'z'} + (b^2 + c^2)(\Omega_{y'z'} - \omega)]\}$$

$$M_{y'} = 16\pi\mu/3\{[1/(b^2\gamma_o + a^2\alpha_o)]\ [(c^2 - a^2)\varepsilon_{z'x'} + (c^2 + a^2)(\Omega_{z'x'} - \omega)]\}$$

$$M_{z'} = 16\pi\mu/3\{[1/(a^2\alpha_o + b^2\beta_o)]\ [(a^2 - b^2)\varepsilon_{x'y'} + (a^2 + b^2)(\Omega_{x'y'} - \omega)]\} \qquad (27)$$

where: $\varepsilon_{z'x'} = 1/2(du'/dz' + dw'/dx')$; $\varepsilon_{y'z'} = 1/2(dw'/dy' + dv'/dz')$;
$\varepsilon_{x'y'} = 1/2(dw'/dx' + du'/dx')$

$\Omega_{z'x'} = 1/2(du'/dz' - dw'/dx')$; $\Omega_{y'z'} = 1/2(dw'/dy' - dv'/dz')$;
$\Omega_{x'y'} = 1/2(dw'/dx' - du'/dx')$

$\alpha_o = \int_0^\infty d\lambda/(a^2+\lambda)\Delta$; $\beta_o = \int_0^\infty d\lambda/(b^2+\lambda)\Delta$; $\gamma_o = \int_0^\infty d\lambda/(c^2+\lambda)\Delta$

$\Delta = [(a^2 + \lambda)(b^2 + \lambda)(c^2 + \lambda)]^{1/2}$

Let x', y', and z' denote a coordinate system that is attached to the particle body. Let x, y, and z denote a coordinate system that is fixed to the tube with the x-axis aligned with the tube centerline. The x', y', z' system then will translate and rotate with the particle at all times. The two coordinate systems are related to one another through the use of the Euler angles, ϕ, θ, and Ψ as shown in Figure 5.1.

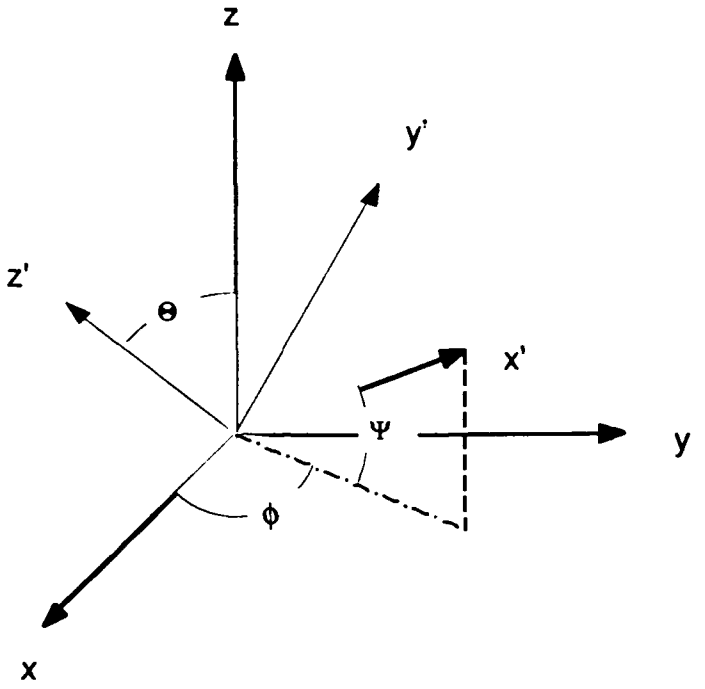

Figure 5.1 The Two Coordinate Systems and Euler's Angles

Looking back at Equation (20), the mass moment and product of inertia terms have a time derivative in the x,y,z coordinate system. This is not convenient for calculations. By transforming the equations into the x',y',z' coordinate systems the time derivative disappears and the result is:

$$I_{x'}\omega_{x'} + \omega_{y'}\,\omega_{z'}(I_{z'} - I_{y'}) = M_{c,f,x'} + \Sigma_i M_{c,e,i,x'}$$

$$I_{y'}\omega_{y'} + \omega_{x'}\,\omega_{y'}(I_{x'} - I_{y'}) = M_{c,f,y'} + \Sigma_i M_{c,e,i,y'}$$

$$I_{z'}\omega_{z'} + \omega_{x'}\,\omega_{y'}(I_{y'} - I_{x'}) = M_{c,f,z'} + \Sigma_i M_{c,e,i,z'} \qquad (28)$$

These equations are called Euler's equations for body-fixed principle axes

(Torby).

The derivatives of Euler's angles will have the following relationship with the angular velocity ω for the coordinate system having a fixed direction in space:

$$\omega = \psi' + \phi' + \theta' \tag{29}$$

or

$$\begin{bmatrix} \omega_x \\ \omega_y \\ \omega_z \end{bmatrix} = \begin{bmatrix} \cos\theta & 0 & \cos\theta\cos\phi \\ \sin\theta & 0 & -\sin\theta\cos\phi \\ 0 & 1 & \cos\theta \end{bmatrix} \begin{bmatrix} \phi' \\ \theta' \\ \psi' \end{bmatrix} \tag{30}$$

or

$$\begin{bmatrix} \omega_{x'} \\ \omega_{y'} \\ \omega_{z'} \end{bmatrix} = \begin{bmatrix} \sin\theta\sin\psi & \cos\psi & 0 \\ \sin\theta\sin\psi & -\sin\psi & 0 \\ \cos\theta & 0 & 1 \end{bmatrix} \begin{bmatrix} \phi' \\ \theta' \\ \psi' \end{bmatrix} \tag{31}$$

The above equations are valid given that the relative velocity of the gas at the surface of the particle is zero. Because the size of the particles dealt with approach the mean free path of the gas medium, the assumption is not valid and a slip correction factor must be taken into account. The slip correction factor is defined as the ratio of aerodynamic force in the continuum regime to the aerodynamic force of interest. The slip correction factor for non-spherical particles obviously is dependent on the particle orientation. For this numerical calculation, a method of approximating the slip correction developed by Dahneke (1973) was used. It is called the Adjusted Sphere Approximation. The slip correction is found using the following expression for a sphere:

$$C = 1 + Kn_a \{1.234 + 0.876\exp(-0.414/Kn_a)\} \tag{32}$$

where Kn_a is the adjusted Knudson number. This adjusted Knudson number or

also called the adjusted sphere radius is calculated by using the slip correction factor in the free molecule regime and assuming the adjusted sphere radius has the same value over the entire range of Kn_a. The slip correction factors were found for particles oriented with their polar axes parallel and perpendicular to the flow direction. Slip correction was only taken into consideration for the acrodynamic drag force and not the aerodynamic torque for this study.

Another restriction on Equations (26) and (27) is the requirement that the particle be Stokesian. If the fluid is incompressible in the presence of a conservative body force field, the Navier-Stokes and continuity equations become:

$$\rho(dU/dt + U \bullet \nabla U) = -\nabla p + \mu \nabla^2 U$$

$$\nabla \bullet U = 0 \qquad (33)$$

For a particle simultaneously translating with velocity U_o and rotating with angular velocity ω, the previous equations can be written in nondimensional form:

$$Re^{(r)} dU^*/dt + Re^{(t)} U^* \bullet \nabla U^* = -\nabla^* p^* + \nabla^{*2} U^*$$

$$\nabla^* \bullet U = 0 \qquad (34)$$

where $t^* = \omega t$ $\qquad r^* = r/\lambda$ $\qquad U^* = U/U_o$

$p^* = (P - P_\infty)\lambda/\mu u_o$ $\qquad \nabla^* = \lambda \nabla$

$Re^{(t)} = \lambda u_o \rho/\mu$ $\qquad Re^{(r)} = \lambda^2 \omega \rho/\mu$

λ is the characteristic particle dimension

In classifying nonspherical particles as Stokesian or Non-stokesian, both the translational and rotational Reynolds numbers should be considered. Because both numbers would be large in this case, a correction for Non-stokesian

particles must be taken into account.

For a small rotational Reynolds number and a large translational Reynolds number, a method given by Fuchs (1964) can be used to find the aerodynamic forces on the particle. The equations are as follows:

$$F_{x'} = -C_D Re_{pe}/24\ (6\pi\mu r_e)\{8/3e^3[-2e + (1 + e^2)\ln\{(1+e)/(1-e)\}^{-1}U_{x'}a/r_e\}$$

$$F_{y'} = -C_D Re_{pe}/24\ (6\pi\mu r_e)\{16/3e^3[2e + (3e^2 - 1)\ln\{(1+e)/(1-e)\}^{-1}U_{y'}a/r_e\}$$

$$F_{z'} = -C_D Re_{pe}/24\ (6\pi\mu r_e)\{16/3e^3[2e + (3e^2 - 1)\ln\{(1+e)/(1-e)\}^{-1}U_{z'}a/r_e\} \quad (35)$$

where r_e is the radius of a sphere having the same volume, Re_{pe} is the Reynolds number based on the equivalent radius r_e, and C_D is the drag coefficient given as:

$$C_D = 24/Re_{pe} \qquad Re_{pe} < 0.1$$

$$C_D = 24/Re_{pe}\ (1 + 0.0916Re_{pe}) \qquad 0.1 \le Re_{pe} \le 5$$

$$C_D = 24/Re_{pe}\ (1 + 0.158Re_{pe}^{2/3}) \qquad Re_{pe} > 5 \quad (36)$$

Only the aerodynamic drag force has been corrected here, the aerodynamic torque was not corrected. Also, the rotational Reynolds number would not actually be negligible for these calculations.

The program written uses the Simpler Program (Patankar 1979) to calculate the flow field for the tube with the abrupt contraction or the APS nozzles. The data from Simpler is then used with Ye and Pui's program (Ye and Pui 1990) to find particle trajectory and orientation. In calculating the flow field one problem was encountered. The APS nozzle exit opens into a larger volume and when the nozzle was modeled this way the program would not converge. The nozzles were then modeled by extending a tube from the nozzle exit of the same diameter as the nozzle exit. The flow field of interest is in the nozzle itself and only for a few hundred micron downstream of the nozzle exit. Because of this, the effect of extending the nozzle exit is not thought to be

great. The flow field results for the standard nozzle are in good agreement with those found by Kinney (1990).

5.1.2 Numerical Results

The fiber alignment program was run for three different cases, a 60^{o} standard APS nozzle, a modified 2^{o} nozzle, and a 90^{o} abrupt contraction. The focus was on the behavior of 2 μm diameter SiC fibers and 8 μm diameter Carbon Graphite fibers but the behavior of fibers of other diameter was also investigated.

The program was run for the three different nozzle configurations using a 2 μm fiber with an aspect ratio of 10 and a density of 1.8 g/cc. The Reynolds number of the flow in the nozzle was about 1000. The flow fields for the three nozzles were calculated using the Simpler program (Patankar 1979) and were in good agreement with the results found in Kinney (1990). Particle trajectory and orientation were monitored for the various nozzles. One nozzle was selected as the best candidate and further study was accomplished for fibers of various sizes and aspect ratios.

60^{o} Standard APS Nozzle

The program was first used to determine particle orientation and trajectory as it passed through the standard 60^{o} APS nozzle. For the program the fibers were released at a point upstream from the nozzle and were released at different y distances from the center line of the nozzle. The resulting trajectories are shown in Figure 5.2.

The fibers were given a diameter of 2 μm and an aspect ratio of 10. This was done because it fairly represents the silicon carbide fibers that were available for use in the experimental evaluation of the instrument.

For the standard nozzle there is not a problem with fiber impaction on the nozzle. The trajectories of fibers of 2 μm diameter with aspect ratios up to 30 were checked and there is not a significant change in their trajectories. This is due to the fact that the aerodynamic diameter of the fibers is a weak function of fiber length when the fiber is oriented parallel to the flow. Notice that the fiber trajectories appear to bounce off of the nozzle centerline after the nozzle. Nothing in the flow field suggests that this should happen and it is thought to be a problem in the program that could not be found. Again, the main concern is for the fiber orientation shortly after the nozzle exit and so

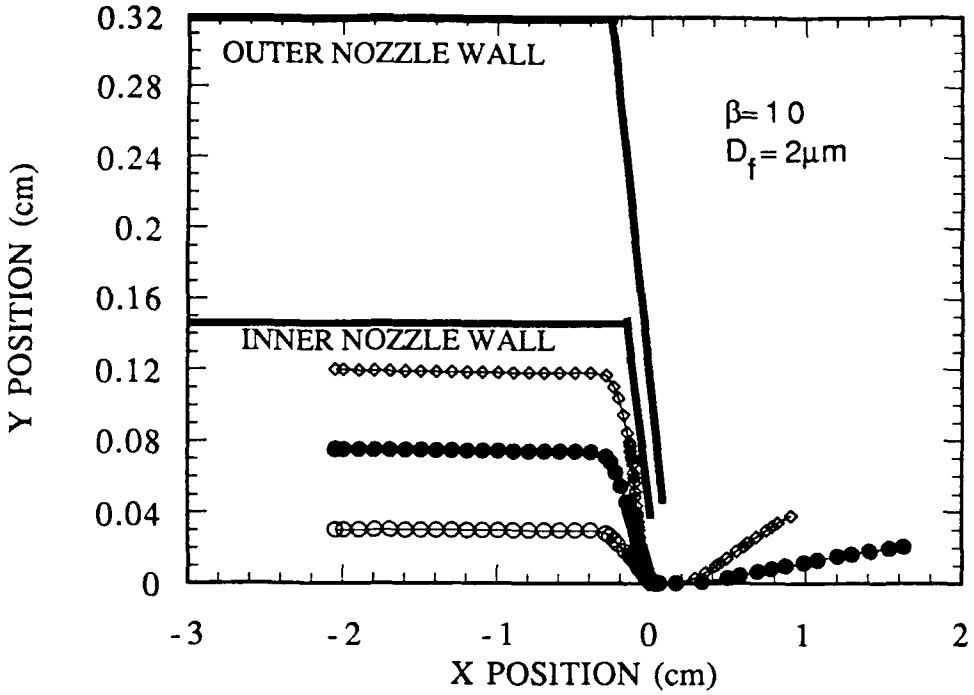

Figure 5.2 Fiber Trajectory in a Standard APS Nozzle (Nozzle Exit at x=0)

this bounce does not affect the orientation of the fibers in the area of interest.

The orientation of these same fibers, with the same starting points, was also calculated. In this analysis, 180° or multiples of 180° are defined as parallel with the flow. The fibers were released with various initial angles for each starting point shown in Figure 5.2. This was done to simulate the random orientation and position the fibers may have as they enter the inlet.

Figure 5.3a shows the orientation of four fibers each released with a different initial angle but all released at the same initial Y position of Y_{init}=0.03 cm, close to the nozzle centerline, and about 2 cm upstream of the nozzle exit.

As the fibers converge on the nozzle they also all become aligned with the flow. As they enter the nozzle itself, their orientation becomes almost the same regardless of initial orientation. They all go through a slight change in orientation once inside the nozzle but exit the nozzle parallel with the flow.

Because the main concern is that the fibers be aligned with the flow as they pass through the instrument's laser beams, Figure 5.3b takes a closer look at the nozzle region as outlined by the box in Figure 5.3a.

For the APS, the first laser beam is located about 200 μm downstream from the nozzle exit. The second laser beam is about 160 μm downstream from the first beam. These beams are outlined in Figure 5.3b. It is apparent that all the fibers are very closely parallel with the flow in the region of the laser beams. The fibers even maintain that orientation well beyond that region.

Figures 5.4a and b through 5.5a and b follow the same format as Figures 5.3a and 5.3b only Figures 5.4a and b are for those fibers released at Y_{init}=0.075 cm and Figures 5.5a and b are for those fibers released at Y_{init}=0.12 cm. Each is successively closer to the nozzle wall.

In Figure 5.4a, the fiber that is released parallel to the flow goes through a half revolution but still passes through the laser beam nearly parallel with the flow as seen in Figure 5.4b. It is thought that the reason for the half rotation may be the fiber end getting caught in the nozzle boundary layer, causing the quick turn. The other fibers shown in these two figures behave similarly to the fibers that were released closer to the centerline. The orientation of the fibers in Figures 5.4a and b however change more while approaching the nozzle than do the fibers in Figures 5.3a and b. Still it appears that all of the fibers pass the laser beams reasonably parallel.

In Figures 5.5a and b, for the fibers released near the wall of the inner

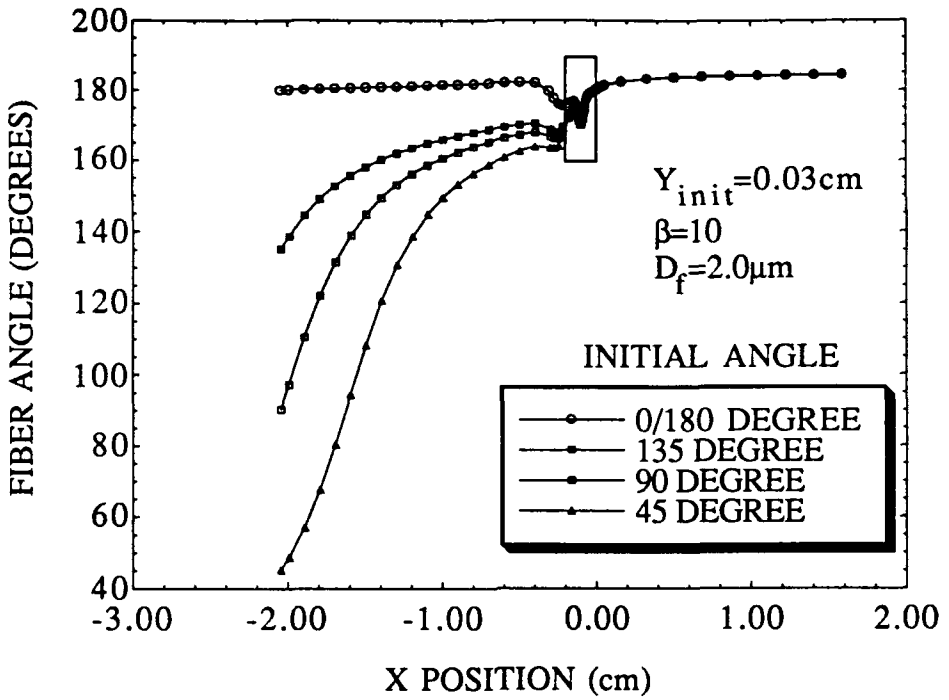

Figure 5.3a Fiber Orientation Through a Standard APS Nozzle for Yinit=0.03 cm (Nozzle Exit at x=0)

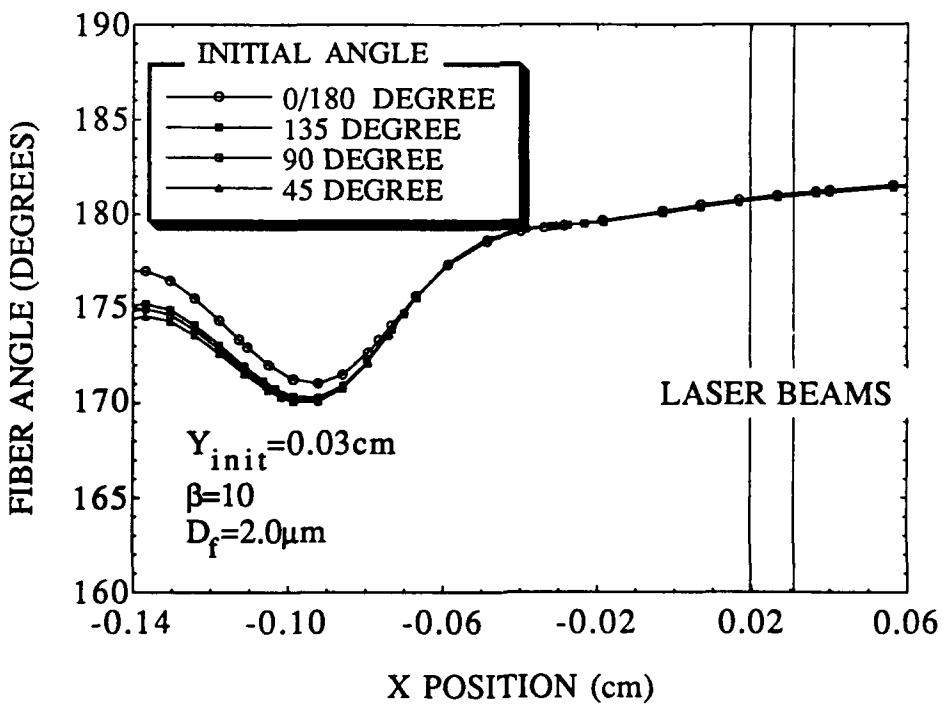

Figure 5.3b Enlarged View of Nozzle Region from Figure 5.3a

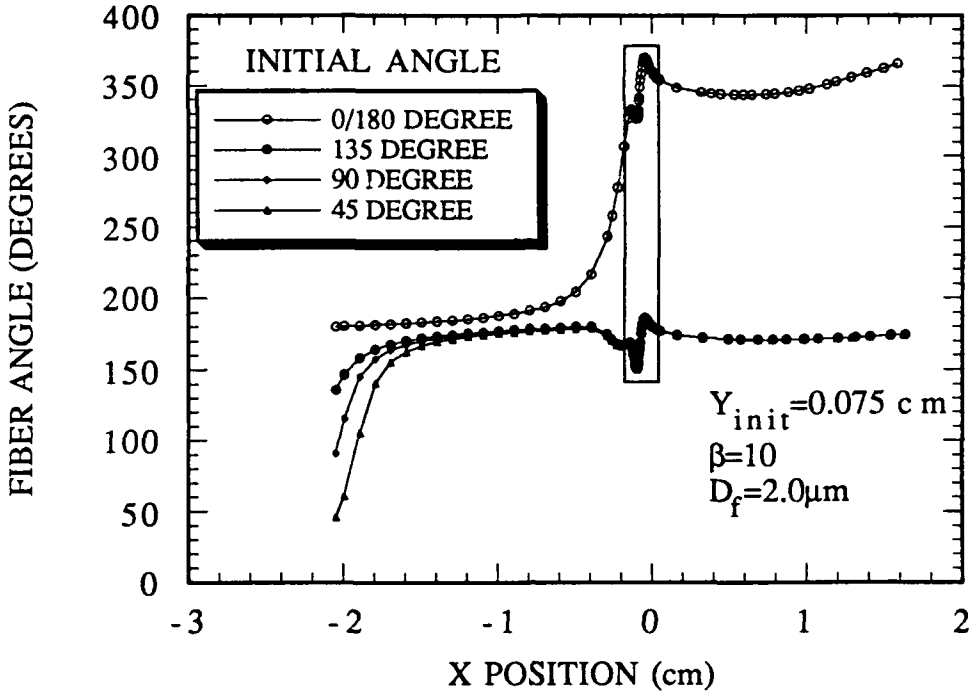

Figure 5.4a Fiber Orientation Through a Standard APS Nozzle for Y_{init}=0.075 cm (Nozzle Exit at x=0)

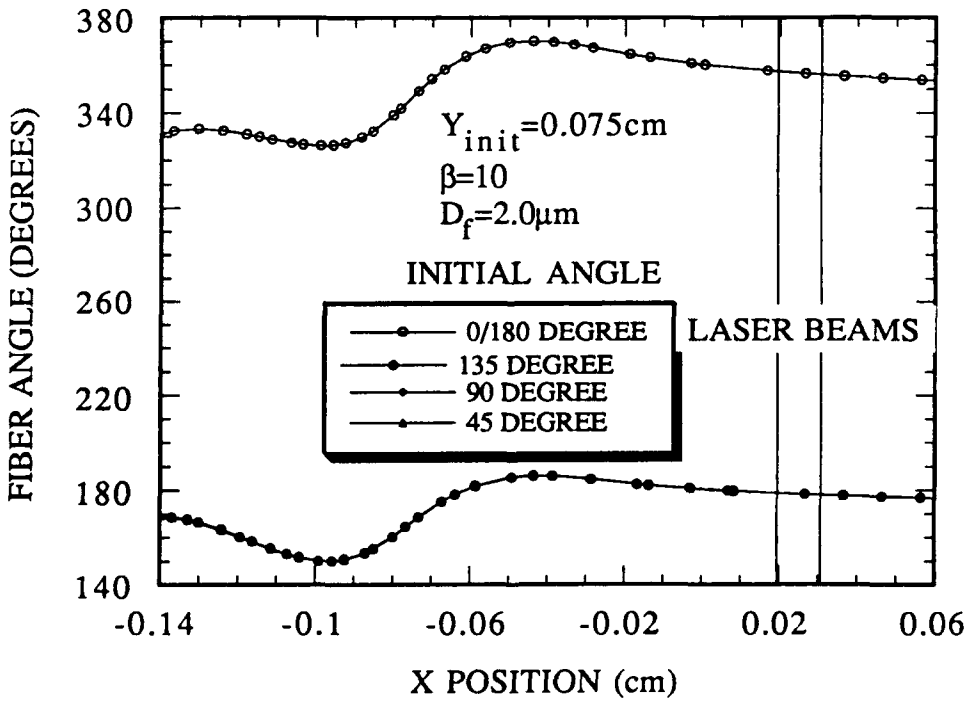

Figure 5.4b Enlarged View of Nozzle Region from Figure 5.4a

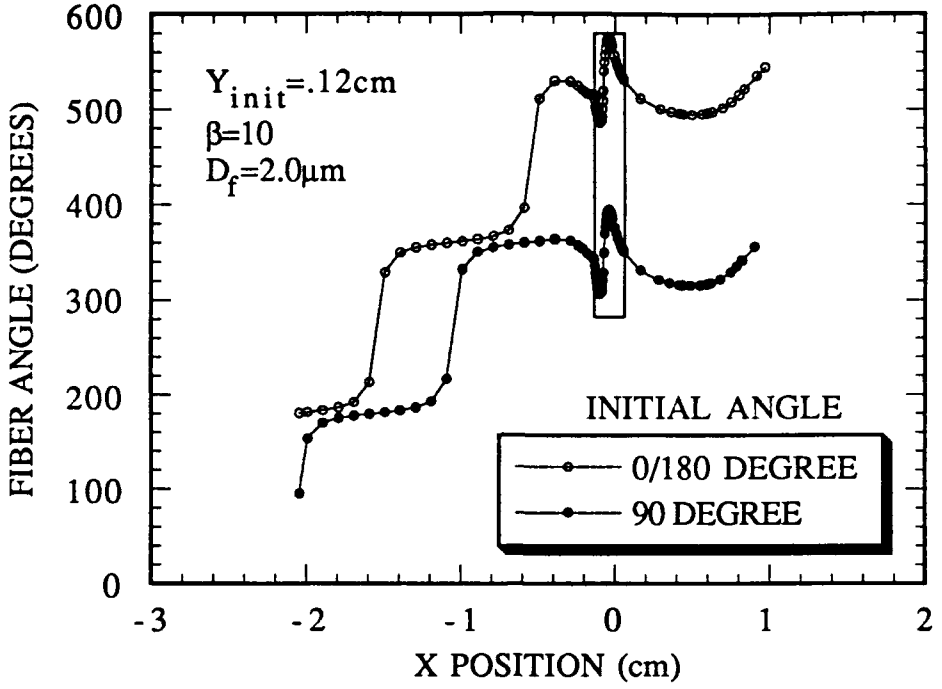

Figure 5.5a Fiber Orientation Through a Standard APS Nozzle for Yinit=0.12 cm (Nozzle Exit at x=0)

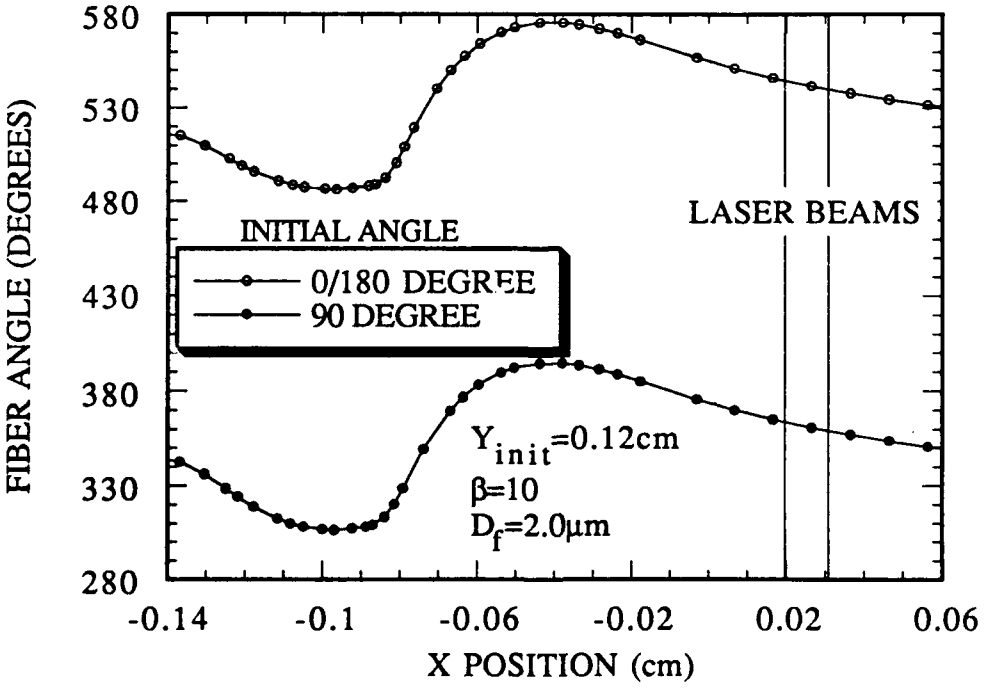

Figure 5.5b Enlarged View of Nozzle Region from Figure 5.5a

inlet, the fiber orientation change is even more dramatic. The fibers go through one or two half rotations as they flow through the tube and then as they approach the nozzle entrance the change in orientation is very pronounced. After passing through the nozzle they reach the laser beams and are still slightly rotating as they pass through them, but yet are still nearly parallel with the flow.

In considering Figures 5.5a and b, however, one thing should be taken into account; how likely is it that fibers will be present in the region close to the inner tube wall? The inner tube inlet is designed in such a way as to focus the particles near the center of the inner tube and nozzle. This was done to help keep the particles in the center of the flow so that they flowed through the center of the laser beams. This can be seen in Figure 5.6 (Kinney 1990).

With this particle focusing to the center of the inner tube, the likelihood of a fiber travelling near the inner tube wall is not as great as for one travelling near the centerline. Therefore we shall not be overly concerned with the fibers located near the wall. That is the reason only two initial angles were modeled for the starting Y position of Y_{init}=0.12 cm.

Modified 2^o Nozzle

A modified 2^o APS nozzle as designed by Kinney (1990), was also modeled for particle trajectory and orientation. The graphical format for the 2^o nozzle is the same as that for the standard 60^o nozzle. First, the fiber trajectories for the various initial starting positions is shown in Figure 5.7.

It is obvious that fiber losses due to impaction will be even a smaller problem for this nozzle design than for the standard nozzle design.

In looking at the orientation of the fibers as they pass through the modified nozzle, the fiber behavior is very similar to that of the standard nozzle. Figure 5.8a shows the fiber orientation for fibers released at the initial Y position of Y_{init}=0.03 cm with Figure 5.8b being the corresponding enlargement of the nozzle region.

The same change in fiber angle occurs as the fiber approaches the nozzle. This change is not as pronounced in the modified nozzle as it is in the standard nozzle. For the modified nozzle, the fibers still become very close to parallel with the flow as they exit the nozzle and pass through the laser beams. However, as the fibers pass through the laser beams from the modified nozzle they are a couple of degrees more from parallel than the fibers exiting the

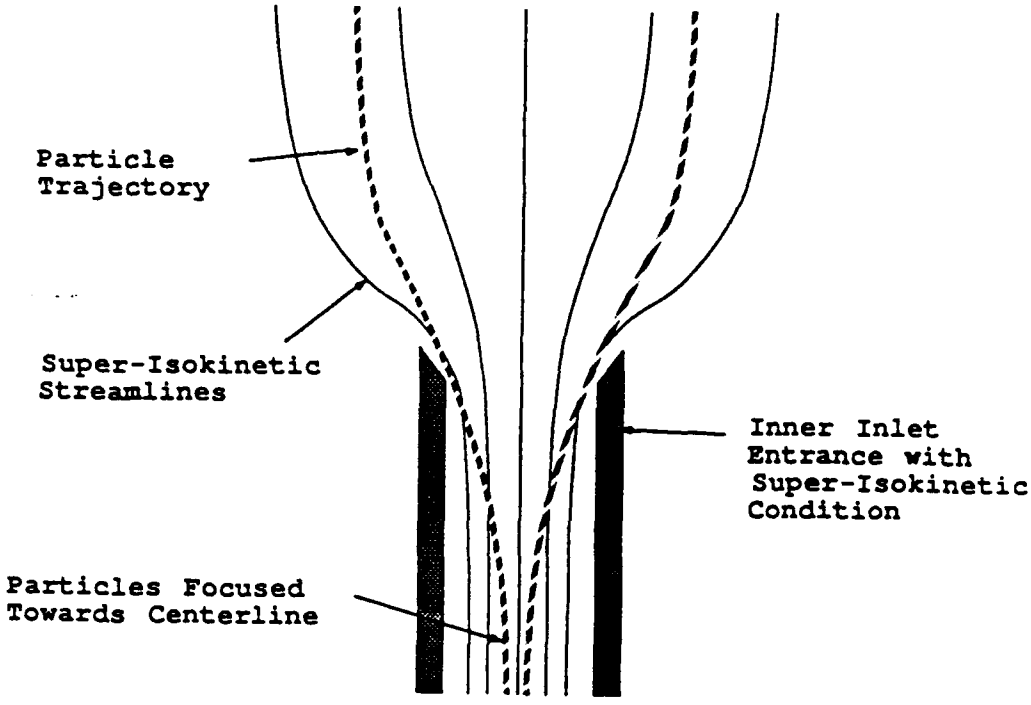

Figure 5.6 Inner Inlet Particle Focusing

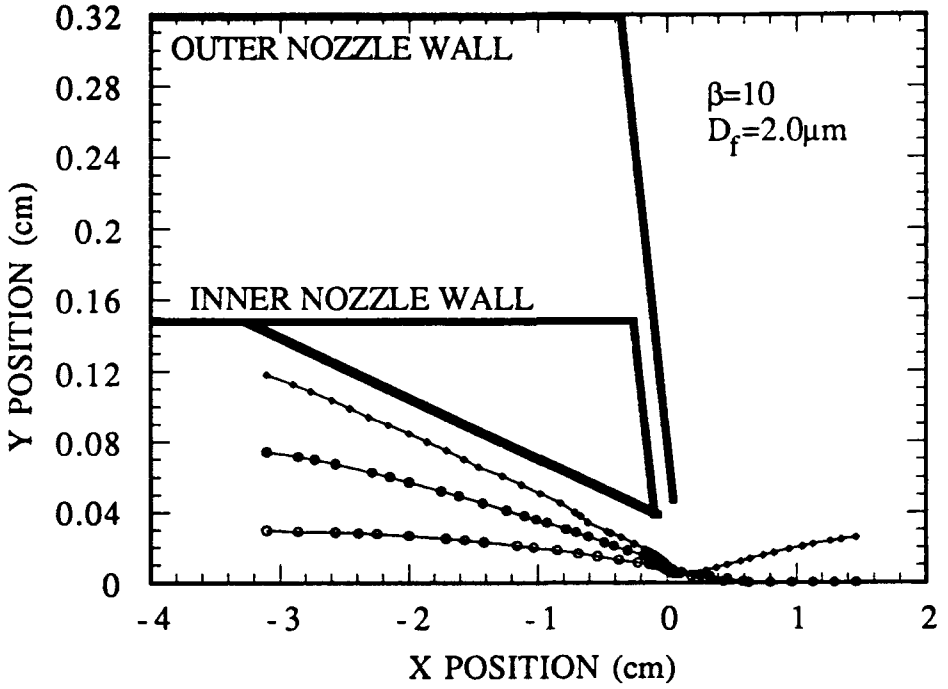

Figure 5.7 Fiber Trajectory in a Modified 2^{o} APS Nozzle (Nozzle Exit at x=0)

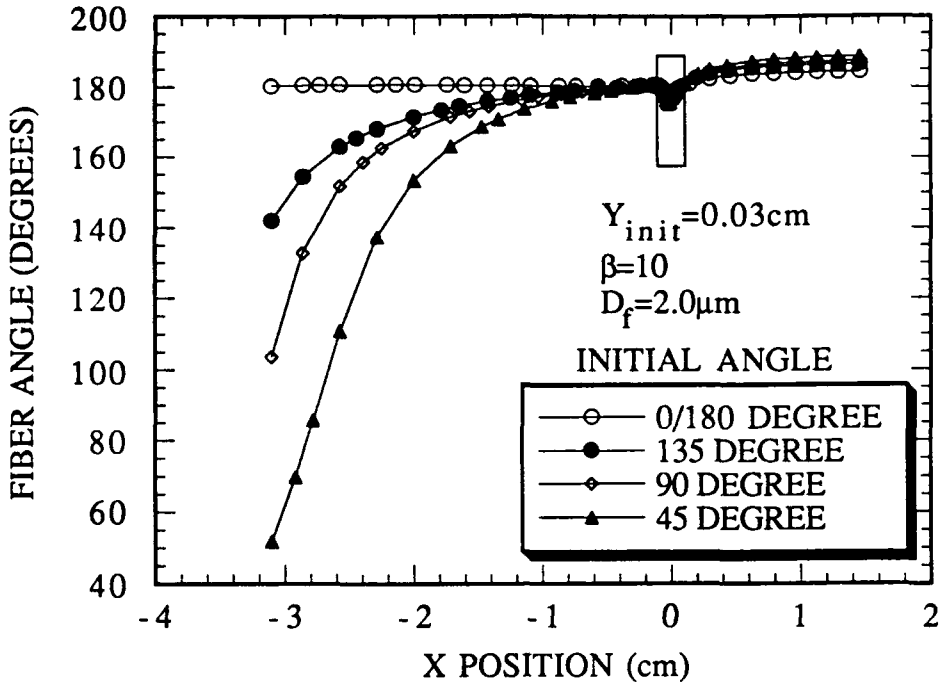

Figure 5.8a Fiber Orientation Through a Modified 2^{o} APS Nozzle for Yinit=0.03 cm (Nozzle Exit at x=0)

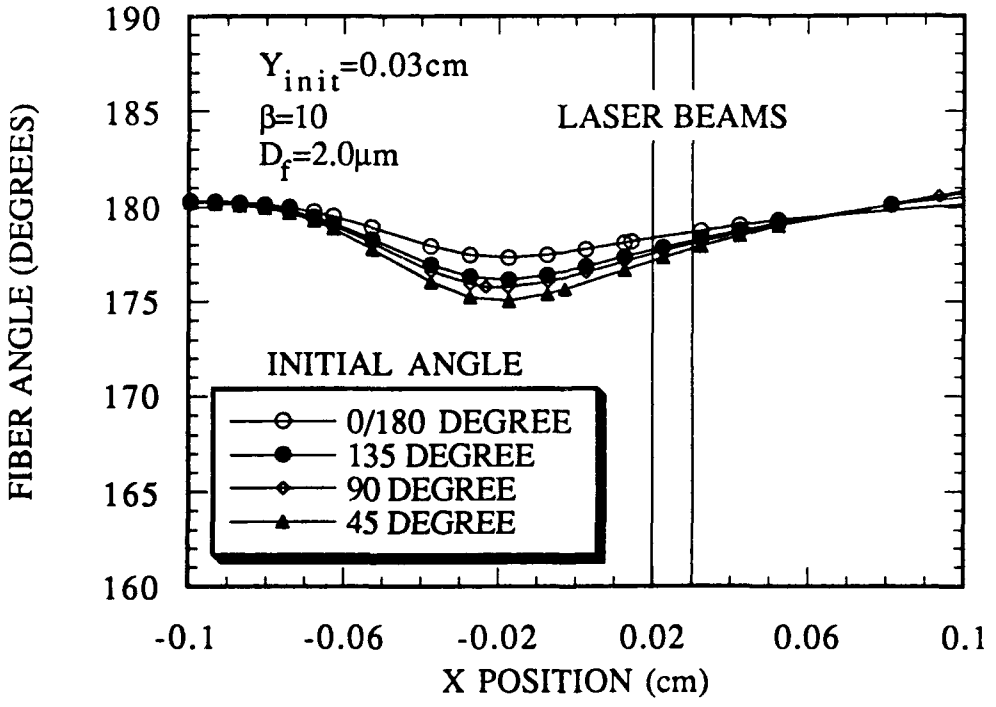

Figure 5.8b Enlarged View of Nozzle Region from Figure 5.8a

standard nozzle. Also, as fibers exit the modified nozzle they still are rotating a small amount while the fibers from the standard nozzle have nearly stopped rotating by the time they reach the laser beams.

This trend in the comparison between the standard nozzle and the modified nozzle holds true for all initial starting positions. This can be seen in Figures 5.9a and b through 5.10a and b.

Perhaps the greatest difference between the two nozzles can be seen in comparing Figure 5.10b with Figure 5.5b. Here the reverse of what was seen before is happening. The fibers maintain a parallel orientation as they exit the modified nozzle while they are rotating slightly as they exit the standard nozzle. As previously noted though, there will be few fibers that travel along the outside of the inner nozzle tube and so this will no longer be considered.

90^{o} Nozzle (Abrupt Contraction)

Figure 5.11 shows the fiber trajectories for the 90^{o} nozzle. Clearly, fiber impaction on the nozzle will be a factor for this nozzle. However, for the fibers which do not impact on the wall, the 90^{o} nozzle appears to align the fibers as well as the other nozzles as shown in Figures 5.12a and b through 5.13a and b.

From the above numerical analysis, it is apparent that the nozzles alone should be sufficient to orient the fibers properly without adding electrostatic alignment to the design. The standard 60^{o} APS nozzle, the modified 2^{o} APS nozzle, and the modified 90^{o} APS nozzle may be suitable for use in the RFA from the stand-point of fiber orientation. The modified 90^{o} nozzle has a problem with fiber losses due to impaction and will therefore be eliminated at this point.

Since the fiber orientation is accomplished well by either the 2^{o} or 60^{o} nozzles, another factor enters into the decision on the best nozzle for the RFA. That factor is instrument resolution. According to Kinney (1990), the resolution of the standard nozzle is superior to that of the 2^{o} modified nozzle. In fact, Kinney suggests that there would be a nozzle design somewhere between 2^{o} and 60^{o} that would optimize resolution. This study indicates that fiber orientation will take place with any nozzle angle. Therefore it is reasonable to assume that there is a better design than what has been presented here. For the purpose of this study however, we will take the 60^{o} nozzle as the best available design and proceed with further numerical and

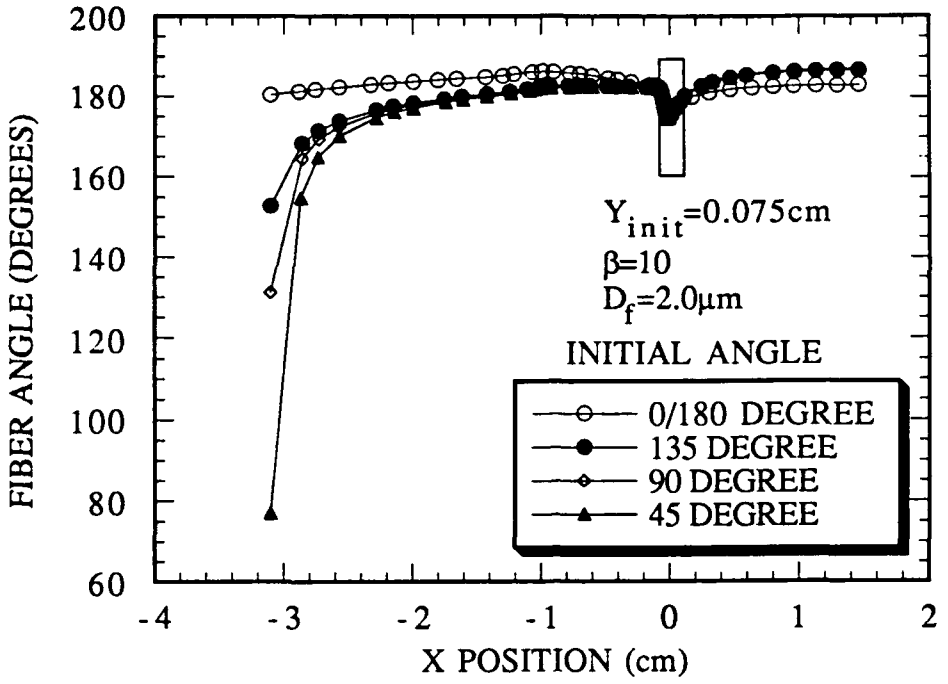

Figure 5.9a Fiber Orientation Through a Modified 2^{o} APS Nozzle for Yinit=0.075cm (Nozzle Exit at x=0)

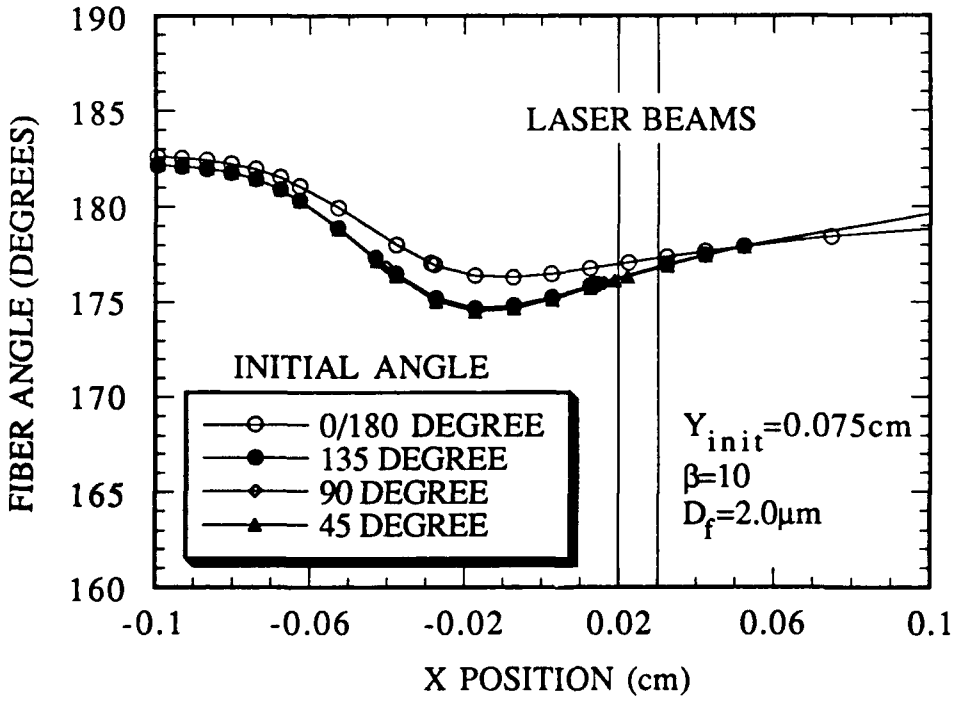

Figure 5.9b Enlarged View of Nozzle Region from Figure 5.9a

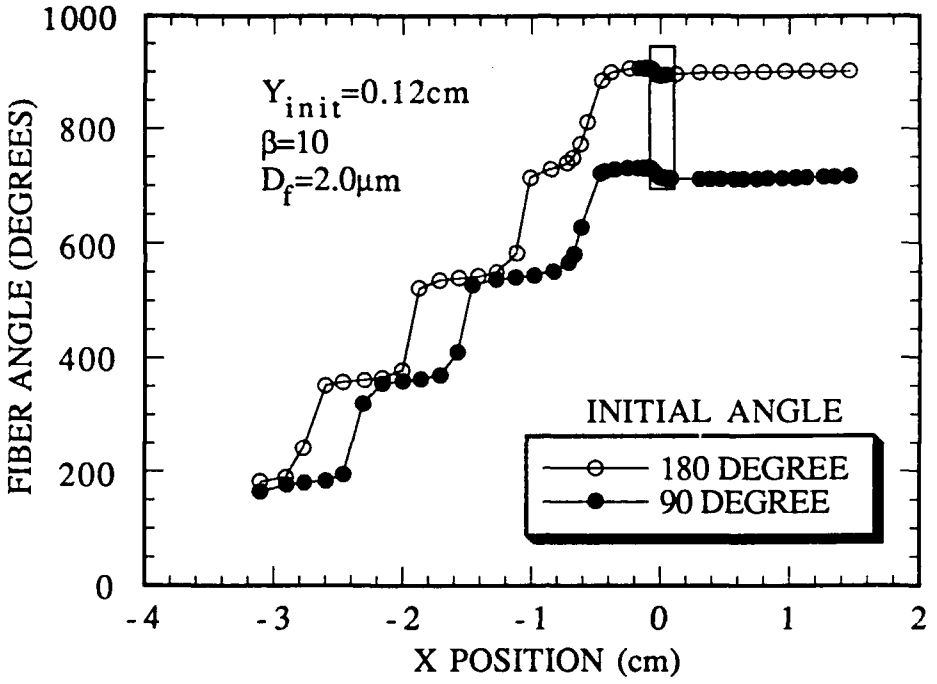

Figure 5.10a Fiber Orientation Through a Modified 2° APS Nozzle for Y_{init}=0.12 cm (Nozzle Exit at x=0)

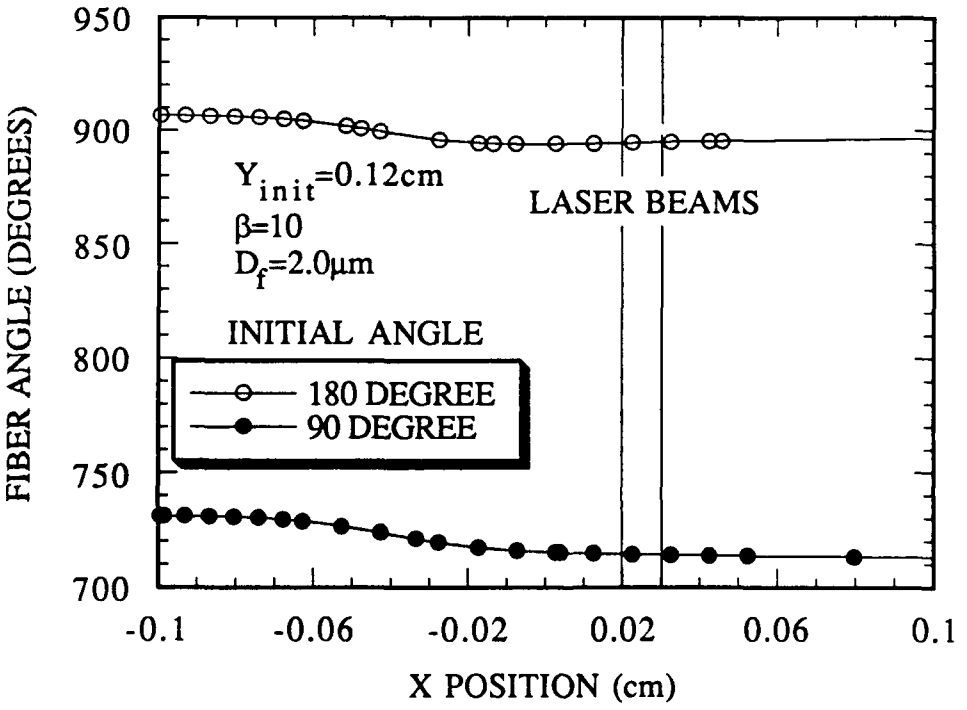

Figure 5.10b Enlarged View of Nozzle Region from Figure 5.10a

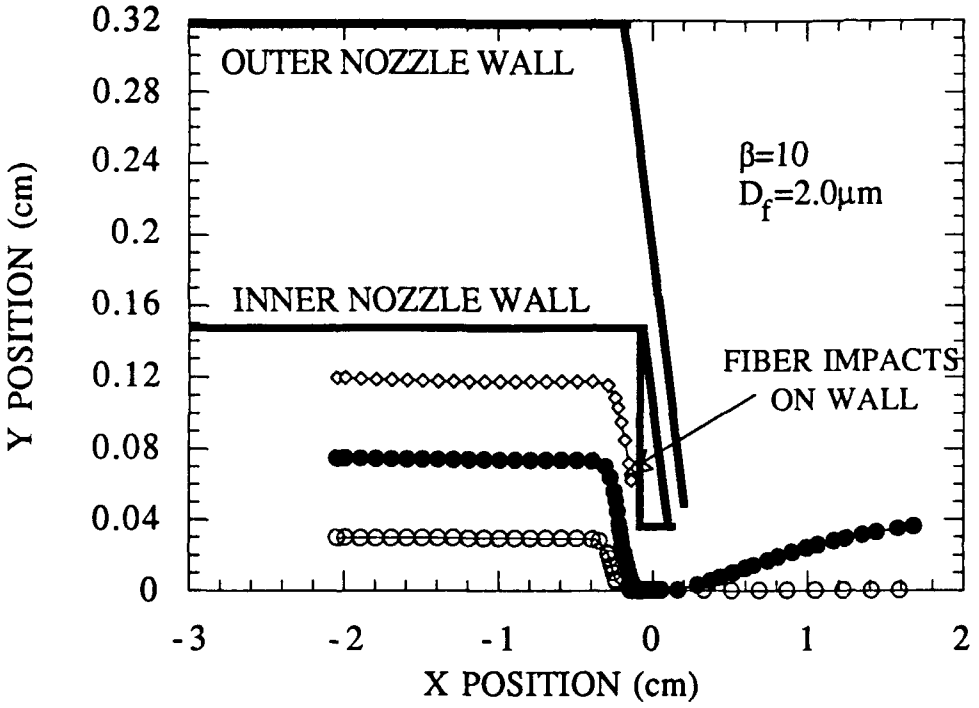

Figure 5.11 Fiber Trajectory in a 90° APS Nozzle
(Nozzle Exit at x=0)

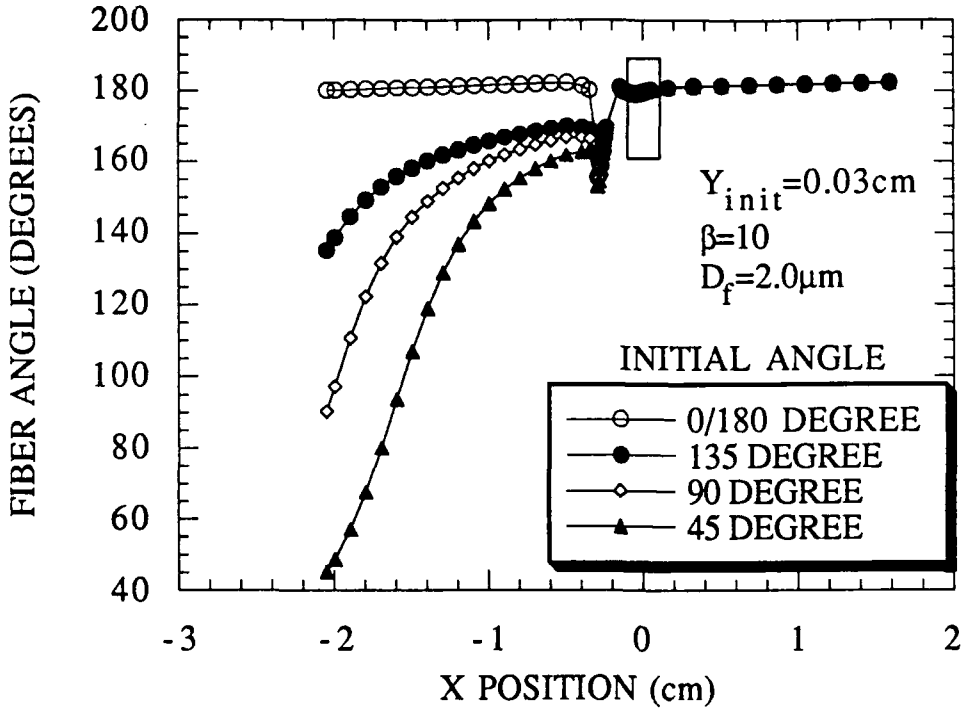

Figure 5.12a Fiber Orientation Through a 90° APS Nozzle for Y_{init}=0.03 cm (Nozzle Exit at x=0)

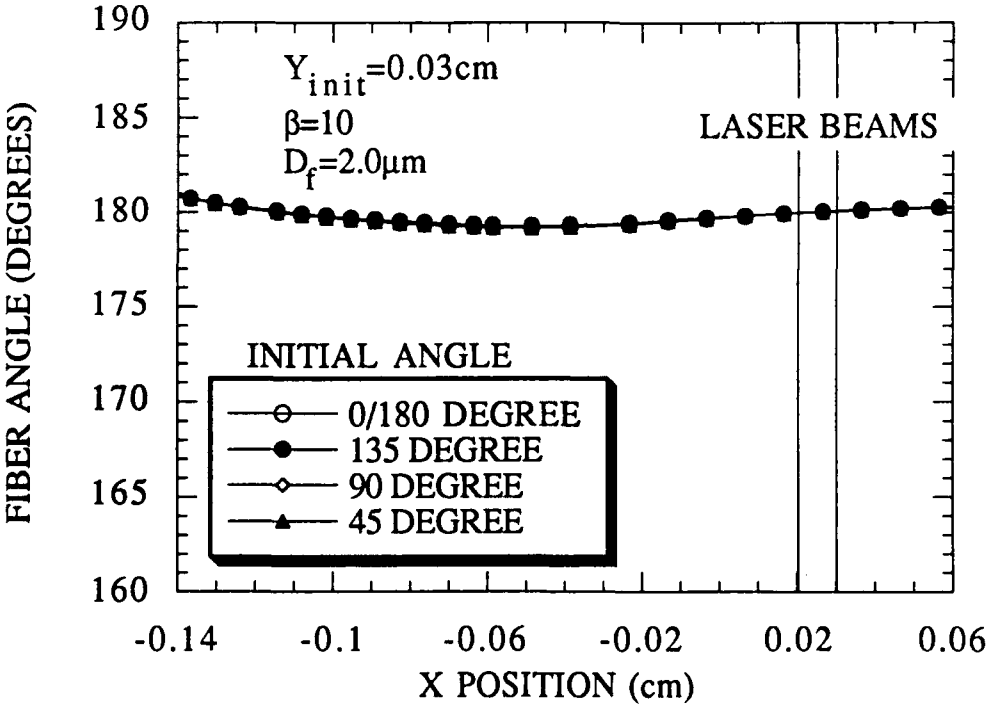

Figure 5.12b Enlarged View of Nozzle Region from Figure 5.12a

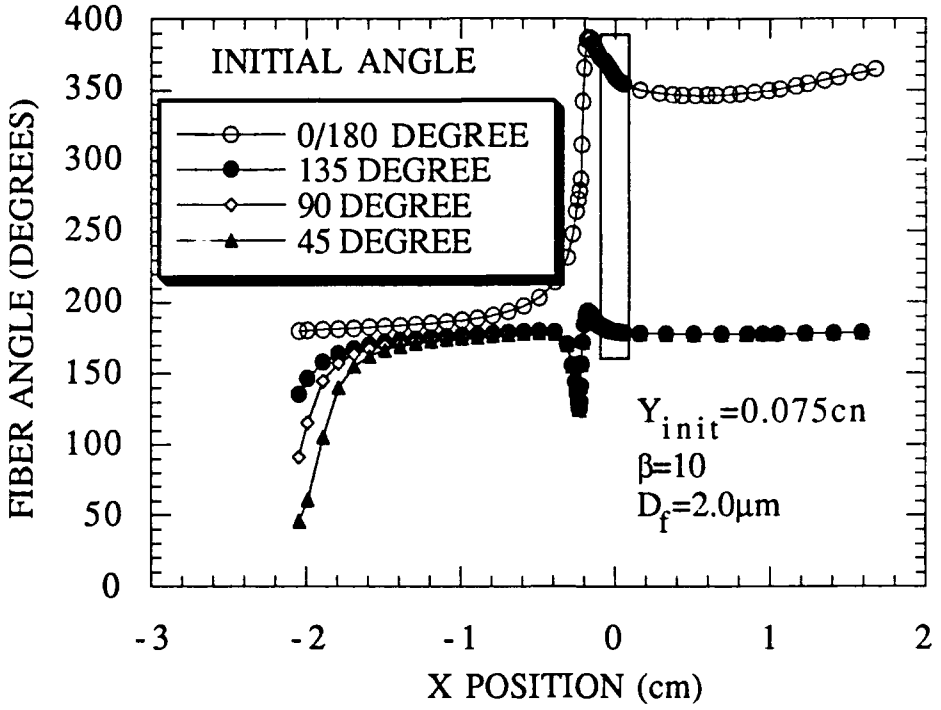

Figure 5.13a Fiber Orientation Through a 90° APS Nozzle for Y_{init}=0.075 cm (Nozzle Exit at x=0)

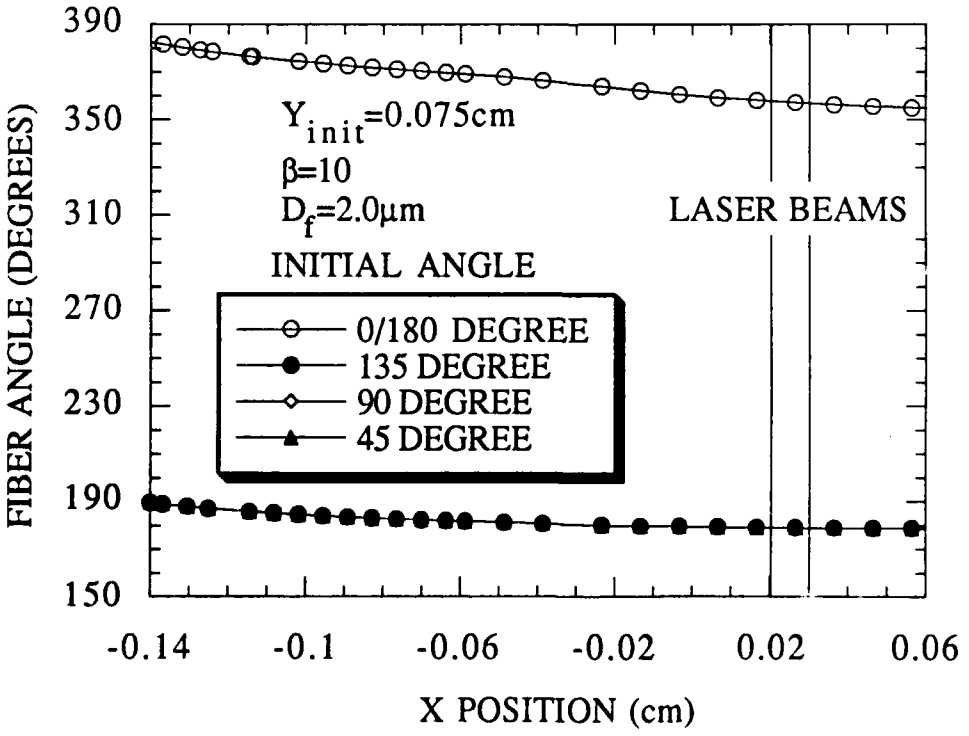

Figure 5.13b Enlarged View of Nozzle Region from Figure 5.13a

experimental investigation.

Up to this point, the fibers modeled have been 2 μm with an aspect ratio of 10. Fibers of various sizes and aspect ratios must be modeled as well to see if the parallel orientation holds true.

Figures 5.14a - 5.15 show the orientation and trajectories of several fiber sizes as they pass through a standard APS nozzle. The orientation modeling was done only for fibers initially starting near the centerline.

Problems occur for the largest of the fibers modeled, 10 μm diameter and 100 μm length, as the orientation may be off by almost 10^{o}. Losses of large particles in the nozzle may also occur due to impaction. Further study of the size limitations of the instrument would be recommended.

5.2. FIBER LIGHT SCATTERING

5.2.1 Numerical Methods

Two programs were used in studying the light scattering response from an APS. One deals with light scattering from an infinite right circular cylinder and the other deals with light scattering from a homogeneous sphere. The light scattering response of the spheres was calculated to provide a reference point from which to evaluate the response of the fibers. Both were based on programs from Bohren and Huffman (1983). A brief description of the theory behind the program for the infinite cylinder follows.

The fibers considered for this work are long compared with their diameter and are modeled as infinite circular cylinders with radius a and refractive index m. The infinite cylinders are being illuminated by a plane homogeneous wave where the angle between the incident wave and the cylinder axis is 90^{o}. Figure 5.16 (Bohren and Huffman 1983) shows the incident beam travelling down the x-axis with the cylinder axis parallel to the z-axis. The angle ϕ is the angle between the incident wave and the scattered wave being considered. The angle ζ is the angle between the incident wave and the cylinder axis. For this study ζ will remain 90^{o}.

The program calculates the scattering coefficients, amplitude scattering matrix elements, and the cross sections for incident light which is either unpolarized, polarized parallel, or polarized perpendicular.

The relationship between the incident and scattered fields is given in matrix form as;

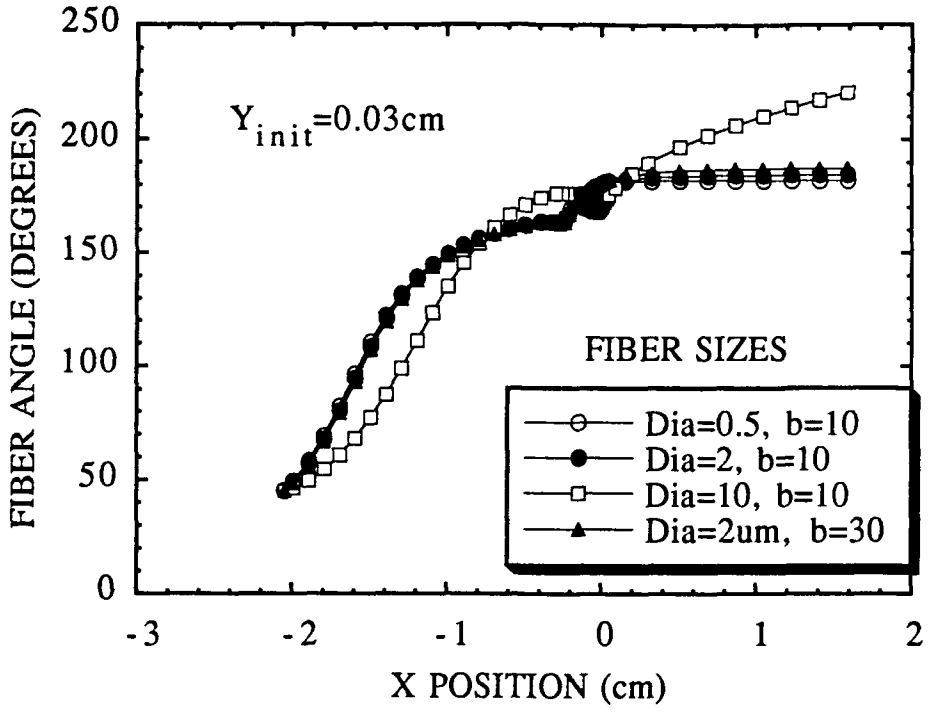

Figure 5.14a Fiber Orientation Through a Standard APS Nozzle for Various Size Fibers (Nozzle Exit at x=0)

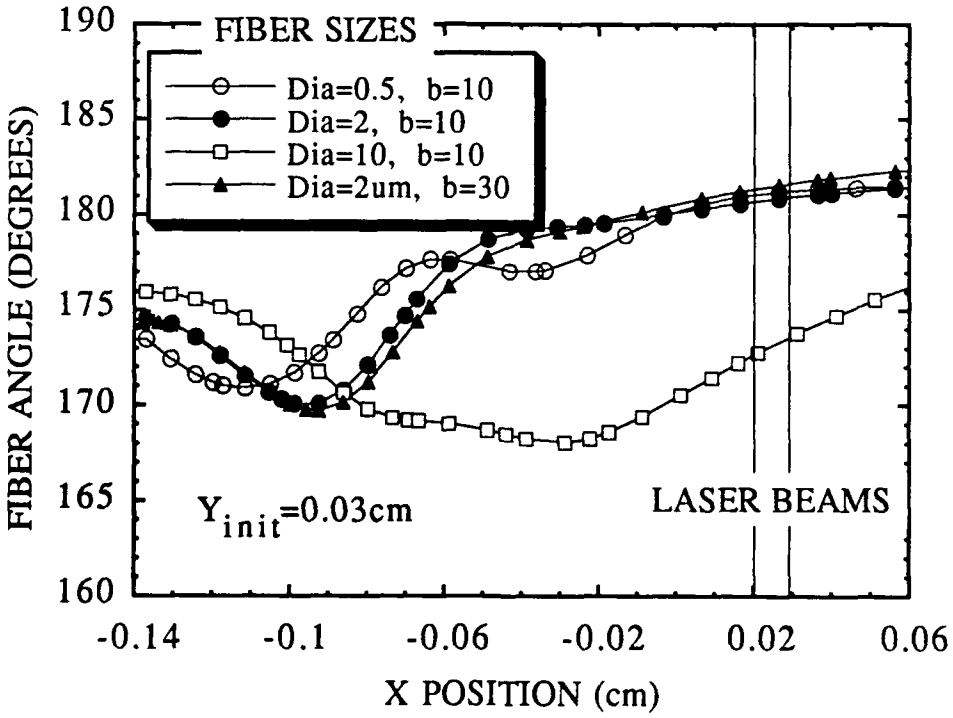

Figure 5.14b Enlarged View of the Nozzle Region from Figure 5.14a

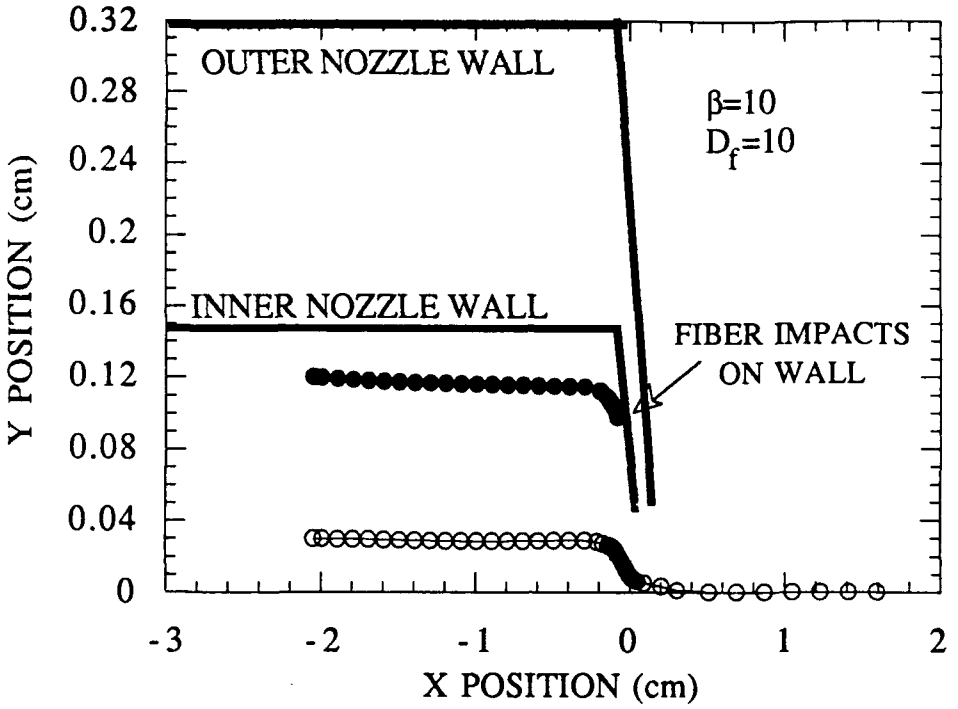

Figure 5.15 Fiber Trajectory Through a Standard APS Nozzle for Fibers of Various Size (Nozzle Exit at x=0)

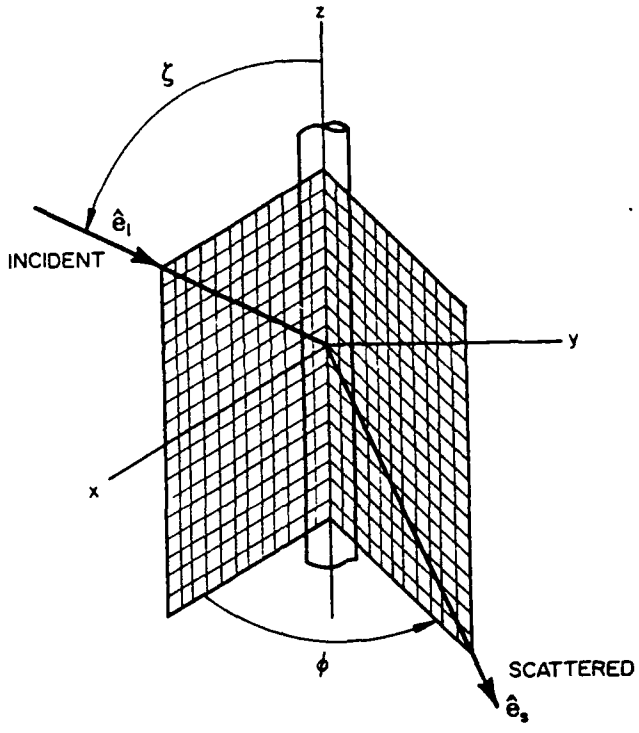

Figure 5.16 Coordinate System for Fiber Light Scattering, Incident Beam Travelling Along the x-axis with the Fiber Centerline on the z-axis

$$\begin{pmatrix} E_{ps} \\ E_{ss} \end{pmatrix} = e^{i3\pi/4}\sqrt{\frac{2}{\pi kr\sin\zeta}}e^{ik(r\sin\zeta - z\cos\zeta)}\begin{pmatrix} T1 & T4 \\ T3 & T2 \end{pmatrix}\begin{pmatrix} E_{pi} \\ E_{si} \end{pmatrix}$$

where

E_{ps} = Parallel component of the scattered field

E_{ss} = Perpendicular component of the scattered fi

E_{pi} = Parallel component of the incident field

E_{si} = Perpendicular component of the incident fie

$$k = 2\pi/\lambda$$

(37)

T1, T2, T3, and T4 make up the amplitude scattering matrix and are the scattering amplitude functions. They are given by;

$$T_1 = b_{0I} + 2\sum_{n=1}^{\infty} b_{nI}\cos(n\Theta)$$

$$T_2 = a_{0II} + 2\sum_{n=1}^{\infty} a_{nII}\cos(n\Theta)$$

$T_3 = 0$ for $\zeta r = 90^\circ$, for all Θ

$T_4 = 0$ for $\zeta r = 90^\circ$, for all Θ

where

$$b_{nI} = \frac{J_n(mx)J_n'(x) - mJ'_n(mx)J_n(x)}{J_n(mx)H_n^{(1)\prime}(x) - mJ_n'(mx)H_n^{(1)}(x)}$$

and

$$a_{nII} = \frac{mJ_n'(x)J_n(mx) - J_n(x)J_n'(mx)}{mJ_n(mx)H_n^{(1)\prime}(x) - J_n'(mx)H_n^{(1)}(x)}$$

(38)

J_n is the Bessel function of the first kind of integral order n and H_n is

the Hankel function. (Bohren and Hufman 1983)
The intensity functions are given by i_1 and i_2, which are the parallel and perpendicular scattering intensities respectively.

$$i_1 = |T_1(\Theta)|^2$$

$$i_2 = |T_2(\Theta)|^2$$

$$i_{unpolarized} = \frac{i_1 + i_2}{2}$$

(39)

The scattering cross section per unit length of fully illuminated infinite circular cylinder is given by Van de Hulst (1957) as:

$$c_{sca}=2/(\pi k)\int_{\theta 1}^{\theta 2}|T(\theta)|^2 d\theta$$

(40)

where θ_1 and θ_2 are the collection angles.

To calculate the scattering cross sections, and thus the APS response, for various fibers, the following methodology was used. Since Equation (40) gives the light scattering cross section per unit length of fiber, all that is needed is to multiply by a given fiber length to get the scattering cross section or APS response for the given fiber. However, the APS laser beam width (in the z direction) is finite, so fibers which are shorter than this width are fully illuminated while fibers which are longer than this width are not fully illuminated. In both cases the fiber is still treated as an infinite cylinder. So then the scattering cross section is given by

$$c_{sca}=2L/(\pi k)\int_{\theta 1}^{\theta 2}|T(\theta)|^2 d\theta$$

(41)

or with $k=2\pi/\lambda$

$$c_{sca}=L\lambda/\pi^2\int_{\theta 1}^{\theta 2}|T(\theta)|^2 d\theta \qquad (42)$$

where L is the fiber length for fibers shorter than the laser beam width or L is the laser beam width for fibers longer than the laser beam width. In other words, the scattering cross section for fibers of constant diameter is a function of fiber length only for fibers whose length is shorter than the laser beam width.

The parameters used for the APS light scattering calculations follow. The laser is a 2mW He-Ne laser with a wavelength of 0.6328μm. The laser beam is split into two beams using a calcite plate. According to Rob Caldow of TSI, the beams are split by polarization. One is polarized with the electric field parallel to the flow direction and one is polarized perpendicular to the flow direction. The scattered light is collected by a lens and focused onto the photomultiplier tube. The collection angle is from 11.9^o to 30.3^o. According to Stan Kaufman of TSI, the calcite plate splits the laser beams so they are approximately 160μm apart. The beam polarization depends upon the orientation of the calcite plate and may vary from instrument to instrument. The beam width was estimated experimentally to be 30 μm and is discussed further in the next chapter.

5.2.2 Numerical Results

The light scattering response of Polystyrene Latex (PSL) spheres, SiC fibers, Carbon Graphite fibers, and asbestos fibers was modeled specifically for the optical system used in the APS. The SiC particles were chosen again for their availability for use in experiment. PSL spheres are uniform, standard particles available in many sizes. They are easily sampled into an APS and the pulse pairs generated by the light scattered from them are easily identifiable. Therefore they were modeled to provide a good reference point on which to evaluate the light scattering response of the APS to various fibers. The refractive indices for an incident light wavelength of 0.6328 μm used for each type of particle are as follows:

PSL	m=1.59	(Chae 1991)

SiC	m=2.63-i2.67	(Chae 1991)
Carbon Graphite	m=1.59-i0.66	(Van de Hulst 1957)
Asbestos	m=1.56	(Lilienfeld 1987 -value used as approximate for typical asbestos fiber)

The first step in the evaluation was to look at the angular scattered intensity function for each of the particles. Since the two laser beams in the APS each have a different polarization, the angular scattered intensity functions for each polarization along with the angular scattered intensity function for an unpolarized beam was plotted. First, the angular scattered intensity function for 2.0 μm PSL spheres is plotted in Figure 5.17. The majority of the scattered light is found to be in the near forward direction as expected. Notice also for the spheres that the intensity functions from incident parallel and perpendicular components are nearly the same from 0^{o} to around 80^{o}.

The angular scattered intensity functions for a 2.0 μm diameter SiC fiber, an 8 μm Carbon Graphite fiber, and a 2.0 μm Asbestos fiber are shown in Figures 5.18-5.20. Again the majority of scattered light is in the near forward direction. But, the intensity functions from the incident parallel and perpendicular components for both the SiC and Carbon Graphite fiber types differ in the near forward direction. This becomes significant as the scattered light in the APS is collected from 11.9^{o} to 30.3^{o}. This difference is not as pronounced for the asbestos fiber until a collection angle of around 60^{o} is reached.

The next step was to calculate the light scattering cross section for these four types of particles over a range of particle diameters. As discussed previously the light scattering cross section of fibers will be dependent on fiber length for fibers shorter that the laser beam width or dependent on the laser beam width for fibers longer than the laser beam width. The light scattering cross section for PSL spheres and for SiC fibers of various diameter is found in Figure 5.21. The same for Carbon Graphite fibers and asbestos fibers is shown in Figures 5.22 and 5.23. The fibers in Figures 5.21-5.23 have some length which is longer than the laser beam width. The laser beam width was determined experimentally to be approximately 30 μm.

The PSL spheres are seen to have close to the same light scattering cross

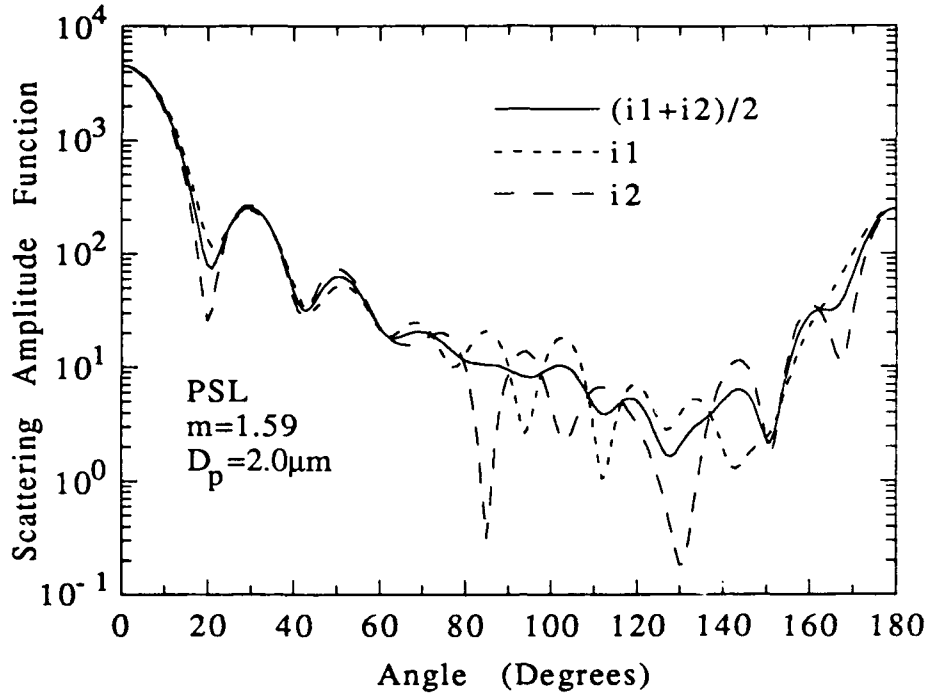

Figure 5.17 Angular Scattered Intensity Distribution of PSL Particle

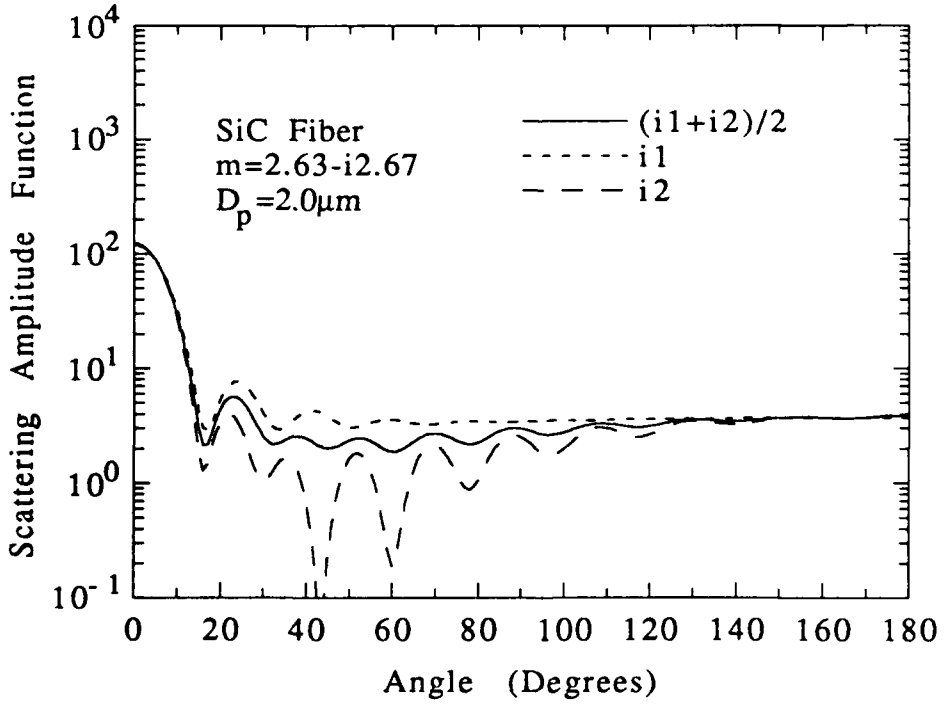

Figure 5.18 Angular Scattered Intensity Distribution of SiC Fiber

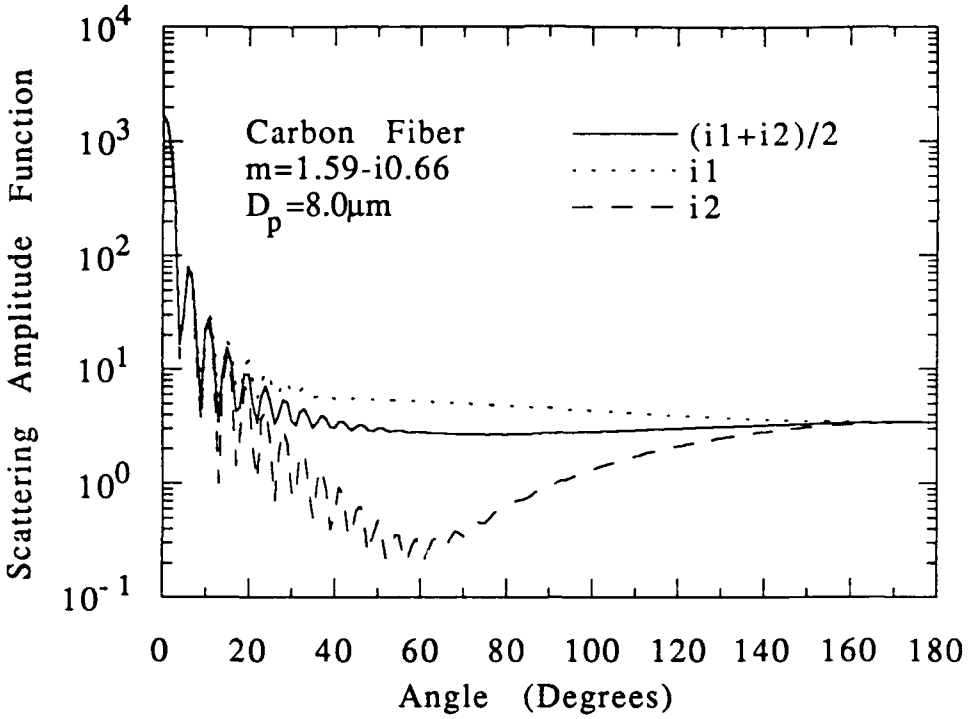

Figure 5.19 Angular Scattered Intensity Distribution of Carbon Fiber

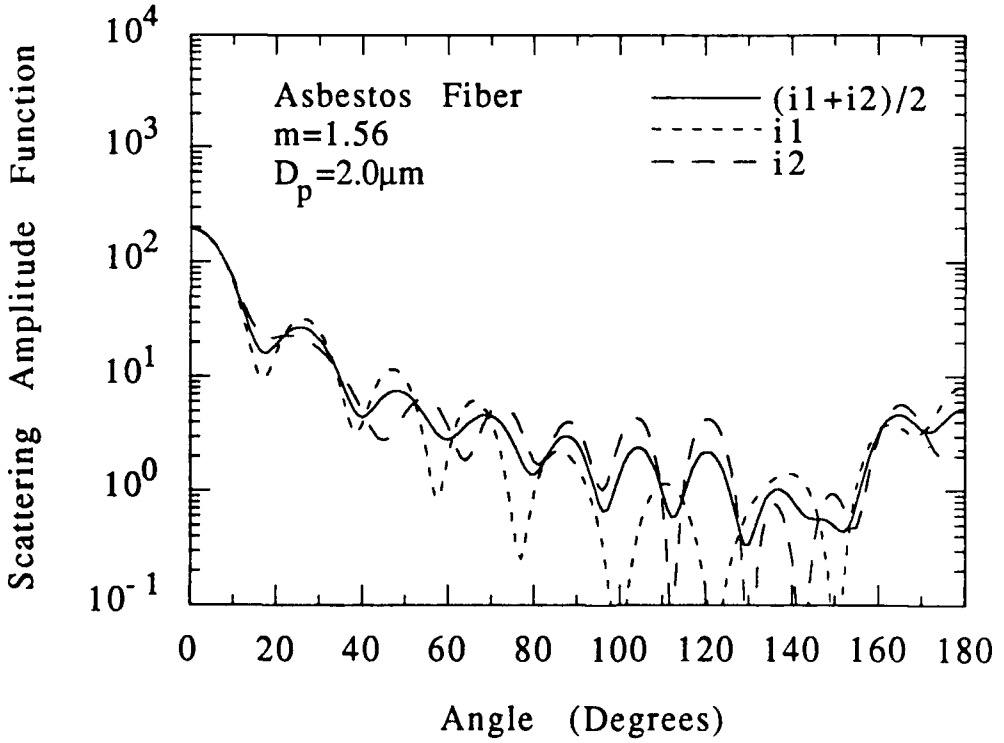

Figure 5.20 Angular Scattered Intesity Distribution of Asbestos Fiber

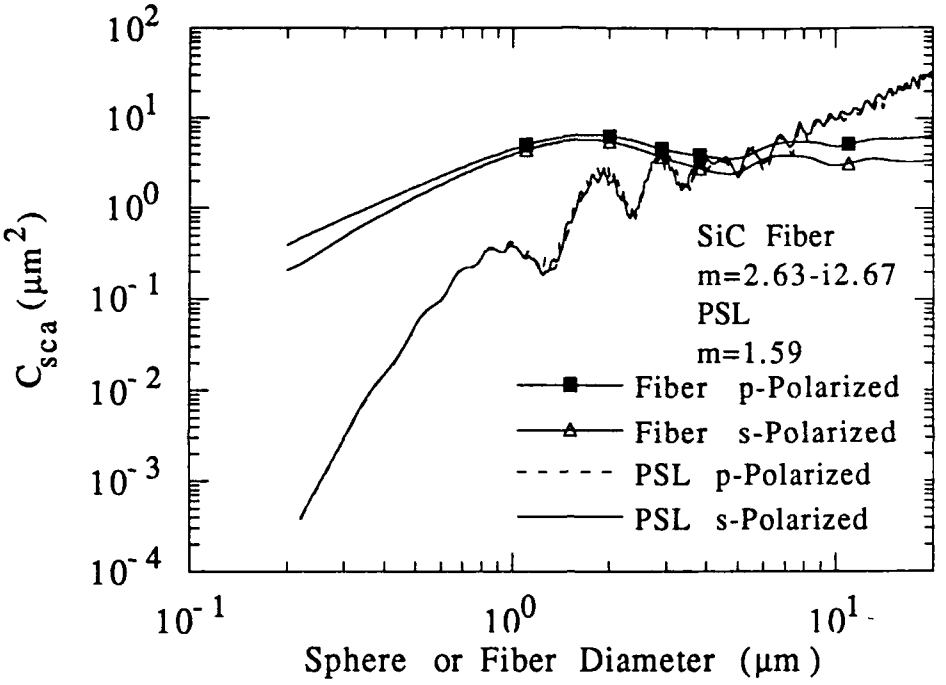

Figure 5.21 Scattering Cross Section (C_{sca}) for PSL Spheres and SiC Fibers in a TSI APS
(Laser Beam Width is Approximately 30 μm)

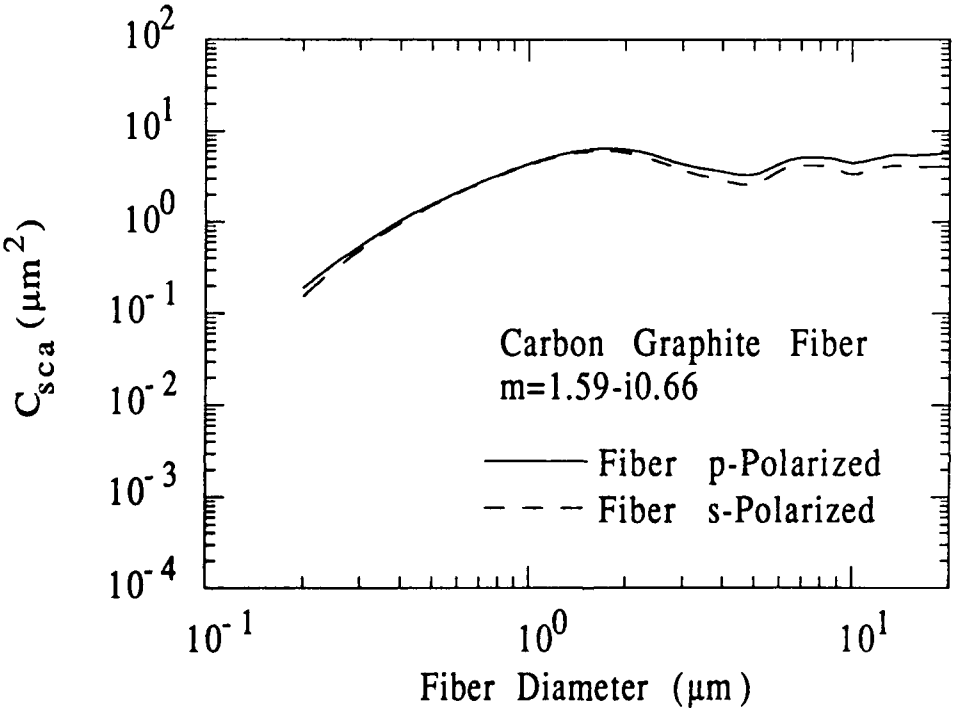

Figure 5.22 Scattering Cross Section (C_{sca}) for Carbon Graphite Fibers in a TSI APS
(Laser Beam Width is Approximately 30 μm)

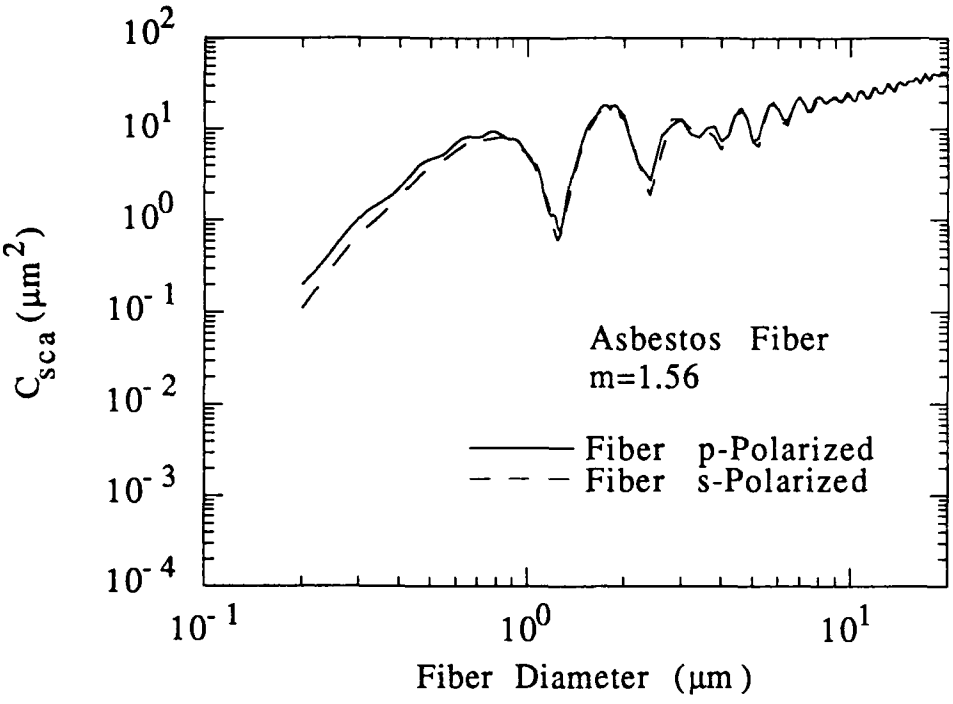

Figure 5.23 Scattering Cross Section (C_{sca}) for Asbestos Fibers in a TSI APS (Laser Beam Width Approximately 30μm)

section for the beam polarized parallel (p-polarized) as for the beam polarized perpendicular (s-polarized). The SiC fibers on the other hand have a larger light scattering cross section for the p-polarized beam than for the s-polarized beam. This is true for the entire range of fiber diameters calculated. Stated another way, PSL particles will generate a pulse pair where the amplitude (height) of each pulse is nearly equal. SiC fibers will generate a pulse pair where the height of one pulse is greater than the other depending on which beam has which polarization. Using this information, SiC fibers can be distinguished from spherical particles.

Figure 5.22 shows that the same idea is valid for the Carbon Graphite fibers but only for the fibers which are greater than about 2 μm in diameter. For the asbestos fibers in Figure 5.23, only the submicron size fibers would be identifiable using pulse height information. So distinguishing fibrous particles by pulse height would not be effective for all types and sizes of fibers. The pulse shape, however, is another way of distinguishing fibers from spherical particle as will be seen shortly.

For fibers which are shorter than the laser beam width, the light scattering cross section depends on fiber length as given in Equation (42). For SiC fibers in this category, the light scattering cross section for fibers of different diameters and aspect ratios is shown in Figure 5.24.

One aspect of the light scattering analysis which is not so obvious is the pulse shapes of the various types of particle. The intensity of each of the laser beams is greater in the center of the beam than on the edges. Therefore, as a spherical particle with a diameter smaller than 30 μm travels through one beam, the pulse strength will gradually increase until the center of the beam is reached. The pulse will have a sharp peak corresponding to the instant when the center of the particle was in the center of the beam, then the pulse strength will gradually decrease until the particle exits the beam. The same would be true of a fiber whose length is shorter than 30 μm, the pulse shape would be that of an upside down "V". For a fiber which is longer the 30 μm however, the shape would be different. As the fiber enters one beam, the pulse strength would gradually increase as before. The maximum pulse height would be reached as the fiber stretches across the entire width of the laser beam. As the fiber is longer than the beam width, this maximum height would be maintained for a certain amount of time. This would give the pulse a flat top or square shape.

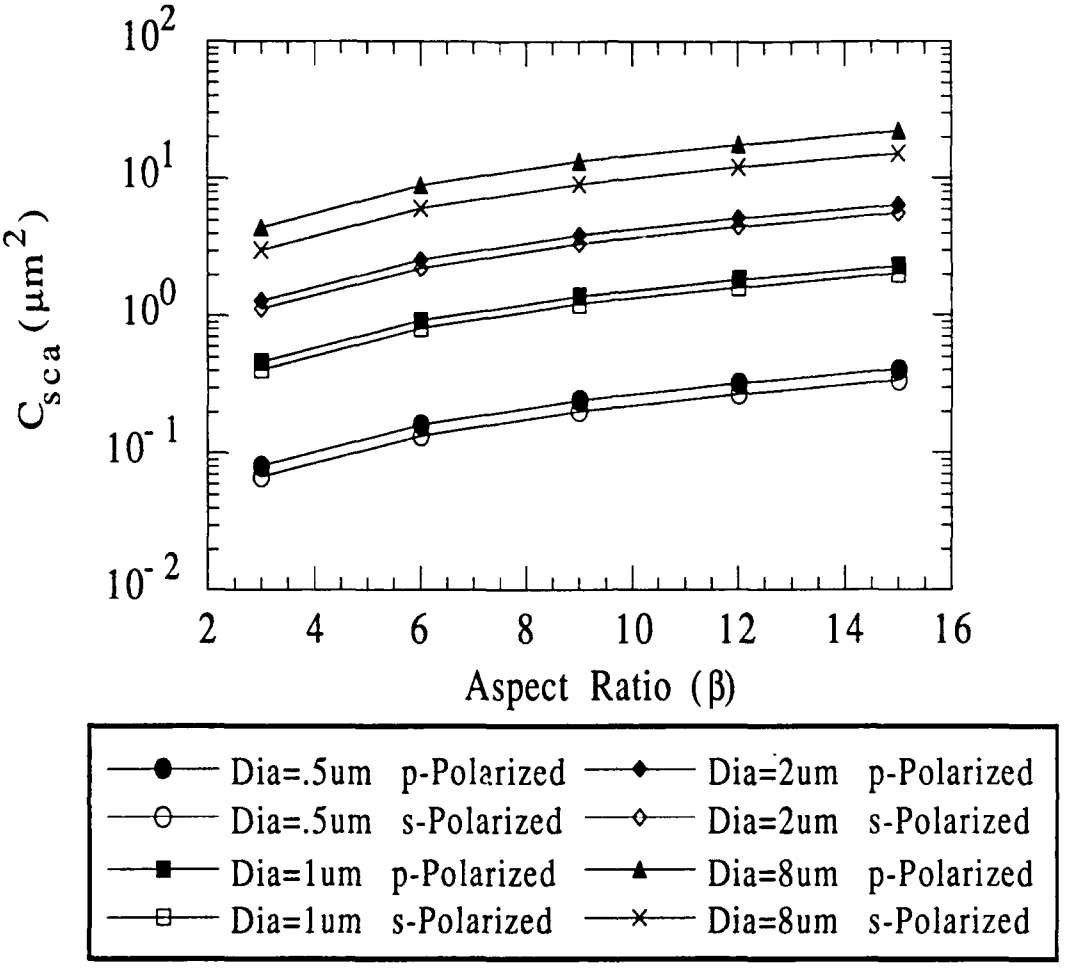

Figure 5.24 Scattering Cross Section vs Aspect Ratio for SiC Fibers in an APS

The light scattering cross sections which were found can be directly converted into a pulse height in volts by comparing the pulse heights of known size spheres and their scattering cross section and determining the correct coefficient. This can then be used to estimate the pulse height in volts for the fibers. This is done in the next chapter.

5.3 CONCLUSIONS

The orientation of fibers of various sizes were modeled for three types of APS nozzle designs to find out if the flow itself was sufficient to align the fibers properly and to determine the best nozzle design. It was discovered that the 60^{o} standard APS nozzle aligned the fibers properly and was chosen as the best alternative. From this numerical analysis, electrostatic alignment was found to be unnecessary. Fiber alignment is sufficient for most fibers except the larger and longer sizes. Although alignment is not perfectly parallel with the flow direction, at this stage it is thought to be adequate.

Light scattering analysis was accomplished for PSL spheres, SiC fibers, Carbon Graphite fibers, and asbestos fibers. This analysis indicates that the light scattering response of the APS will differ for spherical particles and fibrous particles. This will result in spherical particles having pulse pairs where each pulse is nearly the same height while fibrous particles will have pulse pairs where each pulse has a different height. As was seen with the Carbon Graphite and asbestos fibers this difference does not hold true for all types and sizes of fibers. Close inspection of the scattered intensity functions (shown in Figures 5.17-5.20) indicates however, that by varying the collection angle, the distinguishing characteristics of the differently polarized beams could be optimized to cover a wide range of fiber types and sizes. This will be discussed in more detail in Chapter 7. Further analysis of various fiber types would be recommended.

Also it was found that the pulse shape would be the same for spherical particles with a diameter less than 30 μm and for fibers with a length less than 30 μm. Their pulse shape would have a sharp peak. For fibers with a length greater than 30 μm, the pulse shape will be characterized by a flat top creating a square pulse. For these type of pulses, fiber length can easily be calculated. The pulse shape then provides another method of distinguishing long fibers from spherical particles.

CHAPTER 6

RFA EXPERIMENTAL EVALUATION AND RESULTS

Chapter 6 provides the methodology for evaluating the ideas for the RFA and confirming the results of the numerical work in Chapter 5. The experimental methods and apparatus used are presented, followed by the results and a discussion. The experiments were designed to show that the fibers will align themselves as the numerical analysis predicts and that the pulses produced by the fibers would be similar in shape and size to that predicted by the numerical analysis. In short, this chapter will reveal the actual feasibility of the RFA.

6.1 EXPERIMENTAL APPARATUS AND PROCEDURES

The purpose of the experiments performed was twofold. First to see if the pulse pairs produced by a fiber were similar in form and size to what was expected. Second, to determine the actual fiber alignment as it travelled through the APS viewing volume. Two types of fiber were used, a 2 μm SiC fiber with a median length of 48.8 μm (Chan 1991) and 8 μm Carbon Graphite fiber with a median length of 19.5 μm. (Liu 1983)

The method involved in evaluating both fiber pulse form and fiber alignment was similar, the experimental apparatus is shown in Figure 6.1. In each case fibers were generated by a Fluidized Bed Generator (FBG) and sampled through an APS. Individual pulse pairs generated by the fibers as they passed through the two laser beams in the APS were viewed on a digital oscilloscope. The pulse pairs were analyzed for pulse height, pulse width, distance between the pulses or transit time, and general pulse shape. All of these factors were taken into consideration in determining if the corresponding particle was a fiber or not.

As discussed in Chapter 5, for fibers which are shorter than the laser beam is wide, the pulses will be peaked similar to a spherical particle. However, one pulse should be larger than the other pulse due to the different

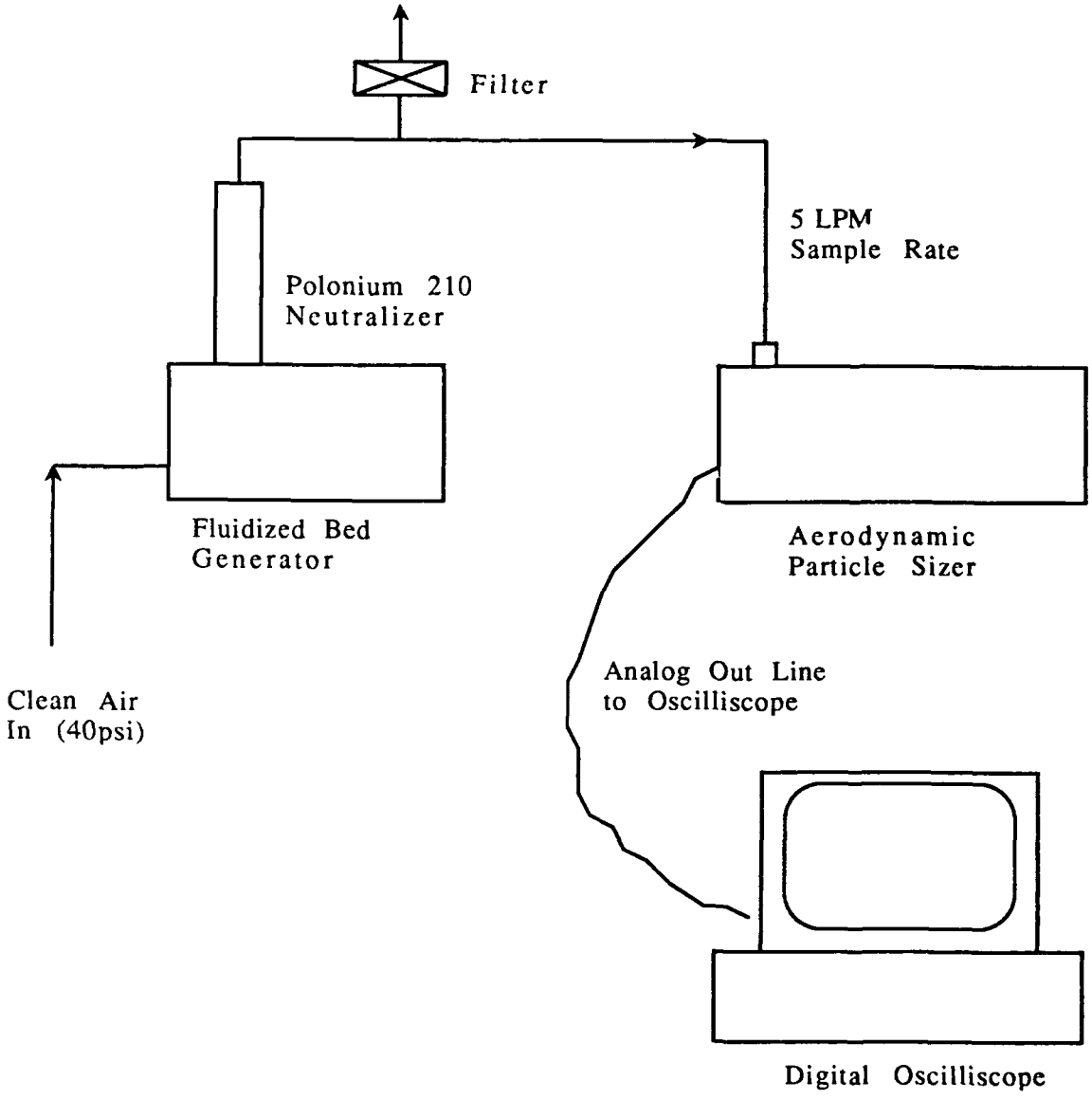

Figure 6.1 Experimental Apparatus Diagram

polarizations of the two beams. For fibers longer than the laser beam width, each pulse should have a flat top, forming a square pulse. This formed the basis or starting point for determining whether or not the particle was a possible fiber.

The criteria identified above, however, does not insure that the particle is a fiber. Careful analysis of the transit time, pulse height, and pulse width were undertaken to verify each possible fiber count. The transit time for each pulse pair leads to two items of interest. First, because the distance between the laser beams of the APS is known (approximately 160 μm) the transit time leads to particle velocity. Second, using the APS calibration curve, the transit time can be converted to a measured aerodynamic diameter. For those pulse pairs which possess a square shape, and only those pulse pairs, the pulse width multiplied by the particle velocity will give the fiber length. Now, knowing the fiber diameter (given) and the measured fiber length, the aerodynamic diameter was calculated and compared with the measured aerodynamic diameter taken from the APS calibration curve. If the particle was truly an individual fiber, the measured aerodynamic diameter would fall somewhere in the limits of the calculated aerodynamic diameter for fibers aligned parallel and perpendicular with the APS flow as shown in Figure 2.2. If the fiber was actually aligned parallel with the flow, the measured aerodynamic diameter and the calculated aerodynamic diameter for a parallel fiber should be the same.

6.1.1 Fiber Generation

Generating the fibers for experimental use proved to be a difficult problem in itself. The main problem being that the fibers become attached to one another and form clumps of two or more fibers. Several methods were used to try to aerosolize individual fibers. Some of these methods involved using a TSI Small Scale Powder Disperser (SSPD). The SSPD is operated by placing a small amount of dry substance on a disk a spreading it out thinly. The SSPD then picks up the substance off of the disk with a capillary tube that has variable suction. The aerosol is diluted with clean air and exits the SSPD. The 8 μm fibers, when placed on the disk dry, remained in clumped form. When sampled and viewed under the microscope very few and often no individual fibers were present.

The 8 μm fibers were also suspended in isopropyl alcohol. Droplets of

the mixture were placed on the disk and allowed to dry. The majority of fibers on the disk in this case were individual fibers. However, as the alcohol evaporated, the fibers were bound to the plate and the suction from the SSPD could not remove them.

Another attempted method was to mix the fibers in filtered, deionized water, and then use an atomizer followed by a diffusion dryer to entrain the fibers in air. This was only attempted with the 2.0 μm SiC fibers. With this method, nothing but very small particles made it to the APS.

The fluidized bed generator provided the best results. A schematic of the FBG is shown in Figure 6.2. The FBG contains a hopper where the particles to be aerosolized are placed. A chain drive carries the particles from the hopper to the fluidized bed. The fluidized bed is made up of relatively large brass beads. As filtered air enters the bed of brass beads the beads begin to "boil" or become fluidized. This boiling action breaks up the agglomerated particles which are then carried into the air. The aerosol then is neutralized, in this case using a Polonium 210 neutralizer. For these experiments the FBG was cleaned and filled with new 100 μm brass beads. The hopper was left empty and small amounts of fiber were placed directly into the brass beads for each experiment. A high bed flow caused a vigorous "boiling" of the beads which broke up the fiber clumps. This method produced the highest concentration of individual fibers although many fiber clumps still were present. As it turned out, all of the experimental results were found using the 2 μm SiC fibers. This is because the Carbon Graphite fibers contained a large amount of Carbon Graphite "dust" particles that made it nearly impossible to capture a fiber pulse with the available oscilloscope.

6.1.2 Pulse Acquisition

As mentioned the apparatus shown in Figure 6.1 was used to perform the experiments. A TSI Model 3400 Fluidized Bed Generator (FBG) fitted with a Polonium 210 neutralizer aerosolized the fibers. The fibers then entered an unmodified TSI Model 3310 APS. For this study two instruments were used, serial numbers APS 153 and APS 309. The photomultiplier tube gain was set on each instrument to produce a 0.2 volt pulse height for a 2.01 μm PSL sphere. The signal from the photomultiplier tube that was generated by a particle passing through the viewing volume can be extracted from the APS through a port on the rear of the instrument. The signal from the APS goes through a

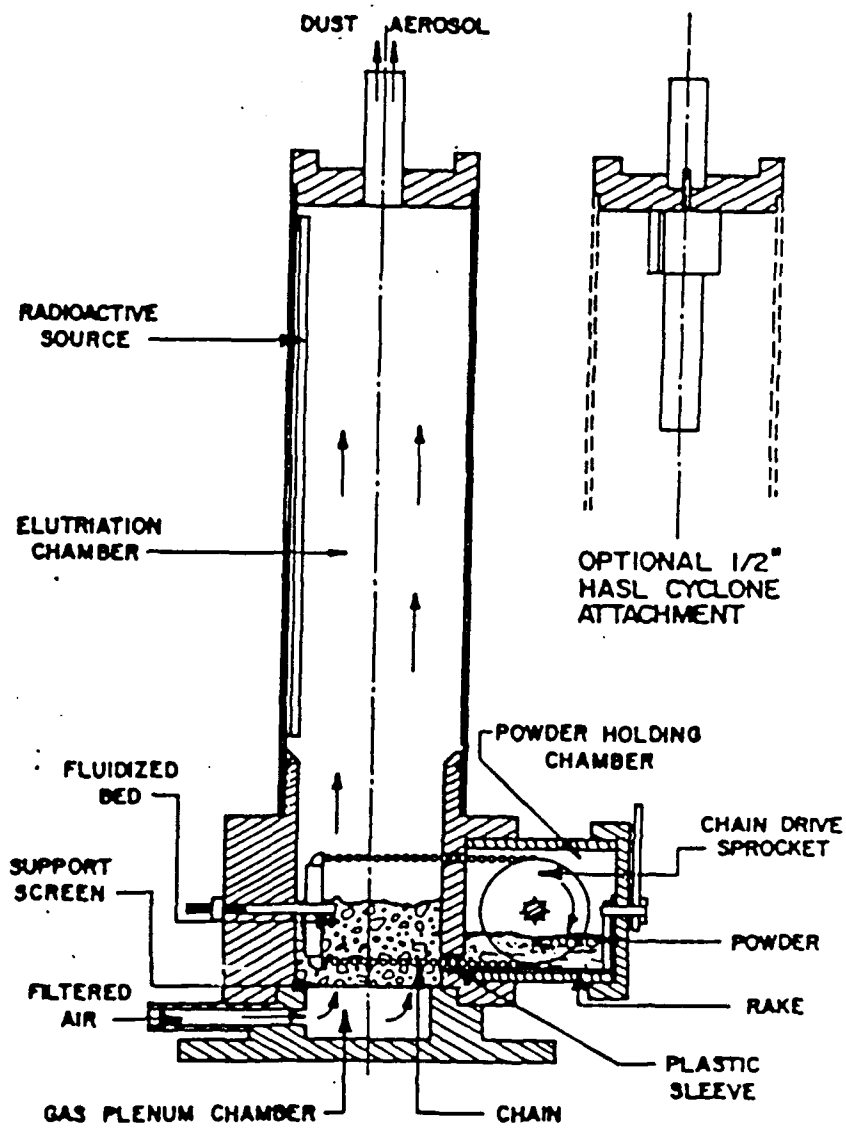

Figure 6.2 Schematic of Fluidized Bed Generator

voltage divider which decreases the voltage of each signal by a factor of 10. This signal was sent to a digital oscilloscope where pulse pairs could be viewed and stored. The oscilloscope was a CyberResearch INST 140 digital scope board with Compuscope 220 software used on a Northgate personal computer. The maximum sampling rate was 40MHz. It is important to point out that the oscilloscope used was not capable of sampling every particle that the APS measured. In fact, one pulse pair at a time was stored in the oscilloscope and had to be transferred to another file before another pulse pair could be stored, making for a rather slow process. So, in some cases, each consecutive pulse pair was stored into a file for later analysis and in some cases, a total count of all pulse pairs viewed was kept while only the possible fiber pulse pairs were stored for later analysis.

6.1.3 Filter Sampling

2.0 μm diameter SiC fibers, generated by the same means, were also sampled to 0.4 μm Nuclepore filters. Samples of 1 minute, 5 minutes, and 10 minutes were taken. The filter samples were viewed under an Ortholux Optical Microscope using 1000x magnification. Over a portion of each of the filters, particles were counted. The count was separated into single fibers, fiber clumps of more than one fiber, and spherical "dust" particles. This count was then compared to the fiber count from the APS as determined by viewing the individual pulse pairs. The filter samples were also viewed under a Scanning Electron Microscope (SEM). From the SEM analysis, an average fiber length and diameter were found by measuring all of the fibers covering a certain area of the filter.

In sampling the fibers onto a Nuclepore Filter the APS was simply replaced by a 47 mm in-line filter holder with the same flow rate as the APS of 5LPM. The flow was drawn through the filter using a vacuum system.

The health risks involved in working with the SiC and Carbon Graphite fibers are not definitely known but it was assumed that they were comparable to asbestos. Even though only small amounts were used, the fibers were always handled with the utmost care and safety. The FBG and APS were contained entirely within a hood and all handling of the fibers took place in the hood.

All of the experimental work presented in section 6.2 was done using the original 60^{o} inner nozzle that is standard for the APS. However, toward the

end of this study, a 2° nozzle was placed in the APS and some fiber was sampled. Also the inner nozzle was removed entirely and fiber was sampled. This was only done for a short time and only a small number of fiber pulses were seen. The main concern in doing this was fiber alignment analysis. Because the alignment analysis did not prove very effective for the 60° nozzle, and because the APS was not calibrated for the different nozzle arrangements, no conclusions on fiber alignment for these cases were drawn.

6.2 EXPERIMENTAL RESULTS

This section includes four main parts. The first part will be the comparison and analysis of individual pulse pairs. The second part will focus on the comparison of fiber counts by means of the APS to fiber counts using an optical microscope. The third part will consider the alignment of the fibers as they pass through the instrument. Finally the fourth part will look at the actual fiber pulse heights compared to the theoretical values.

6.2.1 Individual Pulse Pairs

It will be worthwhile to begin to analyze the results by comparing some actual pulse pairs taken from the same APS. The first pulse pair shown in Figure 6.3 is a 2.01 μm diameter PSL sphere. The second is a 2.0 μm diameter SiC fiber shown in Figure 6.4 whose length is greater than the width of the laser beam. The third is a 2.0 μm diameter SiC fiber shown in Figure 6.5 whose length is shorter than the width of the laser beam.

The PSL particle has a pulse pair in which each of the pulses are of equal height. The pulse shape is that of an upside down "V" with a definite sharp peak. The measured transit time of the pulse pair in Figure 6.3 is 1150ns. The APS calibration curve is then used to find the particle aerodynamic diameter which is 1.995 μm. Since the distance between the laser beams is known to be about 160 μm (Stan Kaufman, TSI) the particle velocity is found to be 139m/s. The width of the first pulse, taken at the 50% height, is 200ns. This together with the particle velocity can be used to estimate the laser beam width at 27.8 μm.

Compare this now to the pulse pair shown in Figure 6.4. The height of the second pulse (about 0.45v) in this pair is much smaller than that of the first pulse (about 0.6v). The peak of each pulse has flattened out as well. These

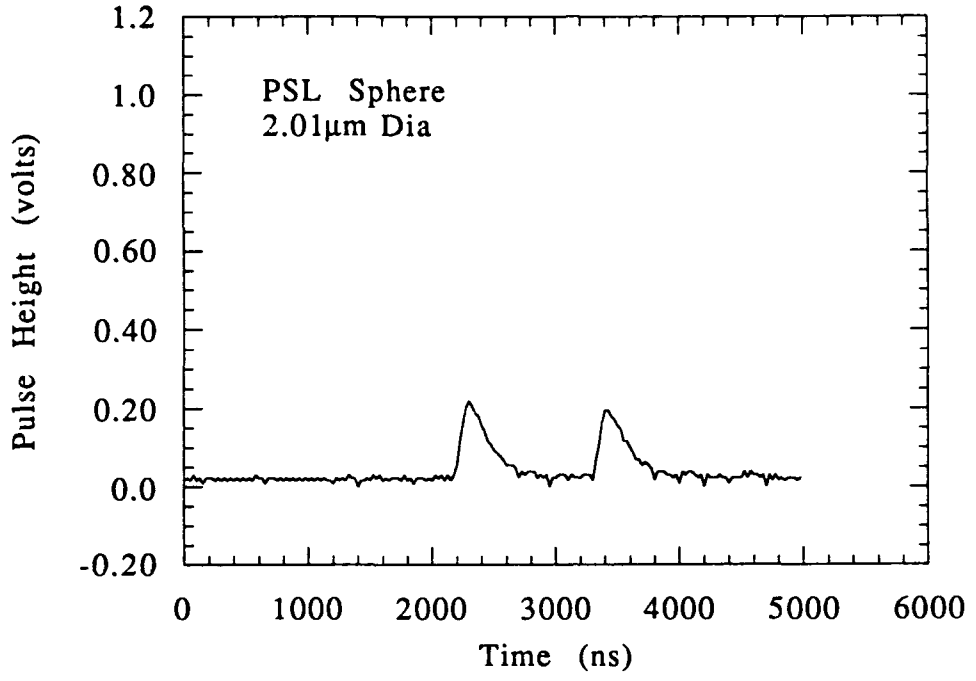

Figure 6.3 APS Pulse from 2.0 μm PSL Sphere

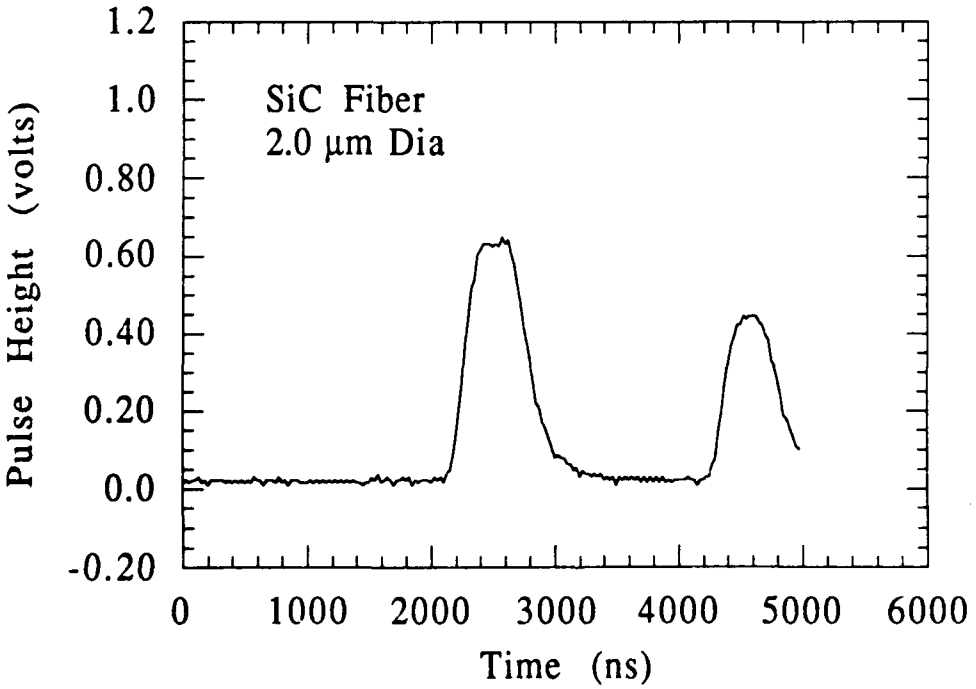

Figure 6.4 APS Pulse from a 2.0 μm SiC Fiber

two items initially mark this pulse pair as a fiber. The difference in shape is the result of the light scattering signal remaining constant for the short time that the fiber entirely fills the laser beam. The difference in pulse height is a result of each laser beam possessing a different polarization as discussed in Chapter 5. For this APS, the polarization of the first beam is parallel while the second beam is perpendicular. The transit time for the fiber pulse is 2100ns and the pulse width of the first pulse taken at the 50% height level is approximately 580ns. The distance between the laser beams is approximately 160 μm so the fiber velocity is 76.2m/s. Then, from the pulse width, the length of the fiber can be calculated to be about 44.2 μm. Using the APS calibration curve, the transit time can be converted to an aerodynamic diameter of 7.09 μm. The limits of aerodynamic diameter for a 44.2 μm SiC fiber parallel and perpendicular to the flow are respectively, 8.12 μm and 6.52 μm. Also, from the light scattering analysis the pulse heights for a fiber of this size should be about 0.9v and 0.62v for the first and second pulse. So it is obvious that this pulse pair does not meet all the criteria perfectly for a fiber of its size aligned parallel with the flow. However, it is reasonable to believe that this is an individual fiber.

The third pulse pair in Figure 6.5 has pulses of different height as a fiber would but the pulse shape is that of a spherical particle. In this case the particle is a fiber whose length is smaller than the width of the laser beam. That gives the pulse shapes the upside down "V" shape of a spherical particle. However, a spherical particle would not generate two different pulse heights. Because the fiber is too short, an accurate length measurement cannot be made and therefore the aerodynamic diameter cannot be calculated to compare to the measured aerodynamic diameter.

After looking at the differences in the pulse pairs of a fiber to a spherical particle and seeing how the pulse pairs are analyzed and counted, further study of many pulse pairs can be accomplished.

6.2.2 Fiber Count Analysis

In this section a comparison will be made between the number of individual fibers that can be identified using the APS and the number of individual fibers that actually passed through the APS. The number of fibers that actually pass through the APS was determined by filter sampling as described in section 6.1. For the 47mm, 0.4μm Nuclepore filters, at the given

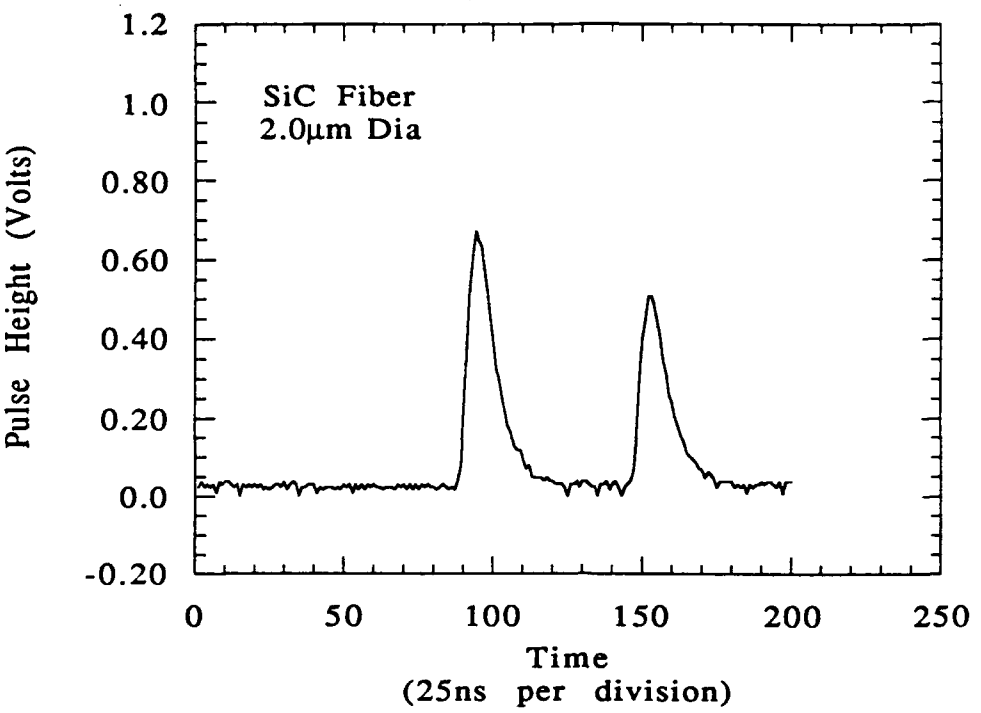

Figure 6.5 APS Pulse from a 2.0μm SiC Fiber

Nuclepore N040, Polycarbonate Membrane, 0.4-μm Pore

ΔP (cm Hg)	1	3	10	30
V (cm/sec)	2.9	9.7	31.9	94.0
D_p (μm)	Collection Efficiency (%)			
0.035	99.95	98.3	88	78
0.10	99.6	95.8	88	90
0.30	99.99	99.8	99.7	99.8
1.0	>99.99			

Figure 6.6 Nuclepore Filter Efficiency

sampling rate of 5LPM, (an approximate face velocity of 4.8 cm/s) the filter efficiencies are shown in Figure 6.6 (Marple 1983).

Basically three types of particles were seen on the filter samples, single fibers, clumps of two or more fibers, and other spherical "dust" particles. Figures 6.7-6.10 show SEM micrographs taken from the filter samples. Figure 6.7 shows that the SiC fibers are very much like a cylindrical rod. The presence of single fibers, fiber clumps, and "dust" particles can be seen in the next 3 figures. It is interesting to note that the fiber diameter is not very monodisperse. This becomes important and will be covered shortly.

Three filter samples were taken with sample times of 1 minute, 5 minutes, and 10 minutes. The results of the particle counts for each of the three samples are shown in Figure 6.11. In each case the majority of particles are single fibers but not a large majority. The single - fiber count ranges between 40% and 50% for all samples but the percentage of fiber clumps ranges from 20% to a little more than 40%. The amount of particles other than fiber hovers around the 20% mark.

As the sample time increases it is not unreasonable to expect the amount of single fibers to decrease and the amount of clumped fibers to increase as fibers deposit on top of one another on the filter. This is not evident between the 1 and 5 minute samples but is evident between the 5 and 10 minute samples. If the average of all three samples is taken the single fibers amount to 45.9% of the total count, the fiber clumps amount to 35.6%, and the "other" particles amount to 18.5%.

In determining the particle counts through the APS by viewing the pulse pairs, it is only possible to distinguish between individual fibers and other (spherical shaped) particles. This was done using the method describe in section 6.2.1. The process for viewing and/or saving individual pulse pairs with the digital oscilloscope available was quite slow as previously mentioned. Therefore, the results given represent the total counts of many separate experiments accomplished on different days but under the same operating conditions.

In viewing hundreds of pulse pairs, it was found that not all pulse pairs fit into the three categories mentioned in section 6.2.1. Some pulse pairs (in fact around 20% of the total pulses counted) had the different pulse height characteristic of a fibrous particle, however the first pulse was smaller than the second, opposite of what would be expected for an aligned fiber. Back in

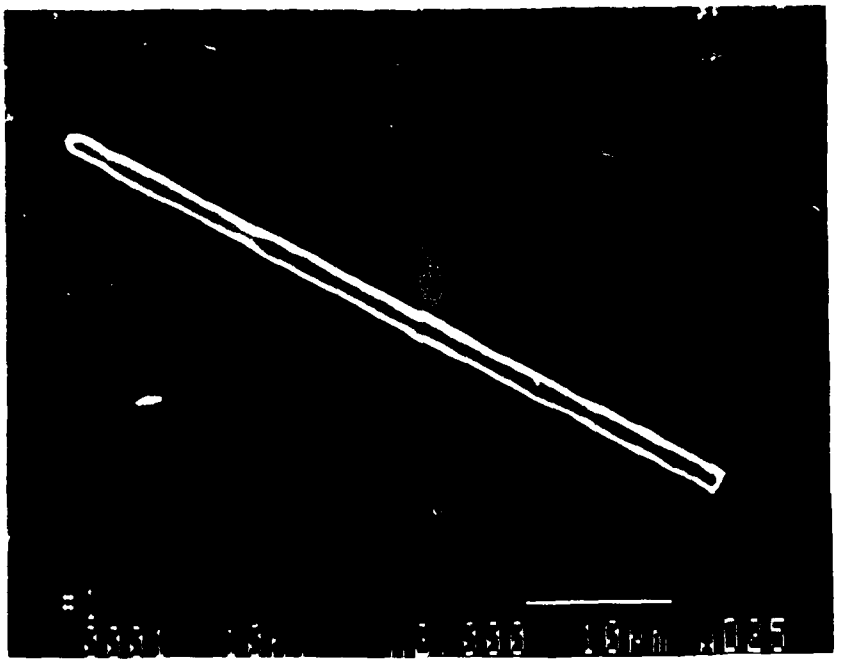

Figure 6.7 SEM Micrograph of 2.0 µm SiC Fibers on a 0.4 µm Nuclepore Filter (Magnification=X2000)

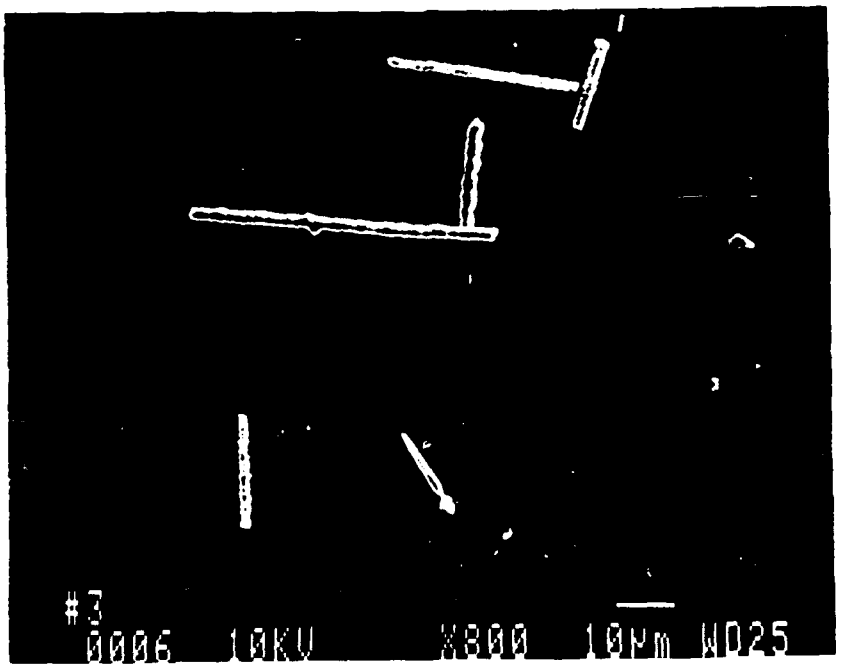

Figure 6.8 SEM Micrograph of 2.0 µm SiC Fibers on a 0.4 µm Nuclepore Filter (Magnification=X800)

Figure 6.9 SEM Micrograph of 2.0 µm SiC Fibers on a 0.4 µm Nuclepore Filter (Magnification=X400)

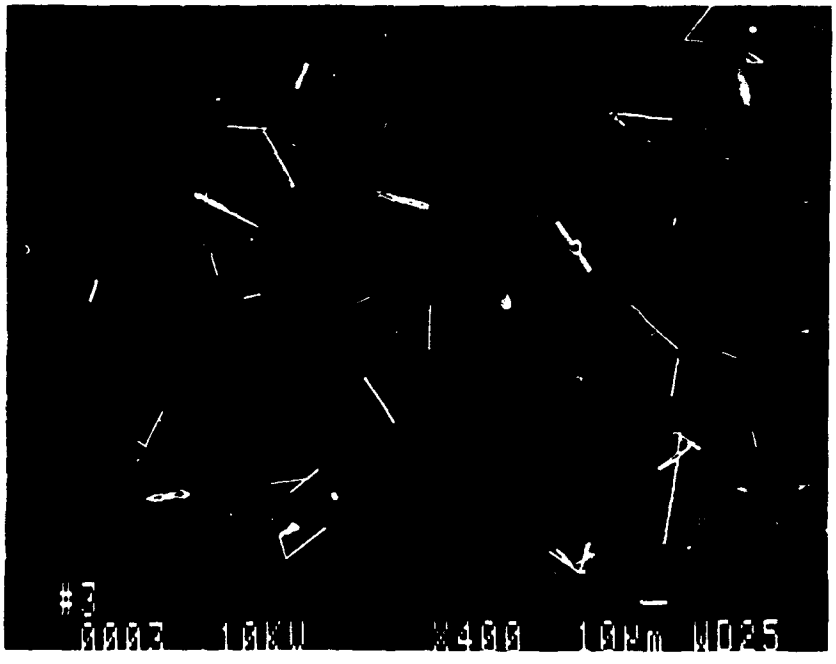

Figure 6.10 SEM Micrograph of 2.0 µm SiC Fibers on a 0.4 µm Nuclepore Filter (Magnification=X400)

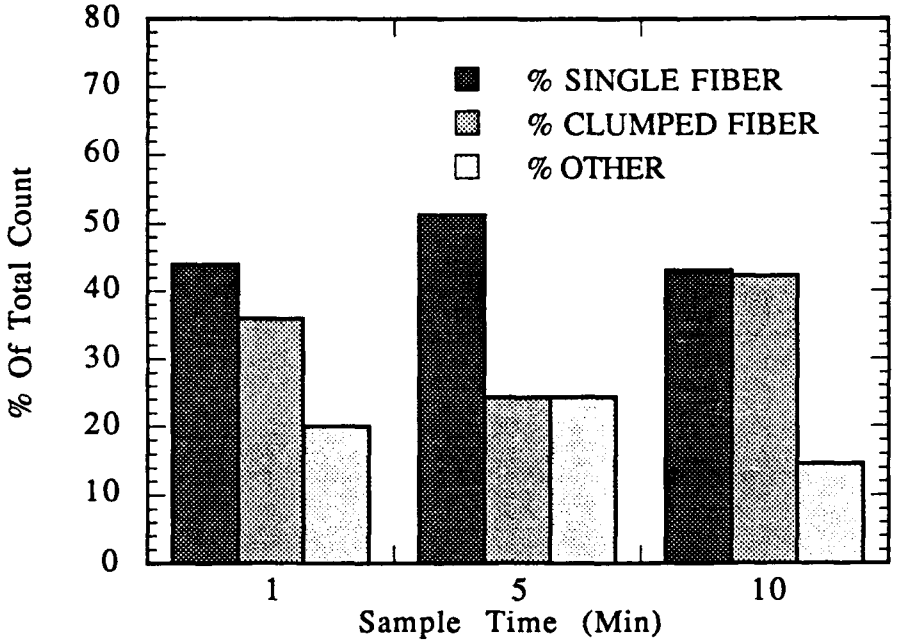

Figure 6.11 Percentages Of Fiber Counts From 2.0μm SiC Fiber Sampled onto a 25mm Nuclepore Filter (.4mm Pore Size) (5LPM Sample Rate)

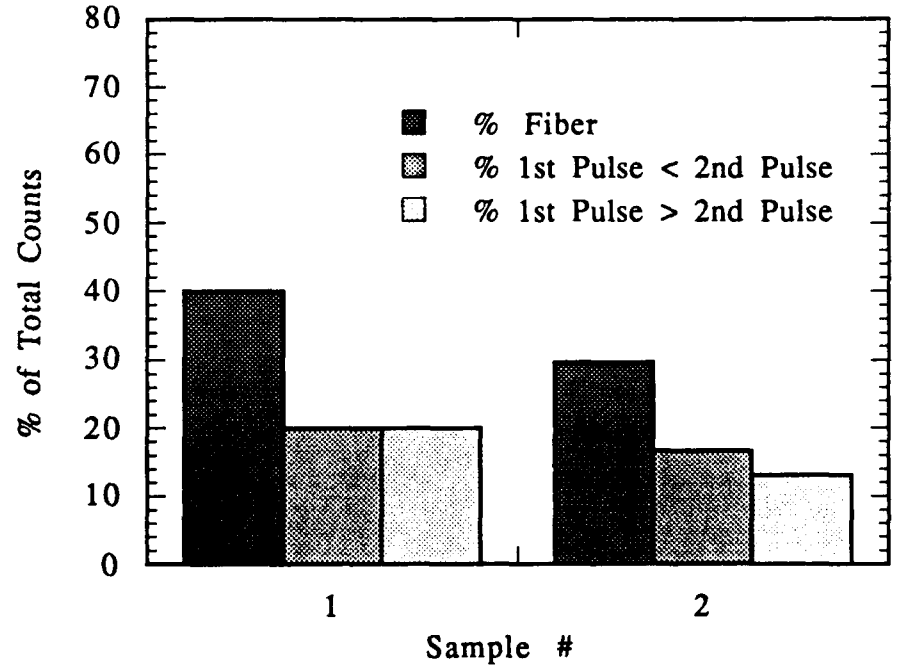

Figure 6.12 Percentage of Fiber Counts from 2.0 μm SiC Fiber Sampled Through an APS, Determined by Evaluating Individual Pulses

Chapter 5, the light scattering characteristics of fibers were discussed. Recall that the majority of scattered light from the fiber is in the plane perpendicular to the fiber polar axis (Van de Hulst 1957). If the fiber is not aligned parallel to the flow direction (i.e. it is tilted so that it is no longer perpendicular to the laser beams) then the scattered light reaching the detector will be less than if the fiber were aligned. A small pulse followed by a large pulse would indicate that a fibrous particle is flowing through the APS viewing volume but that its angle is changing as it proceeds from one beam to the other.

As the APS nozzle arrangement focuses particles to the center of the laser beams (Kinney 1990), it is not likely that a spherical particle would produce this type of pulse pair, but it is possible that a particle with some irregular shape might. To investigate this, atmospheric air was sampled into the APS and more than 1000 pulse pairs were viewed. Of these pulse pairs, 2% had the first pulse smaller than the second. This is significantly less than the amount viewed when sampling the 2.0 μm SiC fibers. From this, though it is somewhat speculative, it was determined to count these type of pulses as individual fibers.

Now that the methodology of evaluating the pulse pairs for fiber counting purposes has been thoroughly discussed, the results are presented. Figure 6.12 reveals that the total individual fiber count as determined by viewing individual APS pulse pairs is slightly less than as determined by counting fibers on the filter samples, however the results are promising. Note that of all the fibers counted, around half are of the type where the first pulse is smaller than the second. This would indicate that not all fibers are aligned exactly parallel to the flow direction as expected from the results of the numerical study. In fact, because the collecting lens is circular as seen by the fiber, the fiber must be out of alignment by about the 30^{o} maximum scattering collection angle to produce a pulse pair where the first pulse is smaller than the second. This leads to the next section where fiber alignment is investigated.

6.2.3 Fiber Alignment

The Fiber Alignment numerical study outlined in Chapter 5 indicates that all of the fibers in the size range used in these experiments should be very nearly parallel with the flow direction as they pass through the laser

beams. Already though, it was seen in counting the fibers, that many fibers are not aligned exactly with the flow and may in fact be rotating as they pass through the laser beams. However, an attempt was made to further evaluate that finding using the pulse pair data taken. The idea is that, for a fiber of known diameter, the pulse pair can be used to find a fiber length and a measured aerodynamic diameter. The fiber length and diameter can be used to calculate the aerodynamic diameter for that fiber travelling parallel with the flow. If the measured aerodynamic diameter and the calculated aerodynamic diameter are the same, the fiber is then properly aligned parallel with the flow.

The length of all the fibers counted cannot be measured. The length could be measured on only those fibers whose length exceeded the width of the laser beam. Only a few fibers met this qualification. Figure 6.13 shows the measured aerodynamic diameter of those fibers along with the calculated parallel and perpendicular fiber aerodynamic diameter for 3 fiber diameters. If the measured fibers were all truly 2.0 μm in diameter and aligned parallel with the flow direction, then all the points would fall on the solid line for a 2.0 μm diameter parallel fiber. It is obvious that not all of the fibers appear aligned. In fact many of the pulse pairs that were evaluated do not even fall within the limits for a 2.0 μm SiC fiber travelling parallel or perpendicular.

There are a couple reasons for this result. First, the fiber diameters are not all exactly 2.0 μm as assumed. As seen from the SEM micrographs, the fiber diameters are quite varied. In fact the average diameter of those measured using the SEM was 1.65 μm with the smallest seen being 0.55 μm in diameter and the largest seen being 4.0 μm in diameter. This is the reason for the limits of 0.55 μm and 4.0 μm shown on Figure 6.13. Second, according to Griffiths (1984) the aerodynamic diameter of fibrous particles whose aerodynamic diameter is less than 5μm is undersized by the APS. Nevertheless, this method of determining fiber alignment is not sensitive enough. Trying to capture the fibers on film as they exit the APS nozzle would be ideal for evaluating their alignment. The procedure was deemed too costly and time consuming for this study but is recommended for any future work.

6.2.4 Fiber Light Scattering Results

The light scattering analysis completed in Chapter 5 found the light scattering cross sections for PSL sphere and for fibers. To convert the light

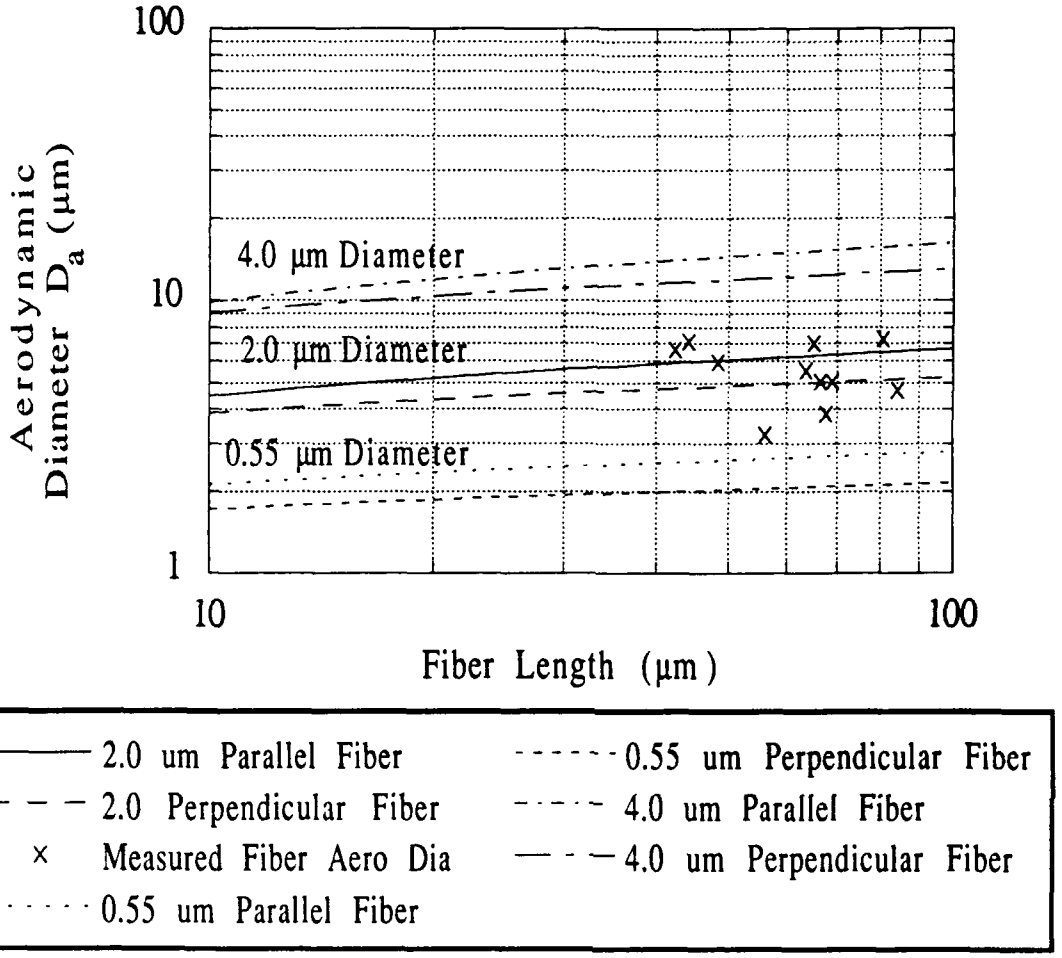

Figure 6.13 Aerodynamic Diameter (D_a) of Fibers Aligned Parallel and Perpendicular to the Flow with Measured D_a of Actual Fibers

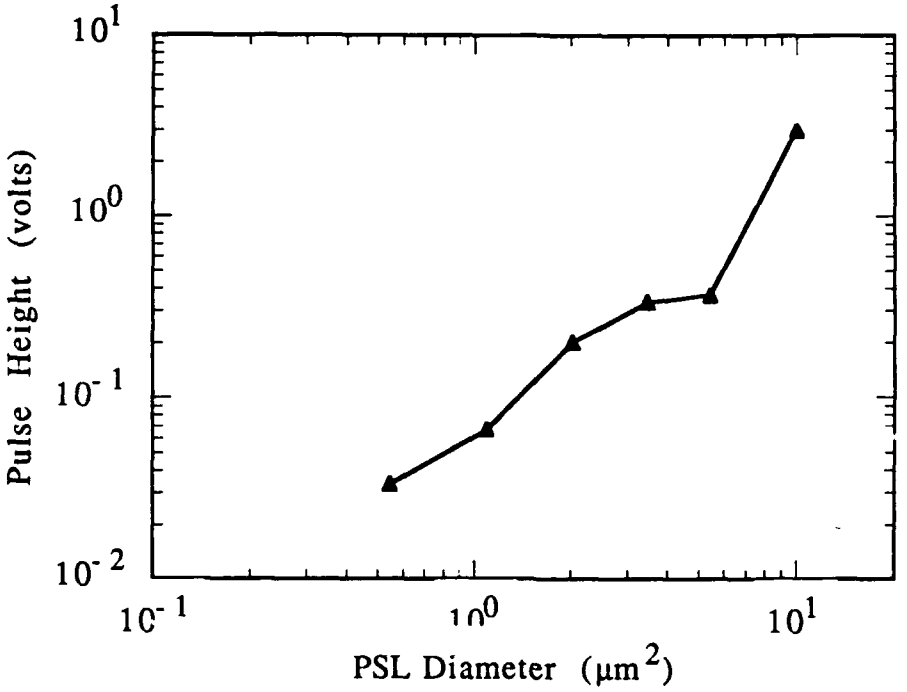

Figure 6.14 Pulse Height vs PSL Diameter, Pulse Heights taken from TSI APS Manual Appendix (Increased by a Gain of 3.3)

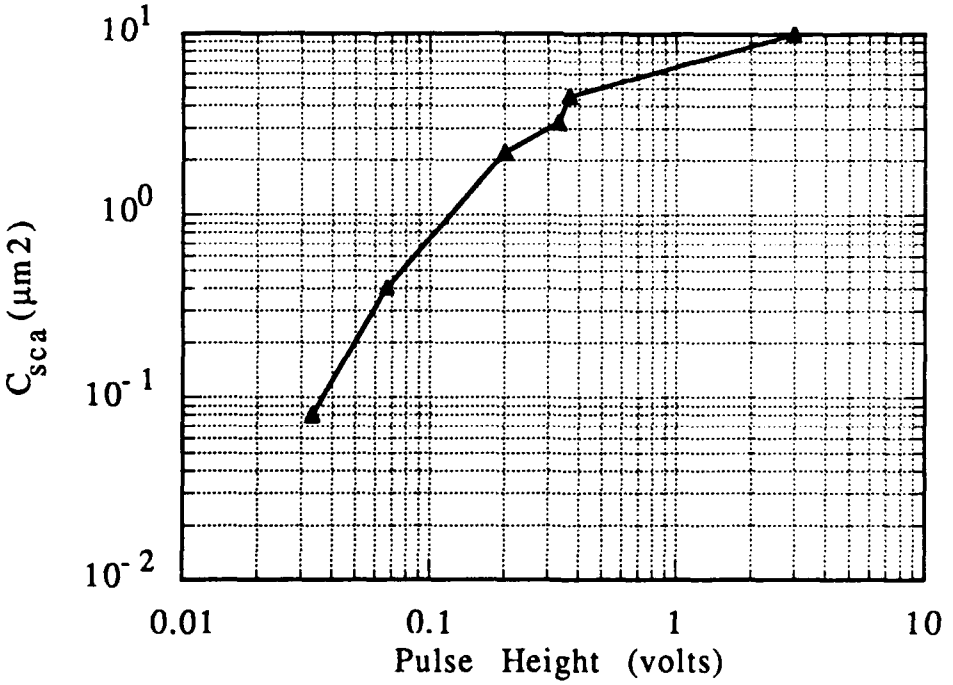

Figure 6.15 Scattering Cross Section vs Pulse Height, Pulse Height Data Taken From APS Manual Appendix (Increased by a Gain of 3.3)

scattering cross sections into a pulse height in volts for any given particle the following was done. Several pulse heights for PSL particles of different sizes were found in the TSI APS Manual. These pulse heights are plotted in Figure 6.14 corrected for the difference in the photomultipler tube gain setting on the APS used in this study. Then from the light scattering cross sections calculated for PSL spheres in Chapter 5, the light scattering cross section versus pulse height in volts was plotted in Figure 6.15. Now knowing the scattering cross section for 2μm SiC Fibers from Figure 5.21 for fibers which are longer than the laser beam width, Figure 6.15 is used to find that the pulse heights will be about 0.9 volts and 0.62 volts for the first and second pulses of each pair.

The pulse heights for the same fibers examined for fiber alignment are shown in Figure 6.16. For three of the pulse pairs, the pulse height could not be determined as they exceeded the limit of 1 volt for the photomultiplier tube. The others are in reasonable agreement with the calculated values. Again, the spread of fiber diameter may account for the smaller heights in some pulses and the pulses that exceeded the photomultiplier tube limit may actually be a fiber with some other particle or fiber adhered to it. There is no proof however of this explanation.

6.3 CONCLUSIONS

Clearly, it is possible to identify and size fibrous particles using the methods proposed for the RFA. Fibers which are shorter than the laser beam width can be identified by the difference in their pulse pair height. Fibers which are longer than the laser beam width can be identified in the same manner, plus their length, aerodynamic diameter, and diameter can be determined.

The experiments showed that the fiber count from the unmodified APS nearly matches the fiber count determined from filter sampling of the fibrous aerosol. This in itself is significant for it shows that the RFA will certainly be able to distinguish fibers from other particles.

The numerical analysis of the fiber alignment from Chapter 5, indicating that the fibers used would be aligned parallel to the flow direction, was not borne out by the experimental results. It is speculated that some fibers are even rotating as they pass from the first to the second laser beam.

Out of all of this, the main conclusion to be drawn from the

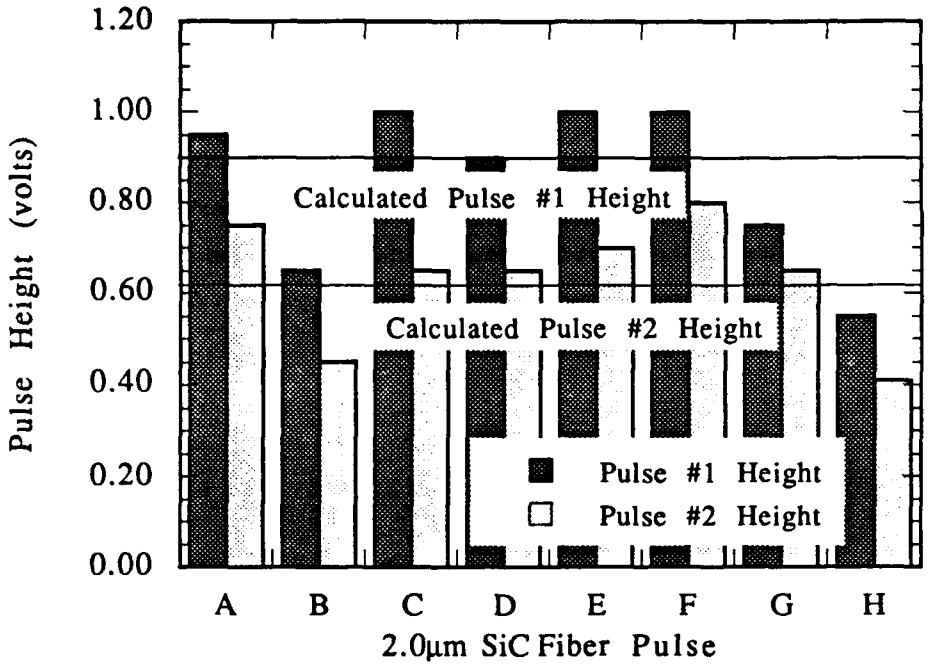

Figure 6.16 Actual Pulse Pair Heights for Several 2.0 μm SiC Fiber Pulses

experimental results is that the RFA is feasible. Much work remains to be done, but these results provide a starting point and also give some direction to the modifications which will be necessary for a working instrument. The modifications and recommendations for future work are discussed in the next chapter.

CHAPTER 7
CONCLUSIONS AND RECOMMENDATIONS

The purpose of this study was to ascertain the feasibility of creating a Real-time Fiber Analyzer by modifying a TSI Aerodynamic Particle Sizer. Simply stated, the end result of the study is yes, it is feasible. Stated in more realistic terms, some of the aspects of the instrument work well while other aspects have problems. This chapter will summarize all aspects studied and explore possible solutions to those aspects with problems. Recommendations will also be made for future study and possible directions for instrument development.

7.1 SUMMARY

7.1.1 Fiber Alignment

The alignment of the fibers as they progress through the instrument was found to be of great importance to the operation of the instrument. The fibers must be aligned parallel with the flow direction of the APS (perpendicular to the incident laser beams). The possible methods of accomplishing this discussed in this study were electrostatic rotation and rotation in a shear flow. Because rotation in a shear flow would require less modification to the APS, it was studied first.

A computer program by Ye and Pui (1990) to calculate the translation and orientation of a prolate ellipsoid as it passed through an abrupt contraction was modified to calculate the same thing for various APS nozzle designs. The designs modeled were a 60^{o} standard APS nozzle, a 2^{o} nozzle, and a 90^{o} nozzle. All exhibited the ability to align the fibers properly but the 60^{o} nozzle was chosen because it provides a better APS resolution. The trajectories and orientation of fibers travelling through the 60^{o} nozzle can be reviewed in Figures 5.2-5.5.

The results show that very large fibers will have problems with both alignment and transport losses as seen in Figures 5.14b and 5.15. The other fibers considered, however, regardless of initial orientation and position will

be aligned very close to parallel with the flow. From this it was determined that the shear flow through the nozzle would be sufficient to align the fibers and electrostatic rotation was no longer considered.

The experimental results showed that perhaps the alignment of the fibers was not as predicted by the numerical analysis. Two items point to this conclusion. First, for the APS used, the pulse pair of an aligned fiber would be characterized by the height of the first pulse being greater than the height of the second. But for around half of the possible fiber pulse pairs identified, the height of the first pulse was less than the height of the second. Because most of the scattered light from a fiber is scattered in a plane perpendicular to the fiber axis, a fiber that is not aligned properly will scatter less light than one that is aligned. This would indicate then, that some fibers are rotating as they travel from one laser beam to the other. The second item that points to unaligned fibers is best seen in Figure 6.13, where calculated fiber aerodynamic diameter is compared to measured fiber aerodynamic diameter for fibers which are longer than the APS laser beam width. If the fibers are all truly 2.0 μm in diameter and were all aligned, then all of the measured points would fall on the line of parallel fiber aerodynamic diameter. The results in Figure 6.13 can be explained by the fact that not all of the fibers are exactly 2.0 μm in diameter and also that the APS may underestimate the aerodynamic diameter of nonspherical particles (Griffiths 1984). Certainly, Figure 6.13 does not prove that the fibers are properly aligned.

7.1.2 Fiber Light Scattering

The light scattering characteristics for an infinite cylinder with a perpendicular incident beam were modeled for the optical configuration within a TSI APS. The program used was based on a program from Bohren and Huffman (1983). Different types of fibers were modeled and compared to the light scattering characteristics of spherical particles. As is seen in Figures 5.21 - 5.23, a spherical particle has approximately the same scattering cross section regardless of the incident beam polarization while the fibrous particles shown have different scattering cross sections for the different incident beam polarizations. Because each of the laser beams in the APS has a different polarization, this will provide a means of distinguishing fibers from other particles. Note that for the Carbon Graphite and asbestos fibers, a range of diameters exists where distinguishing a fiber from a spherical particle by

scattering cross section will not work. By examining the scattering intensity functions as shown in Figures 5.17-5.20 however, an optimum range of collection angles exists where full advantage can be taken of the distinguishing characteristics. This will be discussed further in the next section.

Upon viewing actual pulse pairs taken during experiments with 2.0 μm SiC fibers and 2.01 μm PSL spheres (see Figures 6.3 and 6.4) it is apparent that the distinguishing characteristics identified in the light scattering analysis work. In other words, spherical particles generate pulse pairs in which the first and second pulse are the same amplitude, whereas fibrous particles generate pulse pairs in which the first and second pulse are of different amplitudes. As with everything the information to be gained from the light scattering has limitations. It was found that for fibers whose length is less than the width of the APS laser beam, the pulse pair will be peaked similar to a spherical particle except that the amplitude of the pulse pair is still different. This can be seen in Figure 6.5. In this case the particle can be identified as a fiber but it is not possible to measure its length or diameter as it is for the "square" pulse pair of Figure 6.4. To verify the accuracy of the light scattering program, the pulse heights of the actual fiber pulses were compared to the pulse heights as predicted by the program in Figure 6.16. The two are in good agreement.

The information gained from the light scattering analysis was used to test the viability of the APS as an RFA. The SiC fibers were sampled onto a Nuclepore filter and counted with the results shown in Figure 6.11. Between 40% and 50% of the total particles counted on the filter were individual fibers. SiC fibers were also sampled under the same conditions through an APS and the individual pulse pairs were viewed and a determination was made based on the above light scattering characteristics as to whether or not the particle was a fiber. As shown in Figure 6.12 between 30% and 40% of all pulse pairs viewed were identified as fibers. This is in reasonable agreement with the fiber counts obtained from the filter samples for an APS which was not modified in any way for fiber measurement.

Clearly, it is possible to distinguish fibers from spherical particles with an instrument such as this and it is also possible to measure their dimensions in some cases. However, the instrument is far from being a reality for several reasons which have been previously identified. In the next section possible

solutions for the problems will be discussed.

7.2 Recommendations

The main problems identified with the instrument thus far are:

-fibers not properly aligned parallel to the flow change the light scattering signature seen and impede fiber dimension measurement

-laser beam width limits the ability to measure fiber dimensions

-fibers of different material may not be identifiable over certain ranges of diameter

Of course there are a host of other obstacles to overcome in developing an instrument including things such as instrument sampling efficiency and circuitry development. But this study focused on the former problems as the starting point for any future work.

In attacking these problems some decisions on the direction of the instrument must be made. For instance, is it of prime concern for a particular user to know the fiber dimensions or is it more important to simply identify a particle as a fiber. Will the instrument be used in a specific application for a known type of fiber or will it need to be able to work over a wide range of fiber types. These questions need to be answered from a marketing viewpoint in the long run. For this study, two general directions will be explored. For each direction, possible solutions to the above problems will be presented as a guide for future work.

The directions for instrument development presented here will be: 1) for an instrument that will distinguish fibers from spherical particle with no dimension measurement concern, and 2) for an instrument that will both distinguish fibers from spherical particles and measure their length, diameter, and aerodynamic diameter. Obviously the second will be more expensive to produce than the first.

Before discussing solutions for the two instrument directions, one recommendation must be made and that is for further study of the light

scattering and especially the fiber alignment. As previously noted, the results of the fiber alignment analysis did not conclusively prove the fibers to be either in or out of alignment. It is possible that other explanations exist for the results seen here. The most sure way to do this would be to photograph the fibers as they exit the nozzle although this could prove difficult. The fibers are very small and travel at velocities of around 100m/s.

7.2.1 Instrument With Only Fiber Distinguishing Capabilities

Recommendations

-Provide elliptical mirror or other arrangement in the collection optics to allow the majority of scattered light to be collected regardless of fiber orientation

-Vary the scattered light collection angle to optimize the difference in pulse pair height for fibers while maintaining the constant pulse pair height for spheres

As mentioned, one of the instrument problems is that the fibers may not be aligned or may be changing alignment as they proceed from one beam to the next. Because the majority of light scattered from a fiber is in the plane perpendicular to the fiber polar axis (Van de Hulst 1957), a fiber which is not in alignment will provide a much weaker pulse than one that is in alignment. This is the probable cause for some pulse pairs having the first pulse larger than the second and some pulse pairs being the other way around. Providing an elliptical collection mirror or some other arrangement will allow the instrument to collect the light scattered from the fiber even if it is out of alignment by some margin. This will insure a capability to distinguish fibers from spherical particles.

Also, in looking back on Figures 5.17-5.20, 2 μm PSL Spheres maintain roughly the same scattering intensity function regardless of the incident light polarization until a scattering angle of about 80^{o} is reached. The APS currently is set up with a collection angle of about 12^{o}-30^{o}. For the fibers examined, the difference in the scattered intensity function increases from about 30^{o} to around 80^{o}. This suggests that by changing the collection angle

the ability to distinguish spherical particles from fibers over a large diameter range will be improved.

7.2.2 Instrument With Distinguishing and Measurement Capabilities

Recommendations

-Insure proper fiber alignment through electrostatic means

-Develop a narrower laser beam to improve the length measurement sensitivity

-Vary the scattered light collection angle to optimize the difference in pulse pair height for fibers while maintaining the constant pulse pair height for spheres

As Lilienfeld (1985) has shown, it is possible to align most types of fiber electrostatically. This alignment force can be very strong so that the alignment of the fibers would be positively known and fiber dimension measurements would be that much more accurate. At the same time, it is possible for a Helium-Neon laser to be focussed down to a width of between 5 and 10 μm to increase the instruments sensitivity to length. Recall that fiber length can only be measured for those fibers whose length is greater than the laser beam width. Finally, the collection angle can again be studied to provide increased distinguishing characteristics as discussed before. It is clear that such modifications will require a good deal of study and be more costly than the first set of modifications covered, but the abilities of the instrument in this case have a much greater potential.

REFERENCES

Al-Chalabi, S.A.M., A.R. Jones, H. Savaloni, and R. Wood (1990) "Light-Scattering Method to Discriminate and Size Small Diameter Fibres," Measurement Sci. and Technology 1: 29-35.

Bohren, Craig F. and Donald R. Huffman (1983) Absorption and Scattering of Light by Small Particles, John Wiley & Sons, New York.

Caldow, Rob (1992) Telephone Conversation on 3 January 1992.

Chae, Seung-Ki (1991) Light Scattering Applications For Microcontamination Control and Radiative Properties Determination, Ph. D. Thesis, University of Minnesota.

Chan, Tai L., James B. D'Arcy, and Bradley W. Kibbel (1991) "Exposure Assessment of Silicon Carbide Whiskers and Organic Aerosols for Safe Manufacture of Metal Matrix Composites," Conference on Advanced Composites, ACGIH.

Corpon, Mark (1990) A Feasibility Study of a Fiber Monitor, ME Honors Thesis, University of Minnesota, June 8, 1990.

Dahneke, Barton E. (1973) "Slip Correction Factors for Nonspherical Bodies II and III," Aerosol Sci. Tech. 4: 147-170.

Detenbeck, R.W. (1980) "Feasibility Study for an Asbestos Aerosol Monitor," EPA-600/2-80-200, U.S. EPA, Research Triangle Park, N.C. 27711.

Environmental Asbestos Assessment Manual, "Superfund Method for the Determination of Asbestos in Ambient Air," EPA/540/2-90/005b, May 1990.

Farone, W. A., Kerker, M., and Matijevic, E. (1963) ICES Electromagnetic Scattering (Edited by Kerker, M.) Macmillian, New York.

Fish, B.R. (1974) "Aerosol Physics of Asbestos Fibers: Interception," ORNL-TM-4051, Oak Ridge National Laboratory, Oak Ridge, TN.

Fuchs, N. A. (1964) The Mechanics of Aerosols, Pergamon, New York.

Griffiths, W.D., S. Patrick, and A.P. Rood (1984) "An Aerodynamic Particle Size Analyzer Tested With Spheres, Compact Particles and Fibres Having a Common Settling Rate Under Gravity," J. Aerosol Sci. 15: 491-502.

Jones, A. R. and Purewall, S. S. (1982) J. Phys. D: Appl. Phys. 15: 2135-2147.

Jones, A. R. and Savaloni, H. (1989) Part. Syst. Char. 6: 110-118.

Kaufman, Stan (1992) Telephone Conversation on 16 January 1992.

Kinney, Patrick D. (1990) Inlet Efficiency Study for the TSI Aerodynamic

Particle Sizer, Masters Thesis, University of Minnesota.

Lilienfeld, P. and P.B. Elterman (1977) "Development and Fabrication of a Prototype Fibrous Aerosol Monitor (FAM)," DHEW (NIOSH) Pub. No. 78-125, NIOSH, Cincinnati, OH 45226.

Lilienfeld, P., P.B. Elterman, and P. Baron (1979) "Development of a Prototype Fibrous Aerosol Monitor," Am. Ind. Hyg. Assoc. J. 40: 270-282.

Lilienfeld, P. (1985) "Rotational Electrodynamics of Airborne Fibers," J. Aerosol Sci. 16: 315-322.

Lilienfeld, P. (1987) "Light Scattering from Oscillating Fibers at Normal Incidence," J. Aerosol Sci. 18: 389-400.

Liu, B.Y.H., D.Y.H. Pui, X.Q. Wang, and C.W. Lewis (1983) "Sampling of Carbon Fiber Aerosols," Aerosol Sci. Tech. 2: 499-511.

Marple, Virgil A. and Benjamin Y.H. Liu (1983) Aerosols in the Mining and Industrial Work Environments, Volume 3, Instrumentation, Ann Arbor Science Publishers, Ann Arbor Michigan.

Patankar, S.V. (1979) Numerical Heat Transfer and Fluid Flow, McGraw-Hill-Hemisphere Publication, New York.

Rajhans, G.S., Sullivan J.L. (1981) Asbestos Sampling and Analysis, Ann Arbor Science Publishers, Inc., Ann Arbor, MI.

Rooker, S.J., N.P. Vaughan, and J.M. LeGuen (1982) "On the Visibility of Fibers by Phase Contrast Microscopy," Am. Ind. Hyg. Assoc. J. 43: 505-515.

Van de Hulst, H.C. (1957) Light Scattering By Small Particles, John Wiley & Sons, New York.

Yan Ye and David Y.H. Pui (1990) Numerical Simulation of Translation and Rotation of a Non-Spherical Particle in a Tube with an Abrupt Contraction, University of Minnesota Supercomputer Institute Research Report UMSI 90/249, Minneapolis, Minnesota.

Zumwalde, R.D., and J.M. Dement (1977) "Review and Evaluation of Analytical Methods for Environmental Studies of Fibrous Particulate Exposures," DHEW (NIOSH) Publication No. 77-204, NIOSH, Cincinnati, OH 45226.

APPENDIX A
FIBER ALIGNMENT PROGRAM

```
C
C*********************************************************************
C     THIS IS A PROGRAM TO CALCULATE THE MOTION TRAJECTORY AND
C     THE ORIENTATION OF A PARTICLE IN A SPECIFIED FLOW
C           AUTHOR: YAN YE
C           DATE:       NOV. 15, 1989
C*********************************************************************
      PROGRAM NSPTO
      INCLUDE 'PAT2D.CMN'
      CHARACTER*40,PATTERN
      COMMON/FILES/PATTERN
      COMMON/CONTROL/ISINGLE
      COMMON/PARTICLE/B,EU(3),DE
      COMMON/NSY/NSY1/NSY2,NSY3,NSY4,NSY5,NSY6,NSY7,NSY8,NSY9,NSY10
      COMMON/NSX/NSX1/NSX2,NSX3,NSX4,NSX5,NSX6,NSX7,NSX8,NSX9,NSX10
      DATA LISFIL,INPUTF,SAVEF/'PART.LIS','USER.DAT','PART.DAT'/
      DATA PATTERN/'PATTERN.LIS'/
C-------------------------------------
      CALL GRID
      CALL SETUP1
1     CALL START
      CALL INPUT
      CALL GAMSOR
      CALL IMPINGE
C     CALL SAVE
      STOP
      END
C*********************************************************************
      SUBROUTINE SETUP1
C*********************************************************************
      INCLUDE 'PAT2D.CMN'
      L2=L1-1
      M2=M1-1
      X(1)=XU(2)
      DO 5 I=2,L2
    5 X(I)=0.5*(XU(I+1)+XU(I))
      X(L1)=XU(L1)
      Y(1)=YV(2)
      DO 10 J=2,M2
   10 Y(J)=0.5*(YV(J+1)+YV(J))
      Y(M1)=YV(M1)
      DO 101 I=1,L1
      DO 101 J=1,M1
101   RHO(I,J)=RHOCON
      RETURN
      END
C
C*********************************************************************
      SUBROUTINE FILSPC
C*********************************************************************
C     SPECIFY THE OUTPUT AND INPUT FILENAMES
      INCLUDE 'PAT2D.CMN'
      CHARACTER*40,PATTERN
      COMMON/FILES/PATTERN
      COMMON/CONTROL/ISINGLE
      COMMON/CRITIC/XX(12),RR(7),IXX(12),JRR(7),IXXT(12),JRRT(7)
      COMMON/PARTICLE/B,EU(2),DE
600   FORMAT(' SPECIFY INPUT VEL DATA FILE:'/4X,'DEFAULT= ',A40)
```

```
620   FORMAT(' SPECIFY OUTPUT DATA FILE :'/4X,'DEFAULT= ',A40)
630   FORMAT(' SPECIFY LISTING FILE:'/4X,'DEFAULT= ',A40)
640   FORMAT(' SPECIFY DEPOSITION PATTERN FILE:'/4X,'DEFAULT= ',A40)
      RETURN
C*****************************************************************
C     ENTRY UGRID
C       UGRID FOR NONUNIFORM GRID USED IN THE PROGRAM IS GIVEN
C       USER SUBROUTINE
C     RETURN
C*****************************************************************
C
      ENTRY INPUT
C
      OPEN(UNIT=2,FILE=INPUTF,STATUS='OLD')
      DO 410 NF=1,2
      READ(2,*)
      READ(2,420)((F(I,J,NF),I=1,L1),J=1,M1)
420   FORMAT(1X,10(E12.5,1X))
410   CONTINUE
      CLOSE(UNIT=2)
C--------------NON-DIMENSIONALIZE VELOCITIES
      DO 430 NF=1,2
      DO 430 J=1,M1
      DO 430 I=1,L1
430   F(I,J,NF)=F(I,J,NF)/UIN
C--------------INPUT OTHER PARAMETERS
      OPEN(6,FILE='SOLID.DAT',STATUS='OLD')
      READ (6,424) DP,B,ROP,ISINGLE
      WRITE (*,425) DP,B,ROP,ISINGLE
424   FORMAT (41X,F15.6,/,41X,F15.6,/41X,F15.6/41X,I7,/)
425   FORMAT (4X,'PARTICLE DLAMETER (MICRON)          :',F15.6,/
     +         ,4X,'PARTICLE AXES RATIO (a/b>1)       :',F15.6,/
     +         ,4x,'PARTICLE DENSITY (g/cc)           :',F15.6/
     +         ,4X,'RUN MODE                          :',I7,/)
C
      W=2.*YL      ! CHARACTERISTIC LENGTH
      PR=DP*0.5E-4/W ! CHANGED TO DIMENSIONLESS
C
C       MAKE THE GRID POSITIONS NONDIMENSIONLESS
      DO 499 I=1,L1
      X(I)=X(I)/W
      IF(I.GE.2) XU(I)=XU(I)/W
499   CONTINUE
      DO 502 J=1,M1
      Y(J)=Y(J)/W
      IF(J.GE.2) YV(J)=YV(J)/W
502   CONTINUE
      RETURN
C
      ENTRY SAVE
      IF(ISINGLE.NE.2) RETURN
      OPEN (UNIT=3,FILE=SAVEF,STATUS='NEW')
      WRITE(3,233) ITOTAL
233   FORMAT(2X,I3)
      DO 333 I=1,ITOTAL
C      WRITE(3,244) XP(1,I),YP(1,I)
244   FORMAT(2(2X,F15.11))
333   CONTINUE
```

```
      CLOSE(UNIT=3)
      RETURN
C
      ENTRY PRINT
      RETURN
C
      ENTRY CHECK
C
10     FORMAT('1',26(1H*),3X,A10,3X,44(1H*))
20    FORMAT(1X,4H I =,I7,8I12)
30    FORMAT(1X,1HJ)
40    FORMAT(1X,I2,1P9E12.2)
50    FORMAT(1X,1H )
51    FORMAT(1X,'I =',2X,9(I4,5X))
52    FORMAT(1X,'X =',1P9E9.2)
53    FORMAT(1X,'TH =',1P9E9.2)
54    FORMAT(1X,'J =',2X,9(I4,5X))
55    FORMAT(1X,'Y =',1P9E9.2)
C-----------------
      OPEN(UNIT=5, FILE='CHECK.LIS', STATUS='NEW')
      WRITE (5,50)
      IEND=0
301   IF(IEND.EQ.L1) GO TO 310
      IBEG=IEND+1
      IEND=IEND+9
      IEND=MIN0(IEND,L1)
      WRITE (5,50)
      WRITE (5,51),(I,I=IBEG,IEND)
      IF(MODE.EQ.3) GO TO 302
      WRITE (5,52),(X(I),I=IBEG,IEND)
      GO TO 301
302   WRITE (5,53),(X(I),I=IBEG,IEND)
      GO TO 301
310   JEND=0
      WRITE (5,50)
311   IF(JEND.EQ.M1) GO TO 320
      JBEG=JEND+1
      JEND=JEND+9
      JEND=MIN0(JEND,M1)
      WRITE (5,50)
      WRITE (5,54),(J,J=JBEG,JEND)
      WRITE (5,55),(Y(J),J=JBEG,JEND)
      GO TO 311
C
320   DO 999 N=1,2
      NF=N
      WRITE (5,50)
      IFST=1
      JFST=1
      IBEG=IFST-9
110   CONTINUE
      IBEG=IBEG+9
      IEND=IBEG+8
      IEND=MIN(IEND,L1)
      WRITE (5,50)
      WRITE (5,20),(I,I=IBEG,IEND)
      WRITE (5,30)
      JFL=JFST+M1
```

```
      DO 115 JJ=JFST,M1
      J=JFL-JJ
      WRITE (5,40),J,(F(I,J,NF),I=IBEG,IEND)
115   CONTINUE
      IF(IEND.LT.L1) GO TO 110
999   CONTINUE
      CLOSE (UNIT=5)
      RETURN
      END
C*****************************************************************
C           SUBROUTINE TO CALCULATE CRITICAL POSITION          *
C*****************************************************************
      SUBROUTINE CRITI(XINT,YINT,YF,YCR,KK)
      INCLUDE 'PAT2D.CMN'
      DATA EP/5.0E-4/,YINT1/0.001/,YINT2/0.015/
      IF (KK.GT.0) GO TO 15
C
C      SET START POSITION FOR CALCULATION
5     PRINT 10, YINT1*W,YINT2*W
10    FORMAT('  INPUT INITIAL POSITION IN CENTIMETERS'/'DEFAULT
     +               YINT1=',F10.5,'   YINT2=',F10.5).
      READ(*,*,ERR=5) DYINT1,DYINT2
15    IF (DYINT1.GT.0.0) YINT1=DYINT1/W
      IF (DYINT2.GT.0.0) YINT2=DYINT2/W
C
C     INITIAL CALCULATION
      YINT=YINT1
      CALL IMPACT
      IF(ABS(YF-YV(NSY10)).LE.EP) GO TO 110
      YF1=YF-YV(NSY10)
      YINT=YINT2
C     PRINT*,'YF1=',YF1,'YF=',YF,'YV(NSY10)=',YV(NSY10)
      CALL IMPACT
      IF (ABS(YF-YV(NSY10)).LE.EP) GO TO 110
      YF2=YF-YV(NSY10)
C     PRINT*,'YF2=',YF2,'YF=',YF,'YV(NSY10)=',YV(NSY10)
      IF ((YF1*YF2).GE.0.0) GO TO 5
C
C     REGULAR CALCULATION
100   YINT=YINT2-YF2*(YINT2-YINT1)/(YF2-YF1)
      CALL IMPACT
      IF (ABS(YF-YV(NSY10)).LE.EP) GO TO 110
      YF3=YF-YV(NSY10)
      IF ((YF2*YF3).LT.0.0) THEN
       YINT1=YINT2
       YF1=YF2
      ELSE
       YF1=YF1*0.5
      ENDIF
      YF2=YF3
      YINT2=YINT
      IF (ABS(YINT2-TINT1).GT.EP) GO TO 100
      IF (ABS(YINT2).LT.ABS(YINT1)) THEN
       YINT=YINT2
      ELSE
       YINT=YINT1
      ENDIF
110   YCR=YINT
```

```
      RETURN
      END
C*****************************************************************
C            SUBROUTINE TO CALCULATE PARTICLE TRAJECTORY
C*****************************************************************
      SUBROUTINE IMPINGE
      INCLUDE 'PAT2D.CMN'
      CHARACTER*40,PATTERN
      LOGICAL CRTIC,SAME,CONT
      COMMON/FILES/PATTERN
      COMMON/CONST/C1(2),C2(2),C3(2),C4(2)
      COMMON/CRITIC/XX(12),RR(7),IXX(12),JRR(7),IXXT(12),JRRT(7)
      COMMON/CAL/ISTOKE,STK,STKB,GHAT,REYLOC,CD,SLIP0,SLIP1,VREL,RE
      COMMON /WALL/SOLID
      COMMON /PARTICLE/B,EU(3),DE
      COMMON/CONTROL/ISINGLE
      COMMON/GRAD/GRAD(2)
      COMMON/GRID/I,J
      COMMON/NSY/NSY1/NSY2,NSY3,NSY4,NSY5,NSY6,NSY7,NSY8,NSY9,NSY10
      COMMON/NSX/NSX1/NSX2,NSX3,NSX4,NSX5,NSX6,NSX7,NSX8,NSX9,NSX10
      DIMENSION PAR(6),YT(6),FF(6),ETA(6),TEMP(20),RAT(2)
      DIMENSION YST(30),YP(4)
      DIMENSION PAR1(6),PAR2(4)
      DATA YST(1)/0.005/
      DATA RAT/1.0,1.0/
      EXTERNAL DERIV
      DATA ETB,ETA/1.0E-3,6*1.0E-3/
      DATA CRTIC,CONT,SAME/2*.FALSE.,.TRUE./
      DATA FACTORA,FACTORB,FACTORC/0.5,0.95,0.95/
      DATA PI/3.141592654/
      IF(ISINGLE.EQ.2) THEN    ! SINGLE RUN
          OPEN(UNIT=1,FILE=LISFIL,STATUS='NEW')
      ELSE                     ! PATTERN RUN
          OPEN(UNIT=2,FILE=PATTERN,STATUS='NEW')
      ENDIF
C----------------   RUN MODE 2   ----------------
C  CALCULATE SINGLE PARTICLE TRAJECTORY
      IF(ISINGLE.EQ.2) THEN
      READ (6,7) YINT,XINT,EU(2),IFLAG
      WRITE (*,11) YINT,XINT,EU(2),IFLAG
7     FORMAT (41X,F15.6,/,41X,F15.6,/,41X,F15.6,/41X,I7)
11    FORMAT (4X,'PARTICLE INITIAL POSITION IN Y (CM)   :',F15.6,/
     +          4X,'PARTICLE INITIAL POSITION IN X (CM)   :',F15.6,/
     +          4X,'PARTICLE INITIAL ORIENTATION (degree):',F15.6,/
     +          4X,'PRINT OPTION: 1-SIMPLE, 2-COMPLEX     :',I7/)
C
       YINT=YINT/W
       XINT=XINT/W
       EU(2)=EU(2)*PI/180
       GRAD(1)=-16*YINT
       PAR(6)=-GRAD(1)*(B*B*SIN(EU(2))**2+COS(EU(2))**2)/(B*B+1)
C
         CALL STOKE
       WRITE (1,299)
         WRITE (1,4) XL,YL,W,YV(M1)/YV(NSY),UIN
         WRITE (1,5) DP,B,ROP,STK,PR*2*B,RE
       WRITE (1,8) XINT*W,YINT*W,EU(2)*180/PI,PAR(6)*UIN/W
      GO TO 9
```

```
      ENDIF
4      FORMAT(//,4X,'TUBE LENGTH (CM)                : ',F15.6,/
     +            ,4X,'TUBE RADIUS (CM)                : ',F15.6,/
     +            ,4X,'CHARACTORISTIC LENGTH (CM)      : ',F15.6,/
     +            ,4X,'CONTRACTION RATIO               : ',F15.6,/
     +            ,4X,'INLET VELOCITY (CM/S)           : ',F15.6,/)
5       FORMAT(//,4X,'PARTICLE DIAMETER (MICRON)      : ',F15.6,/
     +                ,4X,'PARTICLE AXES RATIO            : ',F15.6,/
     +            ,4X,'PARTICLE DENXITY (g/cc)         : ',F15.6,/
     +            ,4X,'STOKES NUMBER                   : ',F15.6,/
     +            ,4X,'INTERCEPTION PARAMETER          : ',F15.6,/
     +            ,4X,'REYNOLDS NUMBER                 : ',F15.6,//)
8       FORMAT(4X,'PARTICLE INITIAL POSITION (cm):     X= ',F15.6/
     +          ,4X,'                                  Y= ',F15.6/
     +          ,4X,'PARTICLE INITIAL ORIENTATION(degree): ',F15.6/
     +          ,4X,'PARTICLE INITIAL ANGULER VEL.(1/t)  : ',F15.6/)
C
C---------------  RUN MODE 1  -------------------
      CALL STOKE
      WRITE (2,151) UIN,W,2*YL,W,RE,XU(NSX)*W,U(L2,2)*UIN
      WRITE(2,152)
2     PRINT*, '---------- RUN MODE 1 -------------'
      PRINT*, 'INPUT Dp,DDp,NDP'
      READ(*,*,ERR=2),DP,DDP,NDP
      PR=DP*0.5E-4/W
      DO 160,KK=0,NDP
      CALL STOKE
      PRINT*,'SQRT(STK)=',SQRT(STK),'    ROP=',ROP
      CALL CRITI(XINT,YINT,YF,YCR,KK)
      EFF=(YV(M1)**2-YCR**2)/YV(M1)**2
      EFF1=EFF**2
      PRINT*,'EFF',EFF,'EFF1',EFF1
      PRINT 152
      WRITE(2,154) DP,SQRT(STK),SQRT(STK/2.0),EFF,YCR*W,EFF1,ROP,
     +      REPMAX
      PRINT 154, DP,SQRT(STK),SQRT(STK/2.0),EFF,YCR*W,EFF1,ROP
        DP=DP+DDP
      PR=DP*0.5E-4/W
151   FORMAT(///,9X,'PARTICLE DEPOSITION IN CONTRACTION CHANNEL'//
     +  ' INITIAL VELOCITY = ',F10.5, ' CM/S'/
     +  ' CHARACTERISTIC LENGTH = ',F10.5,' CM'/
     +  ' DIAMETER OF INLET TUBE = ',F10.5,' CM'/
     +  ' DIAMETER OF EXITING TUBE = ',F10.5,' CM'/
     +  ' REYNOLDS NUMBER = ',E12.6/
     +  ' LENGTH OF TUBE =',F12.6/
     +  ' MAXIMUM VELOCITY = ',F12.5//)
152    FORMAT (8X,'DP',7X,'SQRT.STK',4X,'SQRT.STK1',6X,'EFF.',9X,
     +      'YCR',9X,'EFF1',10X,'ROp',6X,'REPMAX')
154   FORMAT (4X,F8.4,4X,F8.5,5X F8.5,4X,E10.5,2X,F10.5,3X,F10.5,
     +             F10.5,3X,E10.5)
160   CONTINUE
162   PRINT*,'DO YOU WANT REPEAT? YES--1,'
      READ(*,*,ERR=162) NCC
      IF (NCC.EQ.1) GO TO 2
      RETURN
C-------------------------------------------------------
C
      ENTRY IMPACT
```

```
C
9       ITOTAL=1
       PRINT*, 'ENTERING IMPACT'
        DT=0.0
        NSTEP=0
C---------SET ENTRY POINT OF A PARTICLE
       PAR(1)=XINT
       PAR(3)=YINT
       PAR(5)=EU(2)
       I=2
       J=2
10          IF(XU(I)-PAR(1)) 20,30,30
20          I=I+1
            GO TO 10
30          IF(YV(J)-PAR(3)) 50,40,40
50          J=J+1
            GO TO 30
40          CONTINUE
C---------CALCULATE PARTICLE INITIAL VELOCITY
       CALL CONSTS(I,J)
       PAR(2)=C1(1)+C2(1)*PAR(1)+C3(1)*PAR(3)+C4(1)*PAR(1)*PAR(3)
       PAR(4)=C1(2)+C2(2)*PAR(1)+C3(2)*PAR(3)+C4(2)*PAR(1)*PAR(3)
       PAR(2)=PAR(2)*RAT(1)
       PAR(4)=PAR(4)*RAT(2)
       TF=0.0
       IF(ISINGLE.EQ.2) THEN ! SINGLE RUN
           TT=0.                                    ! IN SEC
       IF (IFLAG.NE.2) THEN
         WRITE (1,298)
       ELSE
           WRITE(1,300)
       ENDIF
299      FORMAT(/,'************  A TUBE WITH A ABRUPT CONTRACTION
     +  ************')
298        FORMAT(6X,4HTIME,9X,1HX,11X,1HY,9X,5HANGLE,9X,5HA.VEL,/)
300        FORMAT(/,3X,1HI,3X,1HJ,4X,4HTIME,8X,1HX,9X,2HVX,11X
     +     ,1HY,10X,2HVY,9X,5HANGLE,7X,5HA.VEL,9X,5HGRAD1,
     +     6X,5HGRAD2,6X,5HREYLO)
       ENDIF
C-------------------------------------------------------------
C
C      COME BACK HERE IF PARTICLE CROSSED A GRID
66     IID=1
       NTIM=1
        Idd=1
       CALL CONSTS(I,J)
C
C      COME BACK HERE IF PARTICLE DID NOT CROSS A GRID
65     TI=TF
       NN=1
C-------------ESTIMATE TIME TO CROSS A GRID
       CALL TIMCOR(I,J,TZ,PAR)
       IF (TZ.LT.1E-3) THEN
        TF=TI+TZ
        IF (TZ.LT.1.E-6) TF=TI+1.0E-6
       ELSE
        TF=TI+FACTORA*TZ
       ENDIF
```

```
55     NTIM=NTIM+1
       DO 61 II=1,6
61     PAR1(II)=PAR(II)
68     NSTEP=NSTEP+1
       IF(NTIM.GE.200) THEN
         PRINT*,' !!! ERRORS, TOO MANY STEPS !!!'
         RETURN
       ENDIF
C
C     CALCULATE TRANLATION AND ORIENTATION OF THE PARTICLE
C
       CALL RK(TI,TF,PAR1,FF,DERIV,6,ETB,ETA,IID,TEMP,DT)
C
C      CHECK IF THE STEP WAS TOO BIG
C
       IF (PAR1(1).GT.XU(I+1).OR.PAR1(1).LT.XU(I-2).OR.PAR1(3).GT.
      +        YV(J+1).OR.PAR1(3).LT.YV(J-2)) THEN
        TF=TI+0.3*(TF-TI)
        PRINT *, 'LAST STEP WAS TOO BIG. IT HAS BEEN ADJUSTED.'
        GOTO 55
       ENDIF
       DO 62 II=1,6
62     PAR(II)=PAR1(II)
       IOLD=I
       JOLD=J
       EU(2)=PAR(5)
C
C     FOR MODE 2 ONLY
       IF(ISINGLE.EQ.2) THEN
           YT(1)=PAR(1)*W ! IN CENTIMETERS
           YT(3)=PAR(3)*W ! IN CENTIMETERS
           YT(2)=PAR(2)*UIN
           YT(4)=PAR(4)*UIN
         YT(5)=PAR(5)*180/PI
         YT(6)=PAR(6)/(W/UIN)
         TT=TF*W/UIN      ! TIME IN SEC.
       IF (IFLAG.NE.2) THEN
        IF (Idd.EQ.1) THEN
        WRITE (1,304) TT,YT(1),YT(3),YT(5),YT(6)
          ELSE
        GOTO 97
        ENDIF
       ELSE
        IPRA=MOD(NTIM,30)
        IF (I.GT.NSX-3.AND.I.LT.NSX+3) IPRA=MOD(NTIM,2)
           IF(NTIM.LE.10.OR.IPRA.EQ.0) THEN
          WRITE(1,301)I,J,TT,YT,GRAD(1),GRAD(2),REYLOC
C           PRINT 301,I,J,TT,YT,GRAD(1),GRAD(2),REYLOC
           ENDIF
          ENDIF
       ENDIF
97     Idd=-1
C
C----------- CHECK IF PARTICLE IMPACTED OR EXITED
C
       PAR1(1)=PAR(1)+COS(EU(2))*PR
       PAR1(3)=PAR(3)+SIN(EU(2))*PR
       PAR2(1)=PAR(1)-COS(EU(2))*PR
```

```
      PAR2(3)=PAR(3)-SIN(EU(2))*PR
C    SET STANDARD FOR FOLLOWING CHECK
            err1=1.0e-7
C
C      FOR MODE 1. CHECK IF PARTICLE HAS IMPACTED OR EXITED
       IF (ISINGLE.EQ.2) GOTO 99
C       FOR MODE 1 (WITHOUT INTERCEPTION)
       IF ((XU(NSX10)-PAR(1)).LT.ERR1) THEN
       IF (ABS(XU(NSX10)-PAR(1)).LE.ERR1) THEN
          YF=PAR(3)
       ELSE
          YF=YP(3)+(PAR(3)-YP(3))/(PAR(1)-YP(1))*(XU(NSX10)-YP(1))
       ENDIF
       PRINT*,'YF=',YF,' Dp=',DP
       RETURN
       ENDIF
       GOTO 90
C
C     CHECK IF THE PARTICLE IMPACTED ON A SOLID WALL
99     IF ((XU(NSX10)-PAR1(1)).LT.ERR1.OR.(XU(NSX10)-PAR2(1))
      +      .LT.ERR1) GOTO 96
       GOTO 98
96     IF ((YV(NSY10)-PAR1(3)).LT.ERR1.OR.(YV(NSY10)-PAR2(3))
      +      .LT.ERR1) GOTO 110
98     IF ((YV(M1)-PAR1(3)).LT.ERR1.OR.(YV(M1)-PAR2(3))
      +      .LT.ERR1) GOTO 112
C
C     CHECK IF THE PARTICLE EXITED
       IF (PAR1(1).GT.XU(L1-1).OR.PAR2(1).GE.XU(L1-1)) GOTO 115
       GOTO 90
C
110    PRINT *,'PARTICLE IMPACTED ON SOLID WALL'
       PRINT *,'XU(NSX10)=',XU(NSX10),' PAR1,2(1)=',PAR1(1),PAR2(1)
         PRINT *,'YV(NSY10)=',YV(NSY10),' PAR1,2(3)=',PAR1(3),PAR2(3)
       WRITE (1,302)
       RETURN
112    PRINT *,'YV(M1)=',YV(M1),' PAR1,2(3)=',PAR2(3),PAR2(3)
       WRITE (1,302)
       RETURN
115    WRITE (1,303)
       PRINT *,'EXIT'
       RETURN
C
C--------CHECK IF PARTICLE HAS CHANGED GRID POINTS
90     IF ((XU(I)-PAR(1)).LE.ERR1) THEN
           I=I+1
              IF(PAR(1).LE.XU(I-1)) PAR(1)=XU(I-1)
              GO TO 79
             ENDIF
             IF(XU(I-1)-PAR(1).GT.ERR1) THEN
              I=I-1
             ENDIF
79     IF(YV(J)-PAR(3).LE.ERR1)THEN
              J=J+1
              IF(PAR(3).LE.YV(J-1)) PAR(3)=YV(J-1)
              GO TO 81
       ENDIF
       IF(YV(J-1)-PAR(3).GT.ERR1) THEN
```

```
            J=J-1
      ENDIF
81    IF(IOLD.EQ.I.AND.JOLD.EQ.J) THEN
                GO TO 65  ! PARTICLE DIDN'T CROSS THE GRID
C               ! INTERPOLATION CONSTANT DON'T NEED TO CHANGE
      ELSE
C     PRINT*,'PARTICLE CROSSED A GRID!'
       IF (ISINGLE.NE.2) THEN
      PRINT*,'I=',I,'          J=',J
       ENDIF
      REPMAX=MAX(REPMAX,REYLOC)
           GO TO 66   ! PARTICLE CROSSED A NEW GRID,
C            ! RECALCULATE INTERPOLATION CONSTANTS.
      ENDIF
301   FORMAT(2I4,F9.5,1X,F10.6,2X,1P,E11.4,0P,F10.5,2X,E11.4,2X,E12.6,
     +  1X,0P,E12.5,2X,E12.6,2X,E12.6,2X,E11.6)
302   FORMAT(/' PARTICLE IMPACTED')
303   FORMAT(/' PARTICLE EXITS')
304   FORMAT(2X,F10.6,2X,F10.6,2X,F10.6,2X,E12.6,2X,E12.6)
911   FORMAT(3X,I3,2X,I3,3X,F10.5,3X,F10.5,3X,F10.5,3X,F10.5,4X,A8)
928   FORMAT(4X,'SUCCESSFUL!')
      RETURN
      END
C*****************************************************************
C               SUBROUTINE TO CALCULATE THE STOKE NUMBER        *
C*****************************************************************
      SUBROUTINE STOKE
      INCLUDE 'PAT2D.CMN'
      COMMON /CAL/ISTOKE,STK,STKB,GHAT,REYLOC,CD,SLIP0,SLIP1,VREL,RE
      COMMON /PARTICLE/B,EU(3),DE
C  SLIP CORECTION FOR NONSPHERICAL PARTICLE
C
      PRESS=76.0
      DA0=DP*(0.8704 8.1699E-2*B-1.9987E-3*B*B+2.8495E-5*B**3
     +       -2.0612E-7*B**4+5.8835E-10*B**5)   !FOR 0 DEGREE
      DA1=DP*(0.92634+1.6687*LOG10(B))       !FOR 90 DEGREE
        FACTOR0=1/(DA0*PRESS)
      FACTOR1=1/(DA1*PRESS)
        SLIP0=1.0+12.64*FACTOR0+4.02*FACTOR0*EXP(-0.1095/FACTOR0)
      SLIP1=1.0+12.64*FACTOR1+4.02*FACTOR1*EXP(-0.1095/FACTOR1)
      PRINT *,'SLIP  ',SLIP0,SLIP1
C
      DE=DP*B**(1./3.)
      STK=ROP*(DE*1.0E-4)**2*UIN/(18.0*AMU*W)
      GHAT=ROP*(DP*1.0E-4)**2/(18.0*AMU*UIN)
      RE=RHOCON*UIN*W/AMU
      RETURN
      END
C*****************************************************************
C         SUBROUTINE TO FORMULATE THE EQUATION OF MOTION          *
C                          FOR INTEGRATION                        *
C*****************************************************************
      SUBROUTINE DERIV(T,YY,FF)
      INCLUDE 'PAT2D.CMN'
      COMMON/CONST/C1(2),C2(2),C3(2),C4(2)
      COMMON/CONTROL/ISINGLE
      COMMON/CAL/ISTOKE,STK,STKB,GHAT,REYLOC,CD,SLIP0,SLIP1,VREL,RE
      COMMON/PARTICLE/B,EU(3),DE
```

```
      COMMON/GRID/I,J
      COMMON/GRAD/GRAD(2)
      DIMENSION YY(6),FF(6)
      DIMENSION U1(2),U2(2)
      EU(2)=YY(5)
C
C----------CALCULATE LOCAL FLUID VELOCITIES-----------------
      V1=C1(1)+C2(1)*YY(1)+C3(1)*YY(3)+C4(1)*YY(1)*YY(3)
      V2=C1(2)+C2(2)*YY(1)+C3(2)*YY(3)+C4(2)*YY(1)*YY(3)
      VREL=(YY(2)-V1)*(YY(2)-V1)+(YY(4)-V2)*(YY(4)-V2)
      VREL=SQRT(VREL)
      REYLOC=RHOCON*(VREL*UIN)*(DE*1.0E-4)/AMU ! in cgs system
      E=SQRT(1-1/(B*B))
      EE=(1+E)/(1-E)
       IF (ABS(B-1.0).LT.1.0E-6) THEN
      CF1=1.0
      CF2=1.0
       ELSE
      CF1=8/3*E**3/(-2*E+(1+E*E)*LOG(EE))*(B*DP/DE)
      CF2=16/3*E**3/(2*E+(3*E*E-1)*LOG(EE))*(B*DP/DE)
       ENDIF
      CE=COS(YY(5))
      SE=SIN(YY(5))
C     CALCULATE THE DRAG COEFFICIENT
      IF (REYLOC.LT.0.1) THEN
        CD=24.0
      ELSEIF (REYLOC.LE.5.0) THEN
        CD=24.0*(1.0+0.0916*REYLOC)
      ELSEIF (RETLOC.LE.1000.0) THEN
        CD=24.0*(1.0+0.158*REYLOC**0.66667)
      ENDIF
C     EQUATIONS IN RELATIVE COORDINATE SYSTEM
10    FF(1)=YY(2)
      F2=CD/24.*CF1/STK*((V1-YY(2))*CE+(V2-YY(4))*SE)/SLIP0
      FF(3)=YY(4)
      F4=CD/24.*CF2/STK*((V2-YY(4))*CE-(V1-YY(2))*SE)/SLIP1
C     EQUATIONS IN INERTIAL COORDINATE SYSTEM
      FF(2)=CE*F2-SE*F4
      FF(4)=SE*F2+CE*F4
C
C     MOMENT EQUATION OF PARTICLES
      II=I
      JJ=J
      XX=YY(1)+PR*B*CE
      YY1=YY(3)+PR*B*SE
      CALL VELO(II,JJ,XX,YY1,V1,V2)
      U1(1)=V1-YY(2)
      U1(2)=V2-YY(4)
      XX=YY(1)-PR*B*CE
      YY1=YY(3)-PR*B*SE
      II=I
      JJ=J
      CALL VELO(II,JJ,XX,YY1,V1,V2)
      U2(1)=V1-YY(2)
      U2(2)=V2-YY(4)
C     VELOCITIES IN THE RELATIVE COORDINATE SYSTEM IN MINOR AXIS DIREC.
      V1=-SE*U1(1)+CE*U1(2)
      V2=-SE*U2(1)+CE*U2(2)
```

```
      GRAD(2)=(V1-V2)/(B*2*PR)
C
      II=I
      JJ=J
      XX=YY(1)-PR*SE
      YY1=YY(3)+PR*CE
      CALL VELO(II,JJ,XX,YY1,V1,V2)
      U1(1)=V1-YY(2)
      U1(2)=V2-YY(4)
      II=I
      JJ=J
      XX=YY(1)+PR*SE
      YY1=YY(3)-PR*CE
      CALL VELO(II,JJ,XX,YY1,V1,V2)
      U2(1)=V1-YY(2)
      U2(2)=V2-YY(4)
C   VELOCITIES IN THE RELATIVE COORDINATE SYSTEM IN MAJOR AXIS DIREC.
      V1=CE*U1(1)+SE*U1(2)
      V2=CE*U2(1)+SE*U2(2)
      GRAD(1)=(V1-V2)/(2*PR)
C
      E=SQRT(1-1/B/B)
      EE=(1+E)/(1-E)
      IF (ABS(B-1.0).LT.1.E-8) THEN
      CM=1.
      ELSE
      CM=4./3.*E*E*E/(-2.*E+(1+E*E)*LOG(EE))
      ENDIF
      FF(5)=YY(6)
      FF(6)=30*AMU*CM*((-GRAD(1)-YY(6))+B*B*(GRAD(2)
     +      -YY(6)))/((DP/2*1.E-4)**2
     +      *(B*B+1)*ROP)*(W/UIN)
C
      RETURN
      END
C*********************************************************************
C             SUBROUTINE TO ESTIMATE TIME REQUIRED FOR A PARTICLE   *
C                          TO EXIT A GRID                           *
C*********************************************************************
      SUBROUTINE TIMCOR(I,J,TZ,YY)
      INCLUDE 'PAT2D.CMN'
      COMMON/CONST/C1(2),C2(2),C3(2),C4(2)
      COMMON/CONTROL/ISINGLE
      COMMON/CAL/ISTOKE,STK,STK2,GHAT,REYLOC,CD,SLIP0,SLIP1,VREL,RE
      DIMENSION YY(6),FF(6)
      IF (YY(2)) 1,2,2
1     TZ1=(XU(I-1)-YY(1))/YY(2)
      GO TO 3
2     TZ1=(XU(I)-YY(1))/(YY(2)+1.0E-10)
3     IF(YY(4)) 4,5,5
4     TZ2=(YV(J-1)-YY(3))/YY(4)
      GO TO 6
5     TZ2=(YV(J)-YY(3))/(YY(4)+1.0E-10)
6     IF (ABS(TZ1).LE.1.0E-8.OR.ABS(TZ2).LE.1.0E-8) THEN
          TZ=MAX(ABS(TZ1),ABS(TZ2))
      ELSE
        TZ=MIN(ABS(TZ1),ABS(TZ2))
      ENDIF
```

```
      IF(TZ.LE.0.0.AND.ISINGLE.EQ.2) THEN
               WRITE(1,7)
               GO TO 8
      ENDIF
      IF(TZ.LE.0.0.AND.ISINGLE.NE.2) THEN
               WRITE(2,7)
               GO TO 8
      ENDIF
7     FORMAT(' !!!!!! TIME STEP IS NEGATIVE, ERROR !!!!!!!!')
8     RETURN
      END
C*************************************************************
C          SUBROUTINE TO DETERMINE INTERPOLATION CONSTANTS    *
C          FOR APPROXIMATION OF LOCAL FLUID VEL WITHIN A GRID *
C*************************************************************
      SUBROUTINE CONSTS(I,J)
      INCLUDE 'PAT2D.CMN'
      COMMON/CONST/C1(2),C2(2),C3(2),C4(2)
      CALL CONSTA(I,J,C1,C2,C3,C4)
      RETURN
      END
C*************************************************************
C     SUBROUTINE TO DETERMINE INTERPOLATION CONSTANTS
C*************************************************************
       SUBROUTINE CONSTA(I,J,C1,C2,C3,C4)
      INCLUDE 'PAT2D.CMN'
      DIMENSION C1(2),C2(2),C3(2),C4(2)
      DX=XU(I)-XU(I-1)
      DY=YV(J)-YV(J-1)
      DO 10 NV=1,2
      DVDY=(F(I-1,J,NV)-F(I-1,J-1,NV))/DY
      DVDX=(F(I,J-1,NV)-F(I-1,J-1,NV))/DX
      C4(NV)=(F(I,J,NV)-F(I,J-1,NV)-F(I-1,J,NV)+F(I-1,J-1,NV))/
     +(DX*DY)
      C1(NV)=F(I-1,J-1,NV)-DVDY*YV(J-1)-DVDX*XU(I-1)+
     +C4(NV)*XU(I-1)*YV(J-1)
      C2(NV)=DVDX-C4(NV)*YV(J-1)
      C3(NV)=DVDY-C4(NV)*XU(I-1)
10    CONTINUE
      RETURN
      END
C*************************************************************
C     SUBROUTINE TO CALCULATE THE PARTICLE ORIENTATION
C*************************************************************
      SUBROUTINE ORIEN (TI,TF,AN)
      INCLUDE 'PAT2D.CMN'
      COMMON/PARTICLE/B,EU(3),DE
      DIMENSION AN(2),FF1(2),TEMP(20),ETA(2)
      EXTERNAL DERIV1
      DATA ETB,ETA/1.E-4,2*1.E-4/
      IID=1
C   CALCULATE THE CHANGE OF ANGLES IN RELATIVE COORDINATE SYSTEM
      CALL RK(TI,TF,AN,FF1,DERIV1,2,ETB,ETA,IID,TEMP,DT)
      RETURN
      END
C*************************************************************
C     SUBROUTINE TO FOMULATE MOMENT EUATION OF PARTICLE
C*************************************************************
```

```
C      SUBROUTINE DERIV1(T,AN,FF1)
C      INCLUDE 'PAT2D.CMN'
C      COMMON/GRAD/GRAD(2)
C      COMMON/GRID/I,J
C      COMMON/PARTICLE/B,EU(3),DE
C      DIMENSION AN(2),FF1(2)
C      RETURN
C      END
C*********************************************************************
C   SUBROUTINE FOR DETERMINE THE FLUID VELOSITIES AT THE POSITIONS
C      WHERE THE PARTICLE LOCATES
C*********************************************************************
       SUBROUTINE VELO (I,J,XX,YY,V1,V2)
       INCLUDE 'PAT2D.CMN'
       DIMENSION C1(2),C2(2),C3(2),C4(2)
       IF(XU(I)-XX) 20,50,30
20     I=I+1
22     IF (XU(I)-XX) 24,50,50
24     I=I+1
       GOTO 22
30     I=I-1
32     IF(XU(I)-XX) 34,34,36
34     I=I+1
       GOTO 50
36     I=I-1
       GOTO 32
50     IF (YV(J)-YY) 60,80,70
60     J=J+1
62     IF(YV(J)-YY) 64,80,80
64     J=J+1
       GOTO 62
70     J=J-1
72     IF (YV(J)-YY) 74,74,76
74     J=J+1
       GOTO 80
76     J=J-1
       GOTO 72
80     CALL CONSTA (I,J,C1,C2,C3,C4)
       V1=C1(1)+C2(1)*XX+C3(1)*YY+C4(1)*XX*YY
       V2=C1(2)+C2(2)*XX+C3(2)*YY+C4(2)*XX*YY
       RETURN
       END
C-----------------------------------------------
C     EXPLANATION OF VARIABLES
C       PAR(1): PARTICLE X-POSITION
C       PAR(2): PARTICLE X-VELOCITY
C       PAR(3): PARTICLE Y-POSITION
C       PAR(4): PARTICLE Y-VELCOCITY
C       PAR(5): PARTICLE ANGLE
C       PAR(6): PARTICLE ANGLE VELOCITY
C       ROP  : PARTICLE DENSITY ,g/cc
C       DP   : PARTICLE DIAMETER,MICRON
C       UIN  : INLET FLUID VEL  ,CM/SEC
C       AMU : AIR VISCOSITY, POISE
C       W    : CHARACTER LENGTH, CM
C       RHOCON : AIR DENSITY ,g/CC
C       PR   : DIMENSIONLESS PARTICLE RADIUS=DP*0.5E-4/W
C       STK:  STOKE'S NUMBER
```

```
C       STKB: STK*B
C       SLIP: SLIP CORRECTION FACTOR
C       GHAT: GRAVITATIONAL FACTOR
C       TI: INITIAL TIME AT EACH STEP
C       TF: FINAL TIME AT EACH STEP
C       TZ  : ESTIMATED TIME FOR A PARTICLE TO
C             CROSS A GRID, =T/W*UIN ,DIMENSIONLESS
C       C1(1-2),C2(1-2),C3(1-2),C4(1-2): INTERPOLATION
C             CONST FOR LOCAL FLUID VEL APPROXIMATION
C             WITHIN A GRID
C       VREL  : RELATIVE DIMENSIONLESS VELOCITY
C       REYLOC: LOCAL REYNOLDS NUMBER
C       CD    : DRAG COEFFICIENT
C       F(1-4): FOUR EQUATION OF MOTION FOR INTEGRATION
C       VREL  : RELATIVE DIMENSIONLESS VELOCITY
C       REYLOC: LOCAL REYNOLDS NUMBER
C       CD    : DRAG COEFFICIENT
C       F(1-4): FOUR EQUATION OF MOTION FOR INTEGRATION
C       B: RATIO OF THE MAJOR AXIS TO MINOR AXIS, A/B, A>B
C       EU(1-3): EULER ANGERS
C       TT: TIME IN SEC
C       NSX#:  GRID POINTS USED TO FORM DESIRED NOZZLE SHAPE
C       NSY#:  GRID POINTS USED TO FORM DESIRED NOZZLE SHAPE

C*********************************************************************
C          4TH ORDER RUNGE-KUTTA INTEGRATION SUBROUTINE               *
C*********************************************************************
C
      SUBROUTINE RK(XO,XE,Y1,Z,FKT,NNN,EP,ETA,ID,S,DS)
      IMPLICIT DOUBLE PRECISION (A-H,O-Z)
      EXTERNAL FKT
      DIMENSION Y1(NNN),Z(NNN),SS1(6),SS2(6),SS3(6),SS4(6),
     +    ETA(NNN)
C
C-------------SET N TO 0 IN CASE VERY FIRST CALL IS MADE WITH ID.LT. 0
C
      DATA N/0/,DX/0.0/
      X=XO
      XF=XE
      NN=NNN
      EPS=EP
      M=-1
C      IF (ID)25,150,30
C-------------USE PREVIOUS DS IF ID IS NEGATIVE
25    DX=DS
C-----------HOWEVER ,USE XF-X AND CHANGE DS IF ABS(DX).GT.ABS(XF-X) OR
C-----------IF DX=0.0 OR IF XF=X OR IF SIGN OF DX.NE. SIGN OF (XF-X)
      IF (ABS(DX).LE.ABS(XF-X).AND.DX*(XF-X).GT.0.0) GO TO 40
30    DX=XF-X
      DS=DX
      N=0
      IF(DX.EQ.0.0) GO TO 140
C
C-----------CHECK FOR NEAR END OF INTERVAL (NEEDS 1 MORE SHORT STEP) OR
C----------- EXACT END OF INTERVAL
40    IF((X-XF+2.01*DX)*DX.LE.0.0) GO TO 60
C----------SET M POSITIVE FOR LAST (SHORT) STEP. SAVE PREVIOUS DX
C----------IN DS. SET DX FOR SHORT STEP
```

```
      M=1
      DS=DX
      DX=0.5*(XF-X)
C_____________INTEGRATE BETWEEN X AND XF
60    CALL RK1ST(X,Y1,2.0*DX,X1,SS1,NN,Z,SS4,FKT)
C---------INTEGRATE BETWEEN X AND XF/2
70    CALL RK1ST(X,Y1,DX,X2,SS2,NN,Z,SS4,FKT)
C-------- INTEGRATE BETWEEN XF/2 AND XF
      CALL RK1ST(X2,SS2,DX,X3,SS3,NN,Z,SS4,FKT)
C---------COMPARE RESULTS
C
      DO 80 K=1,NN
      IF(ABS(SS1(K)-SS3(K)).GT.
     +ETA(K)) GO TO 110
80    CONTINUE
C---------STEP WAS SUCCESSFUL
      X=X3
      DO 90 K=1,NN
      Y1(K)=SS3(K)
90    CONTINUE
C---------EXIT IF M IS POSITIVE
      IF (M.GT.0) GO TO 150
      N=N+1
      IF(N.LT.5) GO TO 40
C-------- DOUBLE THE STEP IF 5 SUCCESSFUL STEPS HAVE BEEN TAKEN
      N=0
      DX=2.0*DX
      GO TO 40
C---------HALVE THE STEP SINCE THE RESULT IS UNSATISFACTORY
110   DX=0.5*DX
C---------BYPASS IF DX LARGE ENOUGH WITH RESPECT TO X
      IF((X+DX).NE.X) GO TO 120
C--------GIVE UP IF DX TOO SMALL WITH RESPECT TO X
C       DS=DX
C       ID=0
      PRINT 115
115   FORMAT(33H INTERNAL STEP TOO SMALL AT XCUR.,
     +18H-INTEGRATION ENDED)
      GO TO 150
C----------SET M NEGATIVE. MOVE OLD HALF-STEP ARRAY TO NEW
C----------FULL STEP ARRAY SO AS NOT TO REDO FULL STEP
C----------RESTART WITH NEW HALF STEP
120   M=-1
      N=0
      DO 130 K=1,NN
      SS1(K)=SS2(K)
130   CONTINUE
      GO TO 70
C---------EVALUATE DERIVATIVE FUNCTION BEFORE EXITTING
140   CALL FKT(X,Y1,Z)
C---------EXIT RK
150   XE=X
      RETURN
      END
C
C
C
      SUBROUTINE RK1ST(X,Y2,H,XE,YE,NN,Z,W,FKT)
```

```
      IMPLICIT DOUBLE PRECISION (A-H,O-Z)
      DIMENSION Y2(NN),YE(NN),W(NN),A(5),Z(NN)
      EXTERNAL FKT
C----------DO ONE RUNGE KUTTA STEP
      A(4)=H
      A(3)=A(4)
      A(5)=0.5*H
      A(2)=A(5)
      A(1)=A(2)
      XE=X
      DO 10 K=1,NN
      W(K)=Y2(K)
      YE(K)=Y2(K)
10    CONTINUE
      DO 30 J=1,4
      CALL FKT(XE,W,Z)
      XE=X+A(J)
      C=A(J+1)*(1.0/3.0)
      DO 20 K=1,NN
      W(K)=Y2(K)+A(J)*Z(K)
      YE(K)=YE(K)+C*Z(K)
20    CONTINUE
30    CONTINUE
      RETURN
      END
C
```

APPENDIX B
FIBER LIGHT SCATTERING PROGRAM

```
      PROGRAM CALCYL
C
C*****************************************************************
C         THIS PROGRAM IS FROM "ADSORPTION AND SCATTERING OF LIGHT BY
C         SMALL PARTICLES", BOHREN AND HUFFMAN, 1983, APPENDIX C
C
C*****************************************************************
C         CALCYL CALCULATES THE SIZE PARAMETER (X) AND RELATIVE
C         REFRACTIVE INDEX (REFREL) FOR A GIVEN CYLINDER REFRACTIVE
C         INDEX, MEDIUM REFRACTIVE INDEX, RADIUS, AND FREE
C         SPACE WAVELENGTH.  IT THEN
C         CALLS BHCYL, THE SUBROUTINE THAT COMPUTES AMPLITUDE SCATTERING
C         MATRIX ELEMENTS AND EFFICIENCIES.
C
C*****************************************************************
      COMPLEX REFREL,T1(200),T2(200),CSP(200),CSS(200)
      DIMENSION ANG(200),RAD(200)
      OPEN (2,FILE='SCAT DAT',STATUS='NEW')
      WRITE (2,11)
C
C*****************************************************************
C         REFMED = (REAL) REFRACTIVE INDEX OF SURROUNDING MEDIUM
C
C*****************************************************************
      REFMED=1.0
C
C*****************************************************************
C         REFRACTIVE INDEX OF CYLINDER = REFRE + I*REFIM
C
C*****************************************************************
      REFRE=2.63
      REFIM=2.67
      REFREL=CMPLX(REFRE,REFIM)/REFMED
      WRITE (2,12) REFMED,REFRE,REFIM
      PI=3.14159265
C
C*****************************************************************
C         RADIUS (RAD) AND WAVELENGTH (WAVEL) SAME UNITS
C
C*****************************************************************
      WAVEL=.6328
C     WRITE (2,13) RAD,WAVEL
      WRITE (2,22)
C       WRITE (2,14) X
C
C*****************************************************************
C         FIN = FINAL ANGLE (DEGREES)
C         INTANG = NUMBER OF INTERVALS BETWEEN 0 AND FIN
C         ANGINC=ANGLE INCREMENTS FOR SIMP CALCULATION
C
C*****************************************************************
      FIN=180.
      INTANG=180
      ANGINC=1.
C     WRITE (2,15)
      DO 789 K=1,3
      RAD(K)=K*0.5
      X=2.*PI*RAD(K)*REFMED/WAVEL
```

```
      CALL BHCYL (X,REFREL,T1,T2,QSCPAR,QSCPER,QEXPAR,QEXPER,
     1  FIN,INTANG,ANG)
        NPTS=INTANG+1
      T11NOR=0.5*(CABS(T1(1))*CABS(T1(1)))
      T11NOR=T11NOR+0.5*(CABS(T2(1))*CABS(T2(1)))
C         ***************************************************************
C         T33 AND T34 MATRIX ELEMENTS NORMALIZED BY T11
C         T11 IS NORMALIZED TO 1.0 IN THE FORWARD DIRECTION
C         POL = DEGREE OF POLARIZATION (INCIDENT UNPOLARIZED LIGHT)
C         ***************************************************************
      DO 107 J=1,NPTS
      TPAR=CABS(T1(J))
      TPAR=TPAR*TPAR
      TPER=CABS(T2(J))
      TPER=TPER*TPER
      T11=0.5*(TPAR+TPER)
      T12=0.5*(TPAR-TPER)
      POL=T12/T11
      T33=REAL(T1(J)*CONJG(T2(J)))
      T34=AIMAG(T1(J)*CONJG(T2(J)))
      T33=T33/T11
      T34=T34/T11
      CSP(J)=TPAR
      CSS(J)=TPER
  107   CONTINUE
C 107   WRITE (2,68) ANG(J),T11,POL,TPAR,TPER
C       WRITE (2,67)  QSCPAR,QEXPAR,QSCPER,QEXPER
   67   FORMAT (  ,2X,"QSCPAR =",E14.6,3X,"QEXPAR =",E14.6,/,
     1  2X,"QSCPER =",E14.6,3X,"QEXPER =",E14.6//)
   68   FORMAT (1X,F8.2,2X,E13.6,2X,E13.6,2X,E13.6,2X,E13.6)
   11   FORMAT (/,2X,"CYLINDER PROGRAM:  NORMALLY INCIDENT LIGHT",//)
   12   FORMAT (5X,"REFMED =",F8.4,3X,"REFRE =",E14.6,3X
     -  "REFIM =",E14.6)
   13   FORMAT (5X,"CYLINDER RADIUS =",F7.3,3X,"WAVELENGTH =",F7.4)
   14   FORMAT (5X,"SIZE PARAMETER =",F8.3/)
   15   FORMAT (//,2X,"ANGLE",7X,"INTEN",13X,"POL",13X,"i1",13X,"i2",//)
        CALL SIMP(13,31,ANGINC,CSP,RP)
      CALL SIMP(13,31,ANGINC,CSS,RS)
      RP=(WAVEL/(PI*PI))*RP
      RS=(WAVEL/(PI*PI))*RS
  789   WRITE (2,99) RAD(K),RP,RS
   22   FORMAT (//,2X,"RADIUS",2X,"PARA RESPONSE",2X,"PERP RESPONSE",//)
   99   FORMAT (3X,F6.2,8X,E14.6,3X,E14.6)
        CLOSE (2)
        STOP
      END
C
C*************************************************************
C         SUBROUTINE BHCYL CALCULATES AMPLITUDE SCATTERING MATRIX
C         ELEMENTS AND EFFICIENCIES FOR EXTINCTION AND SCATTERING
C         FOR A GIVEN SIZE PARAMETER AND RELATIVE REFRACTIVE INDEX
C         THE INCIDENT LIGHT IS NORMAL TO THE CYLINDER AXIS
C         PAR: ELECTRIC FIELD FARALLEL TO CYLINDER AXIS
C         PER: ELECTRIC FIELD PERPENDICULAR TO THE CYLINDER AXIS
C
C*************************************************************
      SUBROUTINE BHCYL (X,REFREL,T1,T2,QSCPAR,QSCPER,QEXPAR,QEXPER,
     2  FIN,INTANG,ANG)
```

```
        COMPLEX REFREL,Y,AN,BN,A0,B0
      COMPLEX G(1000),BH(1000),T1(200),T2(200)
      DIMENSION THETA(200),ANG(200),BJ(1000),BY(1000),F(1000)
      Y=X*REFREL
        XSTOP=X+4.*X**.3333+2.
C
*****************************************************************
C         SERIES TERMINATED AFTER NSTOP TERMS
C         ***********************************************************
      NSTOP=XSTOP
      YMOD=CABS(Y)
      NMX=AMAX1(XSTOP,YMOD)+15
      NPTS=INTANG+1
      DANG=FIN/FLOAT(INTANG)
      DO 555 J=1,NPTS
      ANG(J)=(FLOAT(J)-1.)*DANG
  555   THETA(J)=ANG(J)*0.017453292
C         ***********************************************************
C         LOGRITHMIC DERIVATIVE G(J) CALCULATED BY COWNWARD
C         RECURRANCE BEGINNING WITH INITIAL VALUE 0.0 +I*0.0
C         AT J = NMX
C         ***********************************************************
      G(NMX)=CMPLX(0.0,0.0)
      NN=NMX-1
      DO 120 N=1,NN
      RN=NMX-N+1
      K=NMX-N
  120   G(K)=((RN-2.)/Y)-(1./(G(K+1)+(RN-1.)/Y))
C         ***********************************************************
C         BESSEL FUNCTIONS J(N) COMPUTED BY DOWNWARD RECURRENCE
C         BEGINNING AT N = NSTOP + NDELTA
C         BESSEL FUNCTIONS Y(N) COMPUTED BY UPWARD RECURRENCE
C         BJ(N+1) = J(N), BY(N+1) = Y(N)
C
*****************************************************************
      NDELTA=(101.+X)**.499
      MST=NSTOP+NDELTA
      MST=(MST/2)*2
      F(MST+1)=0.0
      F(MST)=1.0E-32
      M1=MST-1
      DO 201 L=1,M1
      ML=MST-L
  201   F(ML)=2.*FLOAT(ML)*F(ML+1)/X-F(ML+2)
      ALPHA=F(1)
      M2=MST-2
      DO 202 LL=2,M2,2
  202   ALPHA=ALPHA+2.*F(LL+1)
        M3=M2+1
      DO 203 N=1,M3
  203   BJ(N)=F(N)/ALPHA
        BY(1)=BJ(1)*(ALOG(X/2.)+.577215664)
      M4=MST/2-1
      DO 204 L=1,M4
  204   BY(1)=BY(1)-2.*((-1.)**L)*BJ(2*L+1)/FLOAT(L)
        BY(1)=.636619772*BY(1)
      BY(2)=BJ(2)*BY(1)-.636619772/X
      BY(2)=BY(2)/BJ(1)
```

```
      NS=NSTOP-1
      DO 205 KK=1,NS
  205   BY(KK+2)=2*FLOAT(KK)*BY(KK+1)/X-BY(KK)
        NN=NSTOP+1
      DO 715 N=1,NN
  715   BH(N)=CMPLX(BJ(N),BY(N))
        A0=G(1)*BJ(1)/REFREL+BJ(2)
      A0=A0/(G(1)*BH(1)/REFREL+BH(2))
      B0=REFREL*G(1)*BJ(1)+BJ(2)
      B0=B0/(REFREL*G(1)*BH(1)+BH(2))
      QSCPAR=CABS(B0)*CABS(B0)
      QSCPER=CABS(A0)*CABS(A0)
      DO 101 K=1,NPTS
      T1(K)=B0
  101   T2(K)=A0
        DO 123 N=1,NSTOP
      RN=N
      AN=(G(N+1)/REFREL+RN/X)*BJ(N+1)-BJ(N)
      AN=AN/((G(N+1)/REFREL+RN/X)*BH(N+1)-BH(N))
      BN=(REFREL*G(N+1)+RN/X)*BJ(N+1)-BJ(N)
      BN=BN/((REFREL*G(N+1)+RN/X)*BH(N+1)-BH(N))
      DO 102 J=1,NPTS
      C=COS(RN*THETA(J))
      T1(J)=2.*BN*C+T1(J)
  102   T2(J)=2.*AN*C+T2(J)
        QSCPAR=QSCPAR+2.*CABS(BN)*CABS(BN)
  123   QSCPER=QSCPER+2.*CABS(AN)*CABS(AN)
        QSCPAR=(2./X)*QSCPAR
      QSCPER=(2./X)*QSCPER
      QEXPER=(2./X)*REAL(T2(1))
      QEXPAR=(2./X)*REAL(T1(1))
      RETURN
      END
CCCCCCCCCCCCCCCCCCCCCCCCCCCCCCCCCCCCCCCCCCCCCCCCCCCCCCCCCCCCCCCCCCCCCCCCCCCC
        SUBROUTINE SIMP(MIN,MAX,DX,A,SUM)
CCCCCCCCCCCCCCCCCCCCCCCCCCCCCCCCCCCCCCCCCCCCCCCCCCCCCCCCCCCCCCCCCCCCCCCCCCCC
C
C       SUBROUTINE TO NUMERICALLY INTEGRATE A FINCTION OF DISCRETE
C       VALUES USING SIMPSON'S RULE
C       MUST HAVE EVEN NUMBER OF PANELS
C
        REAL A(181)
      SUM=A(MIN)+A(MAX)
      NM2=MAX-2
      DO 15 I=MIN+1,NM2,2
      AI=A(I)
      SUM=SUM+AI*4.
      AI=A(I+1)
   15   SUM=SUM+AI*2.
        AI=A(MAX-1)
      SUM=SUM+AI*4.
      PI=2.*ASIN(1.)
      SUM=SUM*DX/3.*PI/180.
      RETURN
      END
```